63952

$C. 1$

8232-2//063952

00000001 -

8024

Correlation of Electrical Reactor Cable Failure With Materials Degradation

Otmar M. Stuetzer

Prepared for
U. S. NUCLEAR REGULATORY COMMISSION

938852

CORRELATION OF ELECTRICAL REACTOR CABLE FAILURE
WITH MATERIALS DEGRADATION

Otmar M. Stuetzer

Printed: March 1986

Sandia National Laboratories
Albuquerque, NM 87185
Operated by
Sandia Corporation
for the
U.S. Department of Energy

Prepared for

ABSTRACT

Complete circuit failure (shortout) of electrical cables typically used in nuclear power plant containments is investigated. Failure modes are correlated with the mechanical deterioration of the elastomeric cable materials. It is found that for normal reactor operation, electrical cables are reliable and safe over very long periods. During high temperature excursions, however, cables pulled across corners under high stress may short out due to conductor creep. Severe cracking will occur in short times during high temperatures (>150°C) and in times of the order of years at elevated temperatures (100°C-140°C).

A theoretical treatment of stress distribution responsible for creep and for cracking by J. E. Reaugh of Science Applications, Inc. is contained in the Appendix.

CONTENTS

ILLUSTRATIONS

ILLUSTRATIONS (cont.)

LIST OF TABLES

ACKNOWLEDGMENTS

EXECUTIVE SUMMARY

Degradation of elastomeric cable materials in a nuclear reactor
environment has been widely investigated in the past decade. This
investigation addresses the question how materials degradation correlates
with the actual circuit failure of (safety-related) cables in the
containment building of a nuclear power plant. Mainly total failure is
considered, defined as an electrical shortout or an obvious short path.

In the introduction (Section I), the limitations of the present work are
discussed. A very large number of independent variables (e.g.,
composition, geometry, additives, aging sequences, rate effects) leads to
a high degree of complexity and forces judicious constraints on
experimentation. Cables are basically simple, well understood, and
reliable components with a low failure rate; a large number of
experiments are therefore needed to determine failure probability.
Further complications are introduced by the shortcomings of accelerated
testing methods. Single-conductor, 600 V, power cables with ethylene
propylene rubber (EPR) insulators and Hypalon jacket were chosen for the
experiments. With this configuration, a number of experiments large
enough to be statistically significant were feasible. This approach
furnished sufficient data to form a base for cautious extrapolation by
means of scaling models to other geometries and to other mechanical
boundary conditions.

Literature data and several hundred scoping tests (Section II) are the
basis for a discussion of purely electrical failures; i.e. failures
occurring when cables are not mechanically stressed or handled, and,
therefore, the ideal cylindric geometry is not changed. It is shown that
direct electrical-field breakdown, as well as thermal runaway, is very
unlikely at rated voltages even after long-term exposure to high
temperatures (190°C) and to high total doses of gamma radiation (10^8
rads); rate effects are negligible or perhaps even beneficial. The
deterioration of insulation resistance due to the presence of strong
continuous radiation (10 Mrad/h), during an accident, leads to only
negligibly small shunt currents; also, high humidity has little influence
in the absence of cracks. It is concluded that at normal reactor
environments (temperatures less then 90°C, and radiation less than 200
rads/day) the cable design investigated will not fail in 40 years. Very
high temperatures (>180°C) and radiation fluxes, such as occur during
accident conditions, will last only for days and do rarely, during this
time, fatally influence cable performance. This fact simplifies the
present investigation by limiting it to situations where the geometry of
the cable is affected by mechanical forces.

For the following it is assumed that the cables are operated within
ratings and that no severe nonstatistical flaws (such as cuts) exist.
The remaining failure mechanisms fall into two categories. First, if the
cable is stretched by an applied force (or by its own weight) over an
edge with small curvature, the metal wires may gradually creep through
the soft polymeric insulation resulting in metallic contact between cable

wires or a wire and the cable support, shorting the cable (creep shortout). Second, the polymeric materials, embrittled by aging, may crack under mechanical stress. To permit long-term aging, creep, and cracking measurements, a dedicated facility has been established. It consists principally of seven temperature-controlled heat chambers, in which stressed and unstressed cable samples are exposed to constant elevated temperatures for long periods. Creep distances can be precision measured by X-raying at regular intervals.

Creep shortout is investigated in detail in Section III. The main parameter for creep effects is the average stress at closest proximity between cable wire and (metallic) support. This stress is determined essentially by the wire radius, the support curvature, and the weight of the overhanging cable part. For stranded wires, the position of the strands is also of importance. It has been found that with increasing time two phenomena occur which decrease the likelihood of creep shortout. First, the strands will position themselves such that the effective support areas increase. Second, plastic bending of the wire leads to further increase of the effective support area. With this, the effective stress decreases and creep slows down.

For realistic geometries, creep shortout is observed only at very high temperature (> 175°C) in combination with high stress (> 500 lb./sq.in.) where failure will occur in a very short time (hours or days). Temperature and radiation hardening slow down creeping with increasing exposure time, and the mitigating phenomena described above come into play. The critical stress (~500 psi) causes different lengths of critical overhang for different cable gauge sizes; the scaling equation is presented in Section III.

Under creep loads below the critical stress, and at temperatures higher than 200°C, a temporary shortout phenomenon is observed that involves high embrittlement and even "powdering" of the polymers, but not a touching of wire and counter electrode. After a short while, the cable returns to normal performance. The phenomenon is rare.

Crack failure (Section IV) is different from the above described cases as it requires the presence of a (contaminated) liquid or condensate. The two most important, of the situations investigated, are cracking of undisturbed cables in (long) conduits and cracking due to bending during maintenance activities. In both cases, crack appearance correlates well with the polymers reaching a certain critical strain to break factor (e.g., e/e_0 ~.02). (An example pertaining to "through" cracks, i.e., cracks extending all the way to the conductor: such cracks will, under no outside stress, appear in 5 days at 200°C, and in about a year at 125°C. For bending after cooling, the corresponding times are only one half. If the temperature does not exceed 100°C, through cracks under no outside stress will not appear in 5 years.) It is important to note that even a few days exposure to very high temperatures (200°C) will produce inadmissible cracking, however.

In Section V the conclusions drawn from the above described detailed measurements and accompanying analytical considerations are summarized. The measurements were made without radiation exposure and only for a few years' duration. Arguments are presented demonstrating that the results are applicable and conservative for real containment environments and over long periods, viz. 40 years. Briefly, creep shortout is mitigated by radiation that enhances embrittlement; for cracking, strain to break curves measured under radiation have to be used to make the prediction model valid. The essential fact is, however, that situations of concern occur only at high environmental stress, i.e., high temperature and bending. During the life of a reactor these situations occur rarely and only for brief periods, much shorter than the reported aging and measurement times. Within the uncertainties of the complex overall structures, the above results are, therefore, generally pertinent.

Finally, in Section IV, some brief recommendations to improve electrical system reliability are given. As cracking has been shown to be of most concern, occurring even at relatively brief high temperature excursions, sealing of the cabling system may be advisable. In addition, long cable overhangs over sharply curved corners should be avoided.

I. INTRODUCTION

A. Program

A three-year detailed experimental and analytical study on cable failure
in a reactor containment has been performed. This discussion extends,
improves, summarizes, and attempts to extrapolate data reported
previously.[1,2]

Considerable effort has been expended in the past 10 years to understand
the complex aging and deterioration of polymeric cable materials in a
reactor environment. Some of the pertinent publications are quoted in
references 1 and 2. Of interest is a recent publication by Bustard, et
al,[3] containing U.S. and European deterioration data.

Materials' deterioration may or may not cause deterioration of electrical
circuit performance, however. The present investigation deals with cable
circuit failure and correlates, where possible, electrical performance
deterioration with materials' deterioration.

The cable failure problem is of considerable complexity due to the large
number of variables introduced by materials combinations, additives, rate
effects, circuitry, aging sequences, environments, mechanical support,
and others. Even a conservative compilation (c.f. Reference 1,
Appendix A) shows from 25 to 30 independent parameters leading to
hundreds of thousands of different combinations. The situation is
further aggravated by three additional facts:

(1) Cables, per se, are simple and well-developed components, whose
    failure rate is very low; many experiments are therefore needed to
    determine reasonably reliable and statisically valid failure data.

(2) Many parameters of possible importance, such as additives and
    materials processing sequences, are proprietary, often unknown,
    and/or batch variable; this requires a multiplicity of tests for
    statistical evaluation.

(3) Extrapolation in time requires a deterioration model, such as the
    Arrhenius dependence. Such a model is not known for multicomponent
    devices such as cables exposed to several deterioration mechanisms at
    the same time.

Literature studies and several hundred scoping tests served to bound and
define an acceptable program. The program's aim was to find and
understand the most important operational failure mechanisms for
electrical cables in a reactor containment environment. Extrapolation to
40-year exposure with the possibility of a reactor accident at the end of
this time is desirable.

B. Simplifications

Constraints had to be imposed and simplifications had to be introduced to keep the experimental investigation within feasible limits.

Considerable simplification was possible through the realization that for modern qualified cables operated at design voltages or less, the observed and projected deterioration of most electrical properties of the cable (such as loss factor or breakdown field strength) is unlikely to lead to electrical-system failure. Two electromechanical failure mechanisms are of concern, however: (1) creep shortout, occurring when a mechanically stressed cable is bent over a corner and conductors are pulled towards each other or towards a grounded electrode, and (2) cracking of the insulating layers, which in the presence of electrolytic conduction may lead to current diversion or breakdown.

One constraint which had to be imposed on the experimental program is the use of a single combination of materials (EPR for the insulating material and Hypalon for the jacket) and a single cable geometry (600 V, 20-A rated low-power cable); this cable is typically used in nuclear power plants. By adopting this choice, the number of experiments described below became statistically significant at least for one cable design. An attempt will be made to generalize the results to other cable types by correlating the observed cable damage with the rather well-known materials deterioration. Analytical extrapolation to other geometries and to a variety of mechanical stresses is accomplished by correlation to, and then generalization from, simple scaling models.

A number of additional simplifications are made, that are generally thought to be conservative (i.e., increasing the predicted frequency of damage). First, for cracking, any crack penetrating through the jacket to the cable insulator was assumed to be a "failure." Second, it was known that radiation exposure mitigates creep shortout by embrittling the polymers; hence, in the creep experiments, only temperature exposure is used as an aging mechanism. Third, to extrapolate cracking data, a working hypothesis was used that links cracking to the end value of the breaking strain for the materials, disregarding the combination of radiation and/or time-temperature exposures under which the breaking strain was obtained. Fourth, (and perhaps not necessarily conservative), creep shortout was defined as an impedance of less than some fraction of an ohm. These simplifications decrease the number of necessary experiments.

On the other hand, the experimental effort was increased by extension of a test parameter. Up to now, maximum temperatures during an accident were generally considered to be below 165°C; for this investigation, maximum test temperatures of up to 225°C were included. The reasons are threefold: (1) an expectation that predicted containment temperatures may be increased to account for more severe accident scenarios, (2) the fact that cables may be overloaded and therefore hotter than the environment, and (3) the desire to accelerate the aging process in experiments being conducted.

C. Facility

Extrapolations, scaling laws, and even the general damage mechanism may possibly change radically with future introduction of new cable designs. To be prepared for a subsequent need to repeat (some of) the investigations, a dedicated long-term exposure facility has been established. It consists of seven automatically controlled heat chambers and three large heat pipes, all designed to operate with minimum attention for long periods. Self-calibrating fixtures that permit accurate mechanical measurements over long times have been incorporated. The facility is described in Reference 1, Section III.

II. PURELY ELECTRICAL FAILURE

This section deals with purely electrical and electrochemical cable failure (field breakdown, thermal runaway, internal gas discharge, tracing, and tracking); the cables are assumed not mechanically stressed (tracking) or geometrically deformed. Purely electrical failures are extensively treated in References 1 and 2. A summary of the important results will be sufficient for the present discussion.

While our experiments were all done with EPR-Hypalon cables, the data from literature show, that the results are essentially also applicable for designs using PE, XLPO, or XLPE insulators. The electrical properties of these materials are quite similar; average breakdown field strengths differ by factors of 3, and conductivities by factors of 10 in either direction. For the purpose of this section, order of magnitude arguments are justified; differences between insulator and jacket can then be ignored.

All cables are assumed uniform and operated within ratings; severe overloads (circuit breaker failure) make the analysis invalid. Within ratings, and with no geometry changes, the operational field strengths in power cables and the thermal loads occurring are very small compared to critical values. An order of magnitude change would not lead to failure.

A. Field Breakdown

Considerable breakdown data are reported in literature. Qualification tests with high dose-rate aging have been performed by a number of investigators, including Bennet[4] (XLPO), Thome[5] (XLPE and EPR), and Hosticka et al.[6] (XLPE); all of whom used minor variations of the standard IEEE qualification method.[7] The tests revealed no breakdowns except when cables were cracked by rewinding, for example, and then immersed in water (a case excluded in this section).

Of interest is a report by Grub and Langeset,[8] who exposed unusually long samples of EPR cabling to a total of 300 Mrad of radiation (combined gammas, betas, and neutrons) over 4 years. The authors found no noticeable change in breakdown field strength over this time and dosage.

The average dose rate in the Grub-Langeset test was about 8 krad/h, much less than generally used for qualification aging. Dose-rate effects on the breakdown field strength of EPR, then, must be very low or negligible. The same conclusion is arrived at in dose-rate-effect measurements by Asaka.[9]

Breakdown tests for cables are generally conducted at room temperature. Occasionally, tests are also conducted at the highest temperature predicted during an accident. For EPR, the breakdown field increases with increasing temperature, as Corbelli and Tonioli[10] have found for temperatures below 100°C. One possible explanation is that breakdown-causing gases diffuse outward more easily at higher temperatures. Measurements by St. Onge et al.,[11] verify this dependence up to 170°C for EPR, while measurements for XLPE show a decline of the breakdown field to one-half as temperature increases to 170°C.

Extensive measurements of breakdown field strength above 170°C were performed during our investigations. An example for the EPR-Hypalon cable is shown in Figure 1 for 225°C aging . Over a week the average breakdown voltage increased about 10% over that observed for the room-temperature voltage, while the standard deviation stayed about the same.

It is concluded that increasing temperature and radiation rates do not severely decrease the breakdown field strength and sometimes increase it. Synergistic effects are unlikely and apparently have never been reported.

B. Dielectric Loss Failure

A second purely electrical failure mechanism is caused by a strong increase in dielectric loss (or insulator conductivity) which may lead to circuit starvation or to thermal runaway. Loss factor (for ac) and insulator resistivity (for dc) are related parameters used to assess the damage phenomena.

Radiation treatment does permanently change the loss parameters. It sometimes improves them somewhat, and where it is detrimental, the changes are less than an order of magnitude. As examples, tests by Kuriyama, et al [12] and Bustard [13] may be mentioned. As a few examples below will show, increases of dielectric losses by several orders of magnitude would be of some concern with presently used power cables; for signal cables the effects would be totally negligible.

Dose-rate influences on the two parameters (loss factor and insulation resistivity), were also measured by Kuriyama et al.[12] There is only a small change in each parameter as the dose-rate increases. Seguchi et al [14] have exposed EPR and low-density PE cables to irradiation with dose rates varying from 5 to 500 krad/h and to a total dose of 100 Mrad. The
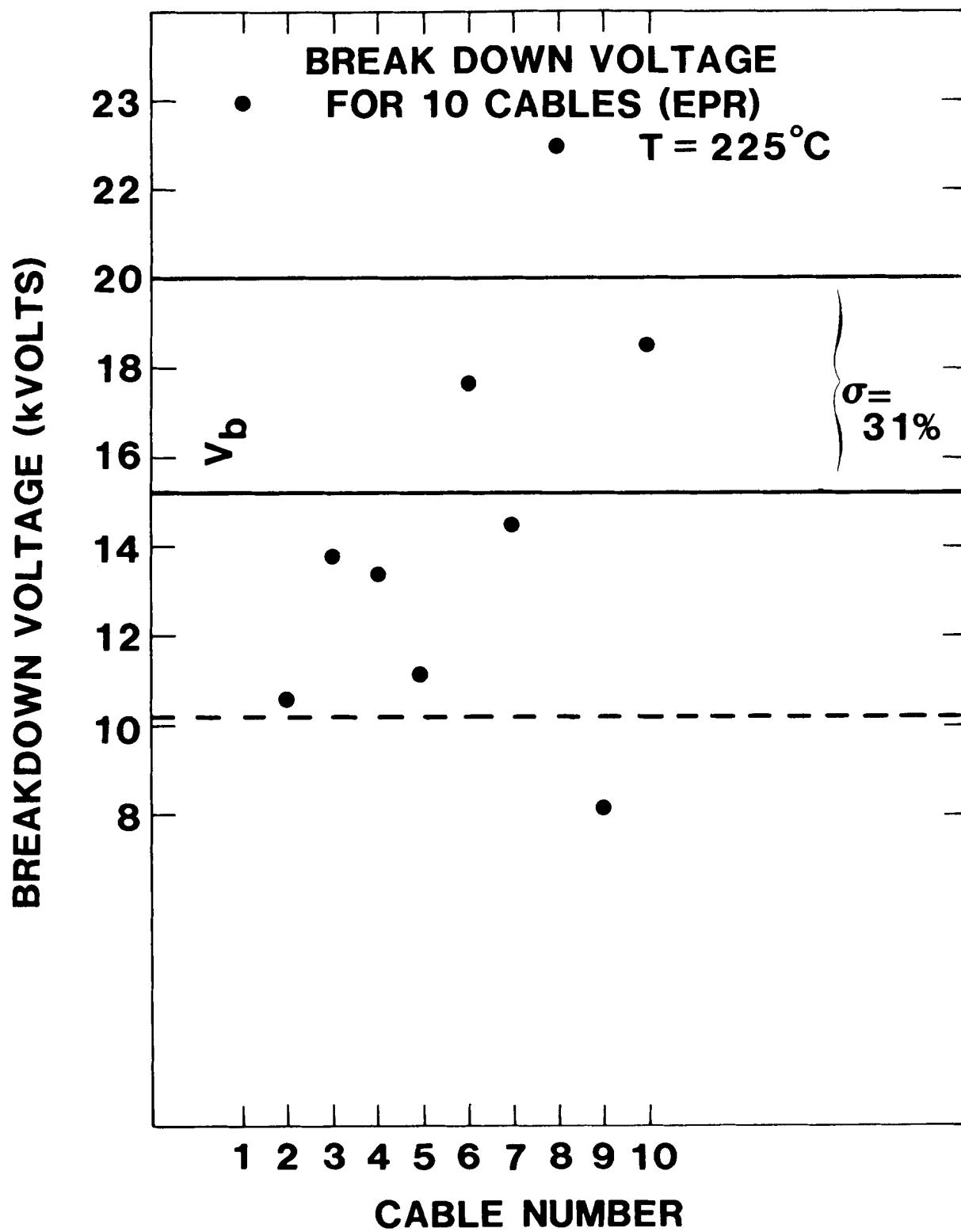
Figure 1:   Breakdown Voltage (V_b) and Its Standard Deviation (σ) at 225°C, measured during aging.

authors find there are no dose-rate effects if the materials contain anti-oxidants; otherwise, the dissipation factor increases by about 50% with decreasing dose rate, which is in agreement with Kuriyama's results. It is concluded that dose-rate effects are small and not important for dielectric losses

In contrast, the influence of temperature on cable losses is substantial, although generally temporary (i.e., they last only as long as the temperature is elevated). In Figure 2, the insulation resistance as measured by Murata et al [15] during a LOCA simulation is plotted. Compared to room temperature, temperatures of 174°C decrease resistivity by nearly 4 orders of magnitude. The data are only slightly affected by the aging methods used.
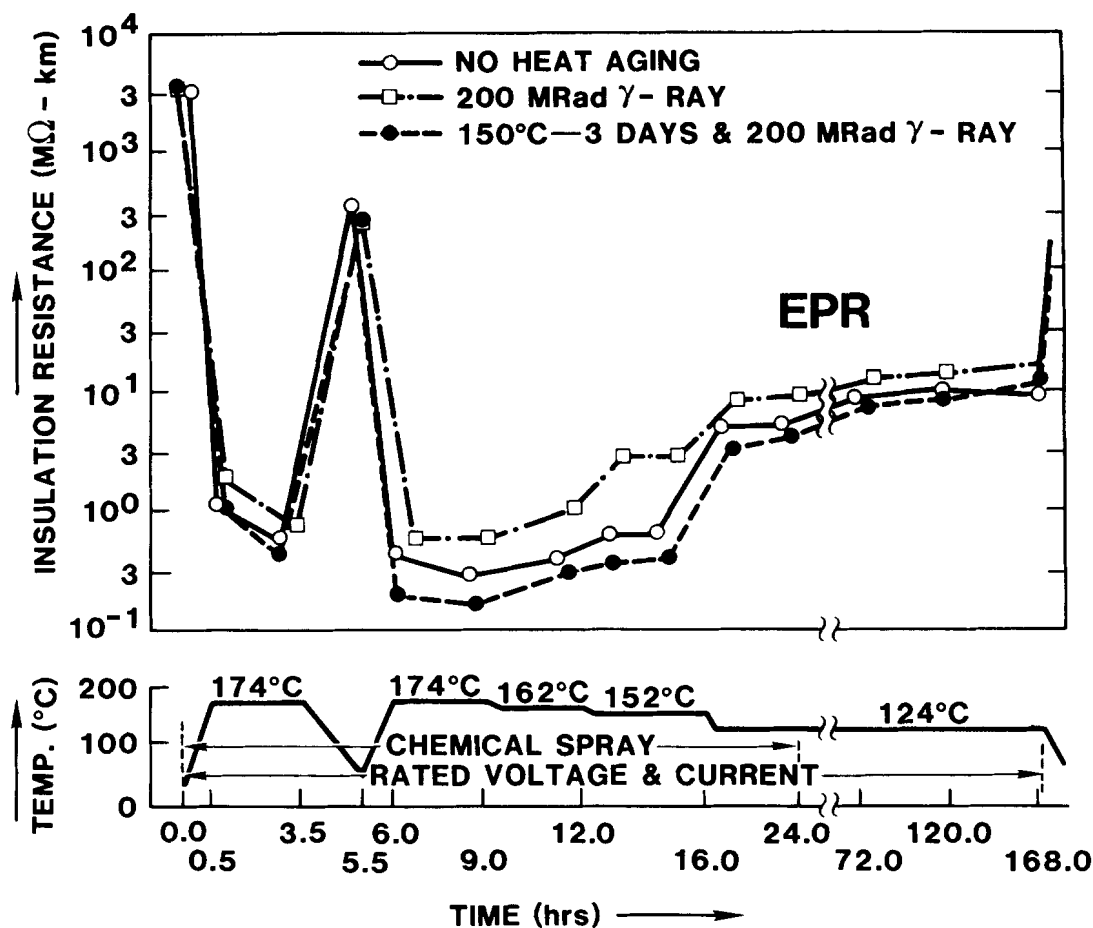
Figure 2: Insulation Resistance in Steam and Chemical Spray Environment (Flame Retardant EPR) (After Murata, Reference 15)

Figure 3 gives an example of higher temperature measurements (up to 225°C) performed in our investigation. The dc leakage current (I_L), averaged over ten 1-m-long cable samples, is seen to increase by nearly 7 orders of magnitude over the current measured at room temperature. The ac dissipation factor (D) first decreases with increasing temperature (as additives perhaps diffuse out of the polymers) and then rises to not quite 0.35; dissipation factors were measured at operational ac voltages and frequencies.

What do these data mean? The following discussion of thermal runaway is based on a comparison of the heat generated by losses in the conductor of the cable which is unavoidable, and the additional heat caused by the dielectric losses in the insulator and the jacket. The first quantity is current dependent, the second depends on the applied voltage. The cable presently under investigation, AWG #12, has a conductor resistance of 0.00828 ohms/m at room temperature. At 100°C, this value is increased by a factor of 1.43. At the maximum rating, 20 A, the cable current causes heat generation of 4.74 W/m at 100°C, and somewhat more at higher temperatures. The installation has to be able to carry this heat flux away, and usually is amply dimensioned to do this. Therefore, dielectric losses may add a comparable amount of heat generation without undue consequences. To be conservative, we will stipulate that additional dielectric heat input will not exceed 20% of the permitted current heat generation. Dielectric losses are therefore limited to 0.95 W/m for the present cable.

For dc, the dielectric losses are U^2/R where U is the applied voltage and R is the leakage resistance of the cable per unit length. For an applied voltage of 480 V, R must be larger than 0.24 Mohm.m to keep the losses under 0.95 W/m. The cable (average) measurement in Figure 3 (with an applied voltage of 500 V and a leakage current of 0.4 mA at an equilibrium temperature of 225°C) yields an average value of 1.2 Mohm·m at the highest experimental temperature. This cable design can thus be assumed to be safe from thermal runaway up to 225°C.

For ac, the losses are essentially electronic and therefore generally less than those for dc, which contain an additional ionic conductivity. For a D-factor of 0.35, the ac losses, $U^2 l C D$, with C being the cable capacitance per unit length, are about 0.015 W/m for the example in Figure 3 and are therefore negligible.

The above deductions assume that the loss resistance and the D-factor are reasonably uniformly distributed along the cable, i.e., that there is no "bad spot" solely responsible for the leakage current. For the measurements in Figure 3, this is assured by the standard distribution value for the 10 leakage current measurements, which reaches only a factor of 2 for the highest temperatures.

Not many measurements in literature are made at temperatures as high as 225°C. If we wish to determine from such lower temperature measurements
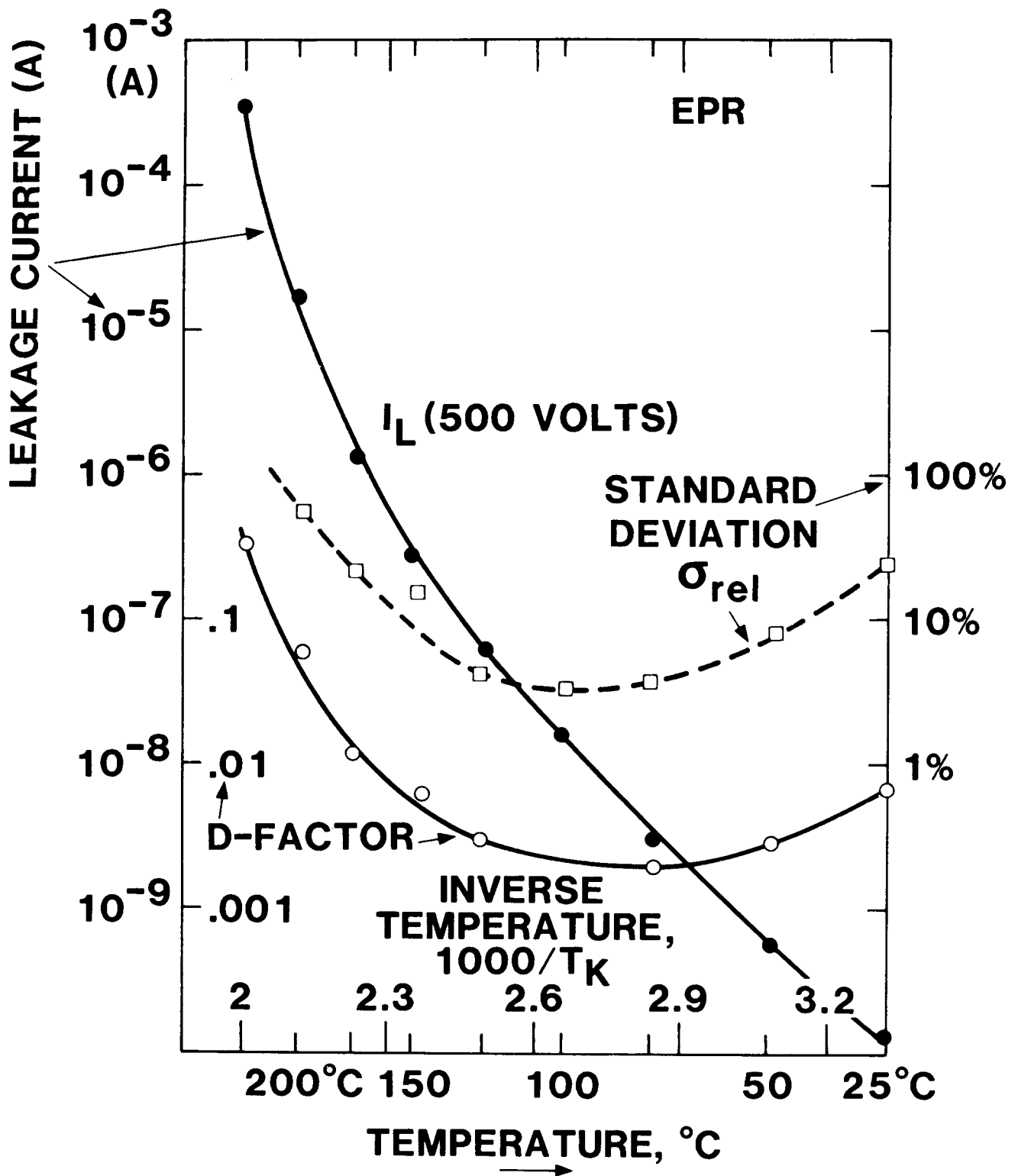
Figure 3: DC-Leakage Current I_L for 1-m Cable Length (Standard Deviation of I_L is σ_{rel} and Dissipation Factor is D).

the highest safe operational temperature, we may (for EPR) use the
leakage current curve in Figure 3 for scaling.

There are many variations in EPR composition;[13] the statistical chance
exists, that the EPRs in the measurements quoted above were better than
average. A safe temperature for EPR power cables would then be 200°C; as
Figure 3 shows, the 25°C decrease would lower the average leakage current
by about an order of magnitude. (As will be shown below, this
temperature has to be lowered more if the cable is mechanically stressed.)

C. Other Phenomena

While radiation is applied, the conductivity of insulating materials is
enhanced due to additional carrier generation. This phenomenon should be
independent of temperature but could conceivably cause excessively high
currents during accidents. Figure 4, taken from a paper by Murata et
al,[15] shows measurements on EPR cables preaged in a variety of ways,
and then, during measurement, exposed to radiation. After an initial
drop, resistivity varies by about a factor of 3, and is not proportional
to the dose rate. Extrapolating to a dose rate of 10 Mrad/h, (a dose
rate comparable to those expected in an accident), indicates that a
parallel resistance of more than 100 Megohm would appear across a 1-km
length of cabling. At higher temperatures, the effect would be
overwhelmed by thermal-carrier generation.

With no cracking, the influence of humidity on cable resistivity is
observable but small. Measurements by St. Onge et al (Reference 11,
Figures 4-3 and 4-5) show an order of magnitude increase in conductivity
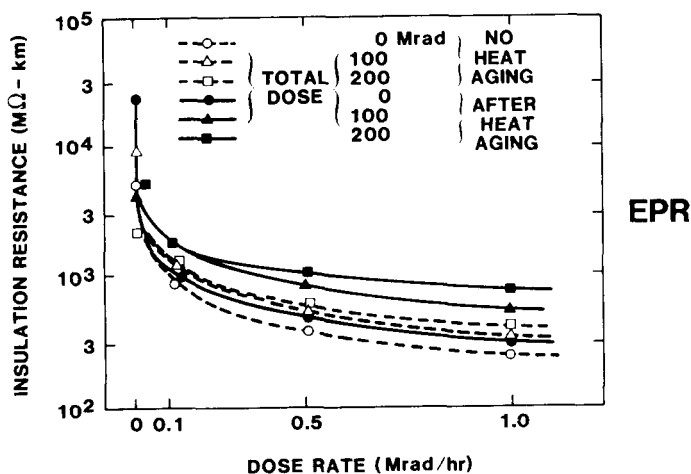
Figure 4:   Effect of Dose Rate on Insulation Resistance (After Murata
            et al, Reference 15)

for XLPE under extreme humidity (soaked cables) compared to dry conditions. A somewhat smaller increase is shown for EPR. The measurements quoted above (e.g., Figures 2 and 3) include the influence of humidity.

Cables immersed in water, as might be the case after an accident, may exhibit a particular form of field breakdown caused by water penetrating the cable along micro-fracture structures. A phenomenon named "treeing"[16,17] develops, where treelike fractures filled with liquid slowly extend into the insulators. This phenomenon is of importance at high field strengths. Data are not available for low operational fields, those smaller than 1 kV/mm for power cables. Treeing becomes less pronounced at high temperatures, while the influence of radiation is unknown. An experiment representing the probable worst case has been operated for 36 months. In this experiment, ten 1-m-long cables have been soaking in a salt water solution at room temperature under field strengths 5-times higher than the operational level. No breakdowns have been recorded.

For a cable with very high insulation resistance, another breakdown effect has been reported in the literature.[18a,b] A space-charge region may build up under irradiation, causing high local fields and a discharge breakdown. In reactor circuits, the effect would be strongly mitigated by low circuit impedance; it can be disregarded at higher temperatures, where higher conductivity would cause the space charge to leak off.

Not directly related to cable properties is surface breakdown at the end of the cable. It is called "tracking" (as carbonized tracks form across the surface) and has been extensively investigated for reactor accident conditions.[19] Breakdown occurs under high humidity on dirty surfaces, across which a voltage of a hundred to a few hundred volts exists. The phenomenon is of concern for armored cables (rarely used) and cable ends clamped to ground in a very short distance from a medium voltage conductor. Cleanliness and sealing of switch boxes will eliminate this problem.

D. Comment on Circuit Failure

The present work deals only with primary cable failure, i.e., complete breakdown of the cable proper. The above discussion of leakage contains data, however, which permit useful comments on other and potentially more common total or partial circuit failures.

The first phenomenon of concern is circuit starvation – loss of so much current through leakage, that the load does not receive enough power. A 100-m long circuit is considered. At 480 V, 190°C, and 0.24 Mohm·m resistance, the circuit would lose 200 mA, which for a power circuit is unimportant. (At 175°C, a circuit using the cable of Figure 3 would only lose 0.6 mA.) For a signal cable operating at 50 V, the losses would be a tenth of the above values or less. A 10% current loss may cause unacceptable misreadings, if the information readout is current dependent (for example, for pressure transmitters).

Similarly important is crosstalk, particularly between power circuits on one side and control circuits on the other side. As stated above, a power circuit with a marginal cable may generate a stray current. However, installation regulations demand total spatial separation of power and signal circuits; where this is the case, no problem exists. Signal-to-signal circuit crosstalk is mitigated by lower voltages. Instead of the 200 mA of stray current in the above example, 20 mA would be available. If a small part of this (e.g., 2 mA) enters a signal line, the accuracy of indication would suffer, but the readings would not be meaningless. As starvation and crosstalk depend strongly on geometry of installation general statements are impossible. Estimates such as those presented have to be made for specific layouts of possible concerns.

E. Summary and Conclusions

The above data and those in references 1 and 2 show that EPR-Hypalon reactor cables, mechanically unstressed and with undisturbed geometry, and operated within rating, are extremely unlikely to generate total circuit failure during a reactor accident, unless the cable temperature exceeds 200°C where thermal runaway may occur. Some data exist predicting the same for XLPE and XLPO insulation.

A method to scale the critical temperature to other cable designs has been discussed.

The importance of making a number of measurements to permit assessment of uniformity of a sample cable design has been established.

With purely electrical effects (in power cables) not of concern for temperatures below 200°C, the investigation had to stress the electrical effects of mechanical phenomena. Creep shortout and cracking will be analyzed in the following sections.

III. CREEP SHORTOUT

A cable is stretched by an applied force, F, over a surface with a radius of curvature, r. The metal wires will creep through the polymeric insulation and cable jacket; after some time, metallic contact between cable wires or between the wires and the cable support may occur. This section will mainly deal with purely mechanical shortout. (At very high temperatures and stresses a [temporary] electrical breakdown may occur without mechanical contact.)

Figure 5 shows an example of cables pulled, by the weight of a vertical section, over a conduit corner. The worst case situation results, if a bottom cable is bent over a sharp edge, the cable is pressed down by the upper layers of cabling, and the vertical section hangs free (i.e., is not supported by friction forces).

The present discussion is limited to the simplest case where the cable consists of a single wire surrounded by an (EPR) insulator and a (Hypalon) jacket. The conducting wire is stranded, and the creep deformation is 3-dimensional. An attempt has been made by Reaugh of Science Applications, Inc. to obtain a computer analysis using state-of-the-art available programs. His findings are described in Section 3 of Appendix A. Even with simplifications (cylindrical wire, predictable materials properties, 2-D treatment), present programs turned out unsuitable.

It has become clear that the main problem for a satisfactory analysis, permitting scaling from one cable design to another, is long term
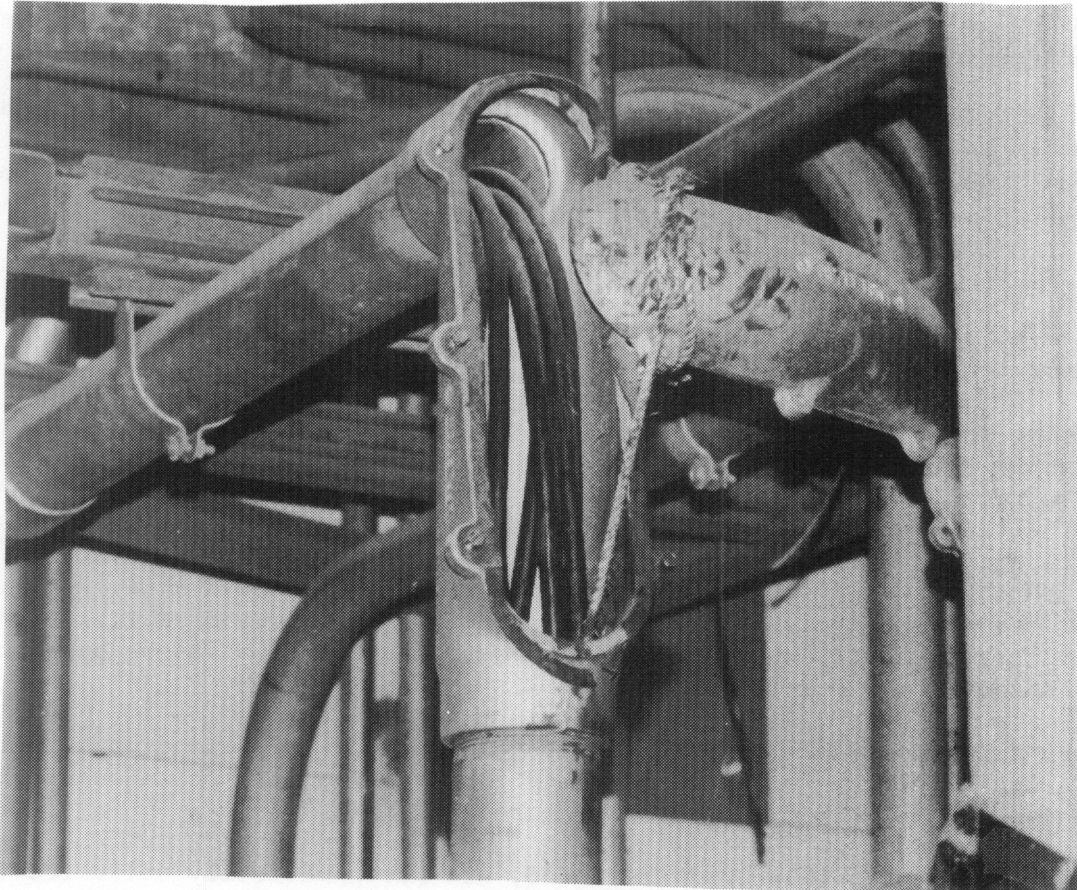
Figure 5: Cables Pulled Around Conduit Corner

deterioration of the cable materials properties, which is largely unknown for times longer than a few years. How deterioration influences creep behavior has not been investigated before.

In this situation a comprehensive and long duration experimental program was necessary. Extrapolation and scaling have to be made cautiously. To obtain a basis for evaluations of measurements, some theoretical considerations are described first.

The creep-shortout of a cable obviously involves very large strains, i.e., strains close to 1. Such cases are not treated in literature.

The low-strain behavior of polymeric materials including rubber has been thoroughly investigated.[20] Even the long-term or "aging" phenomena of these materials are subjects treated in textbooks.[21] Unfortunately, most published work is limited to temperatures below "transition" temperatures, which means that only the lower regions of the temperature range of present interest are covered. (For EPR the transition temperature is not well defined, and the transition is not severe since only a small percentage of the polyethylene incorporated into the compound shows a crystalline melting point; the "transition" lies between temperatures of 70° and 90°C.[22])

At low temperatures and low strain rates, creep is a linear function of applied stress, σ, and a function of a time dependent "creep compliance," $J(t)$, or its inverse, the creep modulus, $M(t)$. The creep strain, ϵ, is given by

$$\epsilon = \sigma \cdot J(t) = \sigma/M(t) \tag{1}$$

where σ is assumed constant, and J or M is measured at a constant temperature, T.

For the same material, curves representing the time dependence of J, measured at different temperatures, starting times, and stresses, are geometrically similar. Consequently, the curves can be obtained from one another by translation of the horizontal or vertical or both axes, and by scale changes. Figure 6 shows a Bell Telephone Laboratories "master curve" obtained by shifting many measurements to obtain overlay with a room- temperature curve.[23] If this creep strain behavior applies also at high strains, a extrapolation of creep shortout data can be based on the shape of the compliance curves.

Some presently available literature creep data for EPR are discussed in Reference 1; the "effective viscosity" approach and its relationship to the compliance method are also discussed there.

The above relationships, as indicated, are not numerically valid for the high strain case; they are used as phenomenological guidance only for the experiments described below.
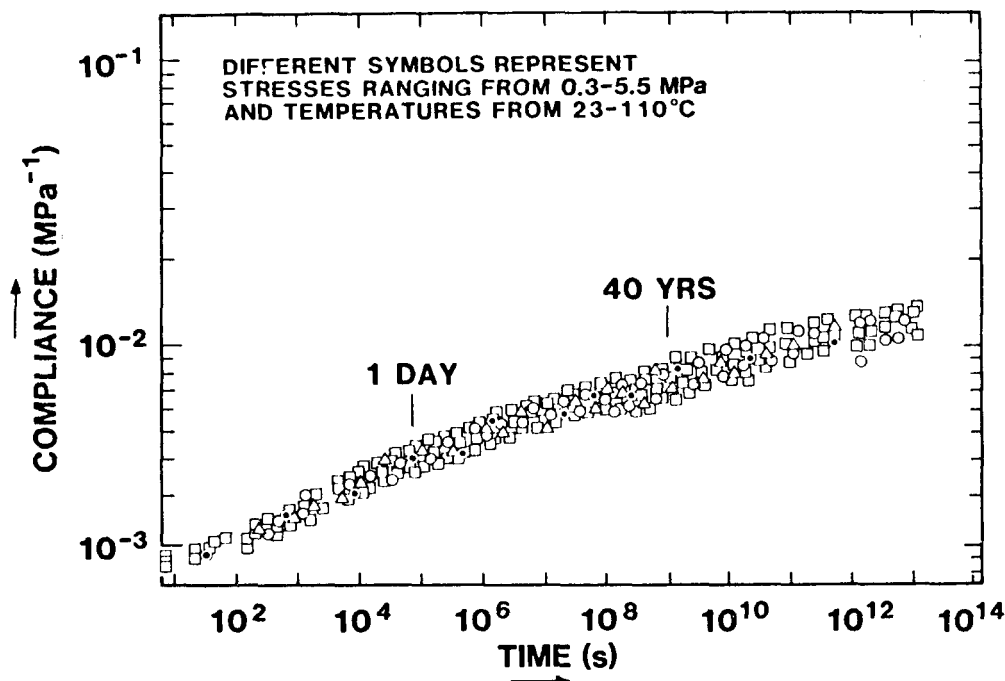
Figure 6: Room–Temperature Master Curve for High–Density Polyethylene in
           Creep (After Aloisio and Brockway, Reference 23)

A. Experiments

All creep experiments were done by hanging cable samples over curved
supports, the curvature radii varying from .2mm ("sharp sheet", Figure 19
of Reference 1) to 3.2mm. Stretching weights were applied in a distance
sufficiently far from the support point to avoid transfer of shear
stresses to the support neighborhood. Some of the stretching
arrangements are pictured in Figure 22, Reference 2. The most often used
arrangement, designed for precision X–ray measurements is shown in
Figure 7.

Six hairpin shaped cable samples are positioned over gooseneck–shaped
supports and stretched by lead weights (visible at the rear of the
mounting struts). For three of the six cables, the maximum operational
electric field was maintained between cable wire and support by applying
the highest operational ac voltage, 480 V. Three short–indicating
circuits are seen located on the right of Figure 7. The other 3 cables
were powered only during brief measurements.
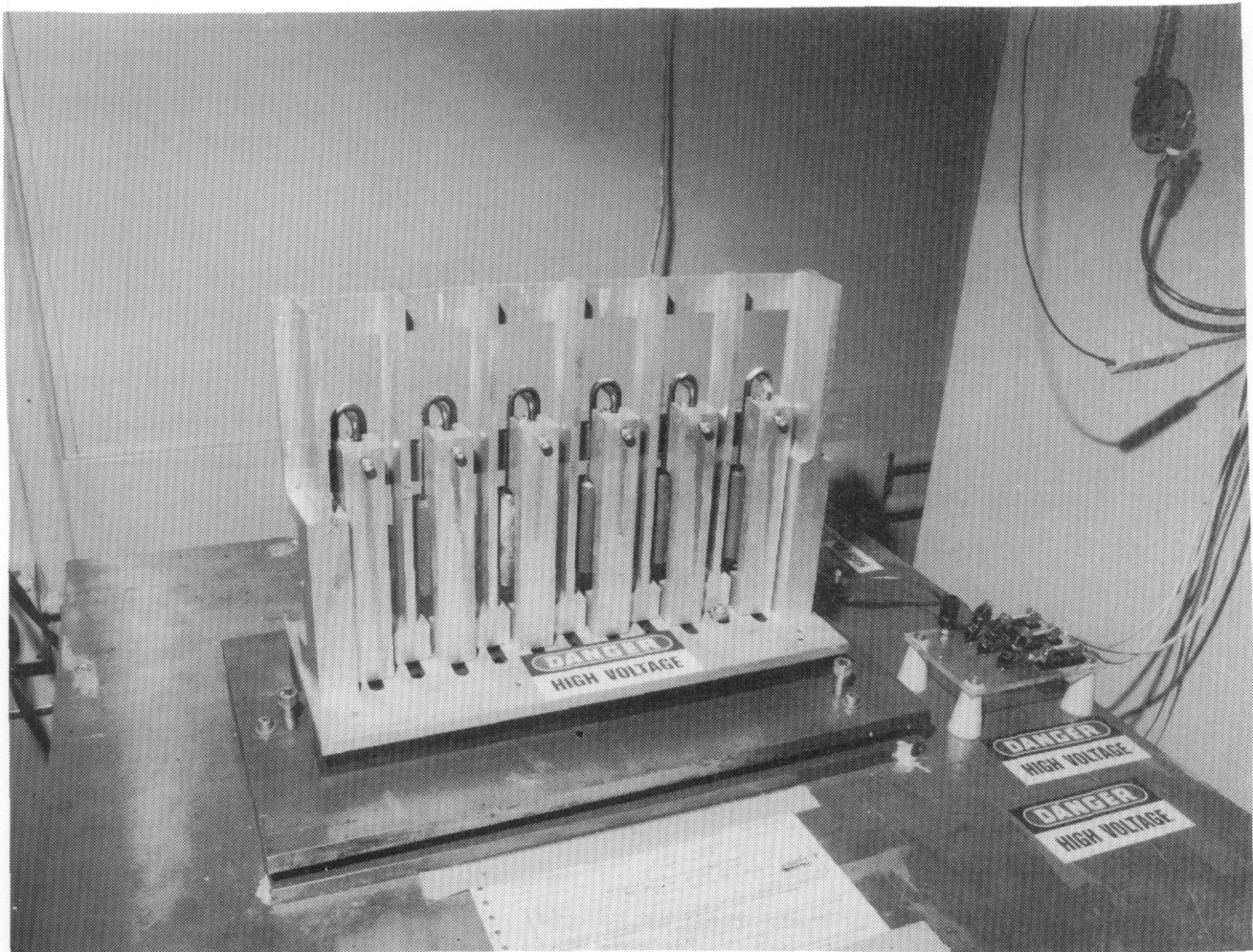
Figure 7: Photograph of a Tensioner

A calibration arrangement, discussed in Reference 1, permitted alignment
of all the (gooseneck shaped) support structures in such a way, that the
axes of the support cylinder passed through the X-ray source. This way
the true distance between wire and support was projected. A correction
method for misalignments occurring during months of heat exposure was
developed. To avoid or minimize sporadic density gradients on the X-ray
film and on subsequent enlargements, the exposure was done very carefully
and the developing and enlargement processes were automated. With this
method, the "creep distance," e.g., between the (hairpin shaped) shadow

of the cable wire and the rounded support cylinders (with calibration hole) pictured in Figure 8 (more fully discussed below) could be determined to an accuracy of about 10 microns.

With the precision arrangements a total of 240 X-ray exposures were made in 2 1/2 years; each X-ray film carrying information on 6 cables which had been exposed to identical environments, half of the cables being, in addition, under electrical stress.

The X-ray measurements had the advantage that the cable was not disturbed by the test and was the same through the full exposure. In early tests, cables were exposed, then carefully cross-sectioned along the plane of the most severe deformation. The remaining thicknesses of insulator and jacket were then measured; Figure 9 shows a cut through a new cable and through a sample exposed to temperatures of 125°C and nominal stresses of 2 MPa for 1 day. (The cuts were made after cooling to room temperature.)

It is seen that deformation is nonuniform, asymmetric and, in this example, accompanied by unraveling of the wire strands. (It is believed that the cutting process itself did not contribute noticeably to these distortions.)

An important evaluation parameter is the stress, s, generated by an applied stretching weight, W. An effective support area A has to be estimated. After the wire has sunk in and the wire-support distance is small compared to the wire diameter, the effective area, A, should be proportional to the wire radius, r_w, and the curvature radius of the support, r_s, such that

$$A = kr_w r_s \tag{2}$$

where k is the proportionality constant.

The proportionality constant, k, should be of the order of unity. In Reference 1, an argument has been presented that k ~.3. Newer results show that k = 1 is more justifiable. This value will be chosen in the present analysis. Equation (2) holds only for cables hung around cylinders. For special geometries, this value has to be modified. For cables lying on a plane and then hanging from a sharp edge (Reference 1, Figure 19) the support area is increased by force transfer from the flat position; replacement of r_s in Equation (2) by the cable radius r_c appears to give a reasonable approximation. At high temperatures (>150°C), cables hanging over a thin flat plate (Reference 1, Figure 18b) stick to the sides of the support. According to Reaugh,[24] the factor in Equation (2) then assumes a value of 3 to 4.

All cables tested were of the design used throughout this investigation. The seven-strand copper conductor had an average radius of 1.15 mm, while the EPR insulation and the Hypalon jacket had thicknesses of 0.74 and 0.51 mm, respectively.
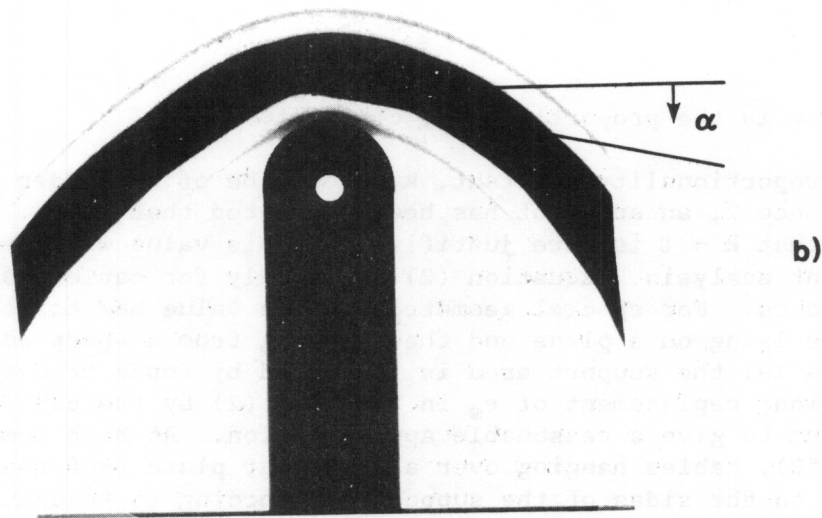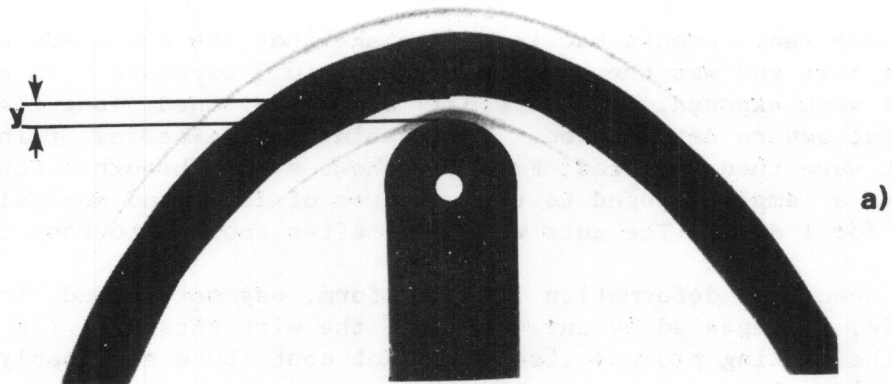
Figure 8: Symmetric (a) and Unsymmetric (b) Hang of Cable, 6 Power Magnification.
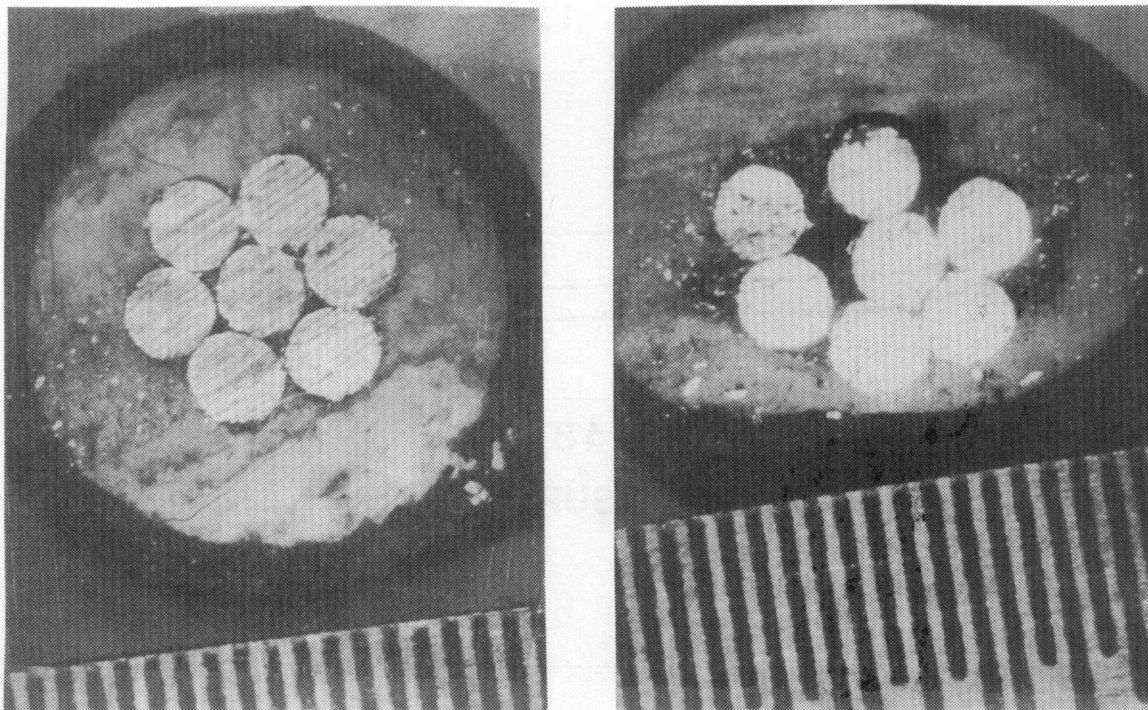
Figure 9:   Cut Through a New Cable (a) and a Cable Stretched by 0.9 kg at
            125°C for 1 Day (b)

B.   Measurement Results

Under mechanical and thermal stress, the distance, y, (Fig. 8) between
the cable wire and the support becomes smaller fast at the beginning of
the test.   This is largely due to the fact that the contact area is very
small in the beginning and the stresses are, therefore, high.   After a
while, the contact area approaches the value defined above in
Equation (2) and the distance reduction becomes much slower.   Figure 10
shows an example taken at various (constant) stresses, each dot
representing the average of two different cables.   In the lower plot a
shortout occurs (for both cables) after 52 hours under 190°C and at a
nominal stress of 6×10^6 N/m^2.   (6900 Newton/m^2 = 6900 Pascal =
1 lb/sq.in.)   For the support used, a cylinder of r_s = 2.4mm radius, a
weight of 4-lb. creates the above nominal stress of 880 lb/sq.in. = 6 x
10^6 Pa.   To generate an equivalent stress for a standard cable, a free
overhang of about 120 ft. would be needed.

From this and similar experiments it is seen that at high temperatures
high stresses can produce shortouts in a short time, a few days or less.

-21-
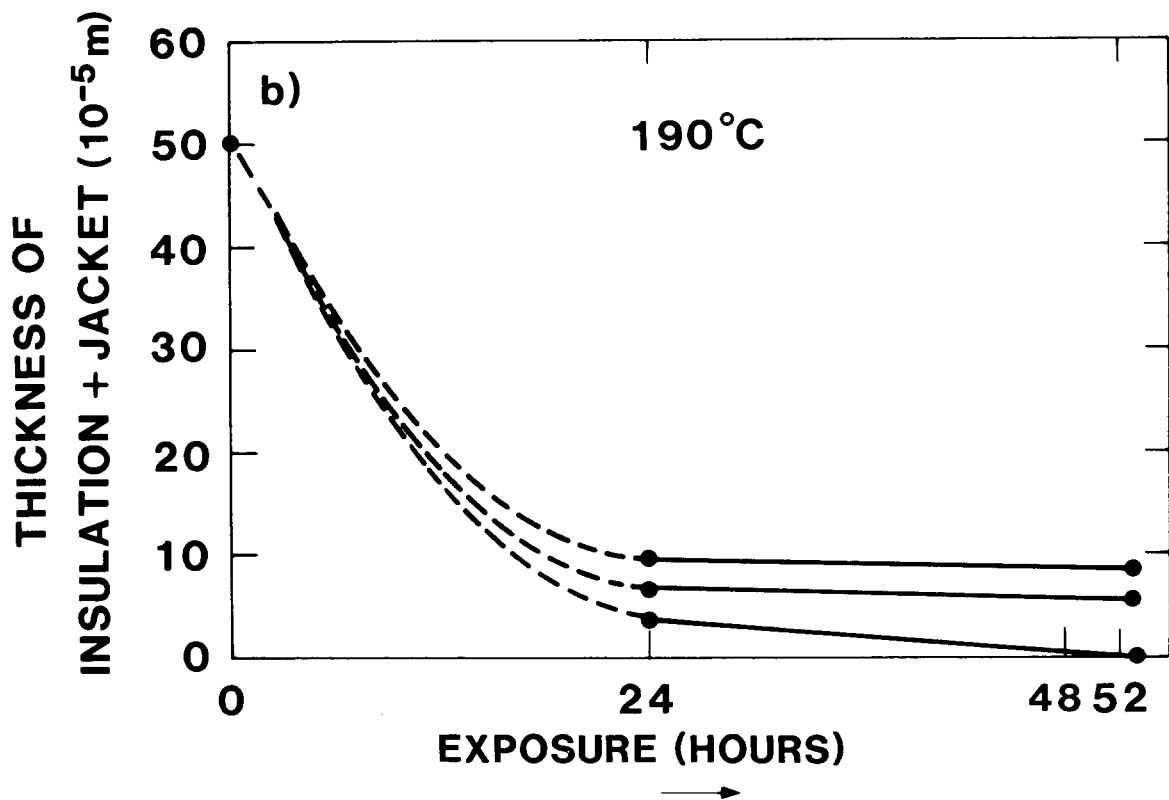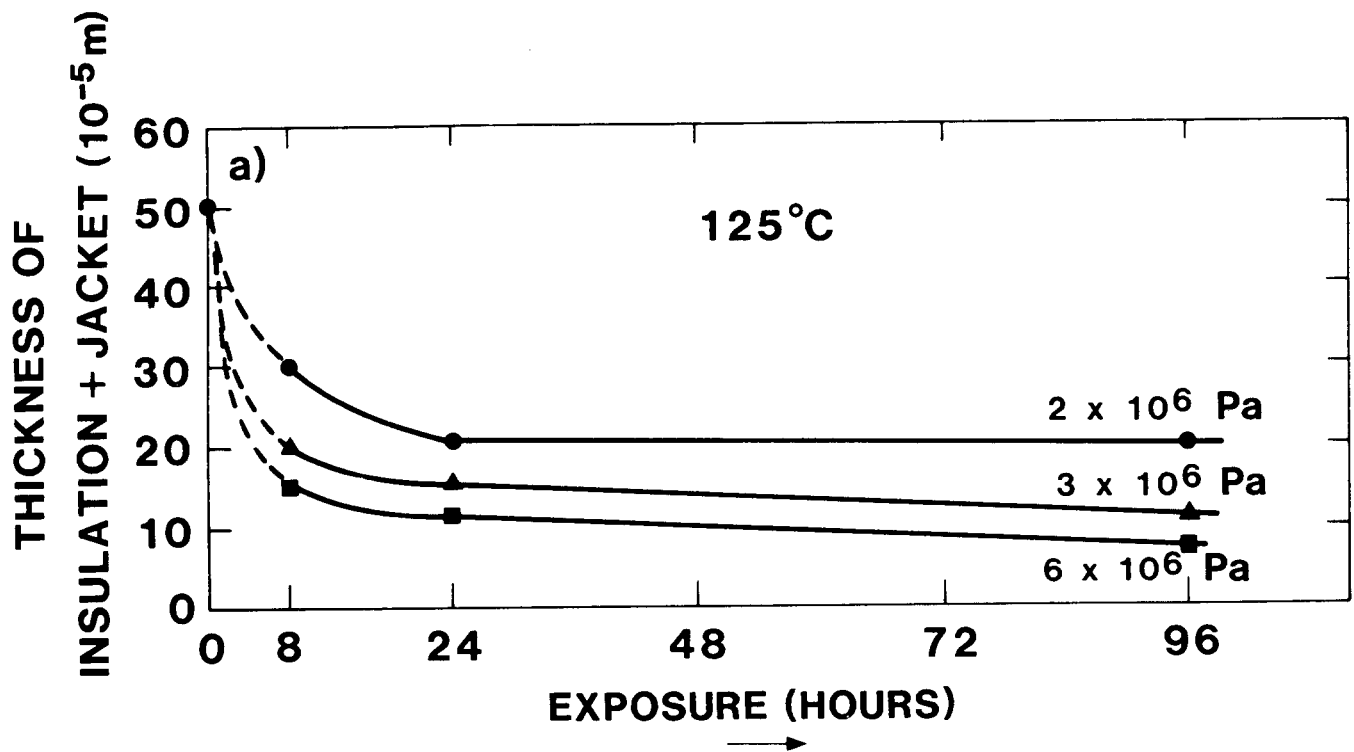
Figure 10: Creep Measurements at 125°C and 190°C. (Average of 2 cables;
2 shortouts occurred at 52 hours.)

With this knowledge, stresses that are not admissible are determined easily and fast. The important and difficult question is, however, which maximum stress is acceptable for long time exposure, preferably 40 years. The experimental activity is, therefore, logically divided into short-time high-stress and long-term low-stress tests.

1. Short-Time Experiments

Examples for short-time stress measurements have already been shown in Figure 10. Table I presents more data, obtained with different support geometries. It becomes clear that stresses of about 6 MPa ($= 6 \times 10^6$ N/m^2 = 870 lb./sq.in.) at temperatures higher than 150°C may lead to shortouts within days, as 190°C temperatures clearly do with very high probability.

The measurements show considerable stray. This is seen, e.g., from Figure 11, where strain (thickness change/thickness; a strain of 1 means a shortout) is plotted versus time for some measurements. (The figure shows some unusual situations; the curvature of the strain curves is not as expected, and a measurement at 14 MPa does not approach shortout.)

The large scatter in measured data is of concern. A main contributor to the measurement variations is the relative position of the wire strands with respect to the support structure.

For two situations where the nominal stress (e.g. Reference 2) may be the same, the effective stress will depend on whether a single wire strand or two wire strands lie opposite the support. The two extreme cases are sketched in Table II, which show measurements where the lie of the strands had been ascertained by X-raying.

It is seen that the average thickness of the composite layer (insulator plus jacket) may vary by a factor of almost 3, depending on whether a single strand or two parallel strands lie opposite the support and take up the weight of the cable.

In the three measurements where the strands are in the (unfavorable) position of case (a), the insulation thickness has been reduced to zero, i.e., the EPR has been moved to the sides as shown in Figure 9. Such squeeze-outs are also indicated in Table I. The cable electrical properties now depend on the properties of the jacket material. Both the resistivity and the dielectric strength of Hypalon are, at room temperature,[25] lower than those of EPR. There is, therefore, some concern about cable performance if squeeze-out conditions are present. Experiments were performed to assess the situation.

Leakage currents, which are very temperature dependent according to Figure 3, were monitored. There was no statistical difference between cables in position a) and position b). (Actually, leakage currents were noticeably lower than scaling of the contact areas between the stress experiments and the sleeved cables of Figure 3 would predict.)

Table I

Creep Shortouts
(Short time experiments)

Experiments	Nominal Stress N/m^2	Temperature Exposure	Exposure Time	# of Exp.	# of Shorts	# of Insulator Squeeze-outs
Bar Hanger (Cylinder Support)*						
r_s = 1.2 mm	6.1×10^6	190°C, Constant	2.2 days	2	2	—
1.2 to 3.6 mm	1.0 to 3.1×10^6	190°, 175°C, Const.	2.2 days	10	0	1
Wire Stretcher (Flat Plate)						
r_s = .4 mm	3×10^6	175°C, Constant	21 days	2	0	2
r_s = .4 mm	3×10^6	190°C, Constant	1 day	12	0	4
Wirehanger (corner geometry)	6.5×10^6	0-225°C, Rising	5 days	10	10	—
	2.1×10^6	0-225°C, Rising	5 days	20	1	
	2.1×10^6	0-225°C, + heat spikes	3 days	10	2	

*No electric field

1 psi = 6900 N/m^2

The support geometries indicated in parentheses are described in detail in Reference 2.
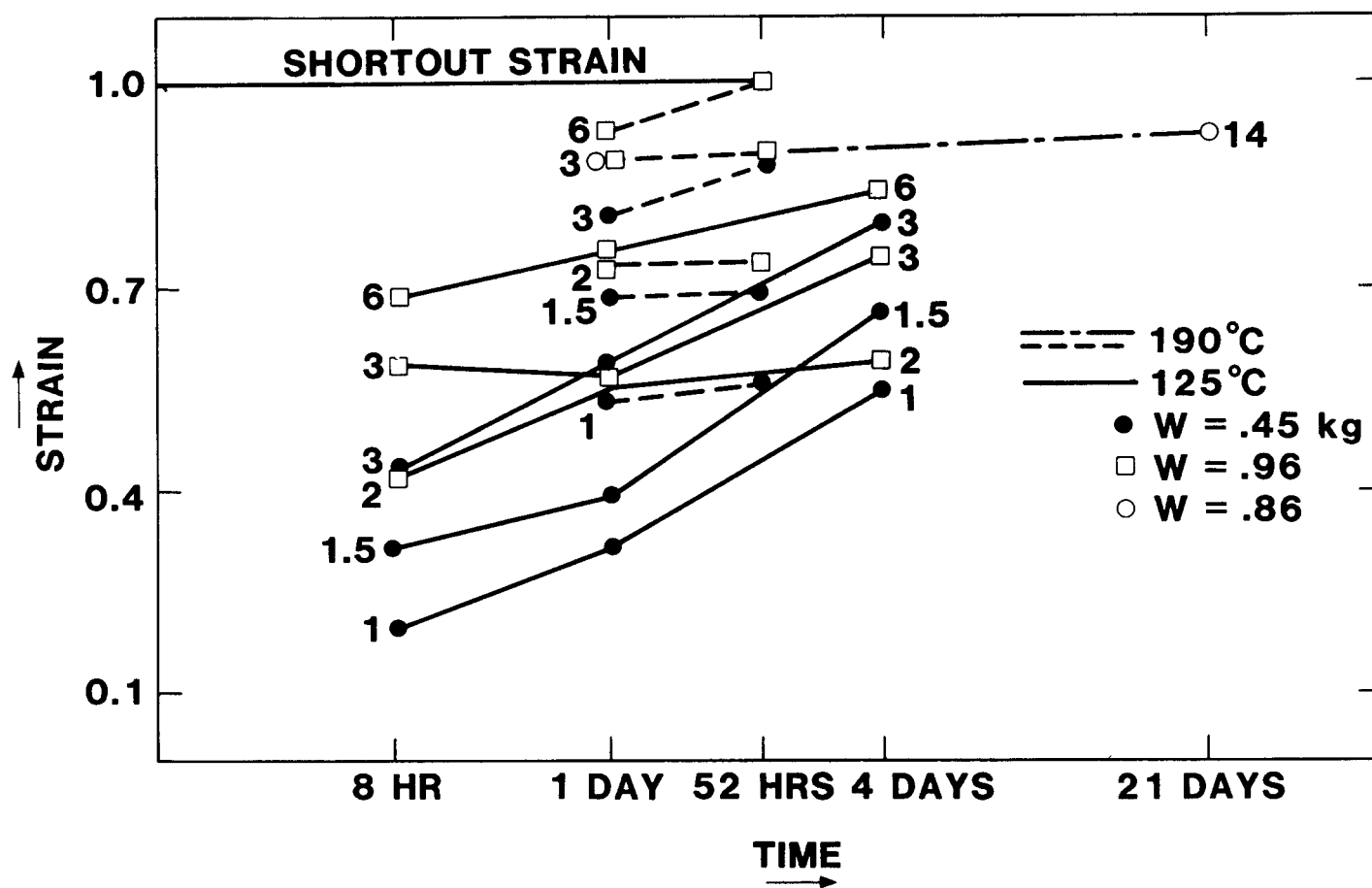
Figure 11: Composite Strain for Various Loads and Temperatures, including unusual observations. The numbers indicate estimated stress in Megapascals, obtained with different weights and support curvatures.

Table II

Position Dependence of Deformation

| | Remaining Thickness (mm) | | | Strain | | Composite |
	Insulator	Jacket	Both	Insulator	Jacket	Strain
ORIGINAL VALUES	0.74	0.51	1.25	0	0	0
Case (a)	0	0.07	0.07	1	0.86	0.94
	0	0.09	0.09	1	0.82	0.93
	0	0.10	0.10	1	0.80	0.92
Av =	0	0.0867	0.0867	1	0.83	0.93
s =	0	.015	.015	0	.031	.01
Case (b)	.01	.20	.21	.98	.61	.83
	.05	.21	.26	.93	.98	.79
	.06	.23	.29	.92	.55	.76
Av =	.040	.147	.253	.95	.71	.79
s =	.036	.119	.045	.032	.23	.35
Average of both cases Av =	.020	.117	.170	.972	.77	.86
s =	.026	.083	.095	.037	.16	.08

Nominal stress: 14×10^6 N/M^2
Exposure time: 24 hours at 190°C

(a)

F

SUPPORT

(b)

r_w

SUPPORT
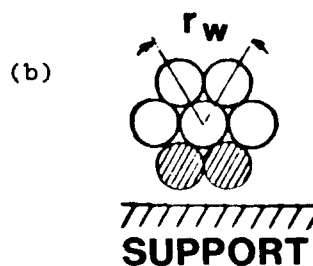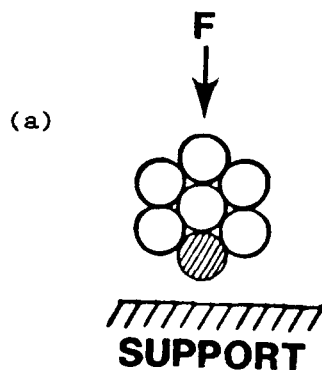
The dielectric breakdown behavior at high voltage exposure showed an even more surprising effect. As Figure 12 shows, breakdown voltages measured for 18 cables at 225°C do not vary significantly with the thickness of the remaining layer. The explanation for this may be that mechanical compression near the support improves the insulating material (e.g., by removing bubbles, closing microcracks, and densifying the polymers). Using an experimental facility developed by K. Gillen,[26] a 5% density increase was measured for EPR samples removed from a location just above the support point. Cable breakdown in the support region therefore becomes less likely with increasing exposure; breakdown along flaws at other locations remains unaffected.
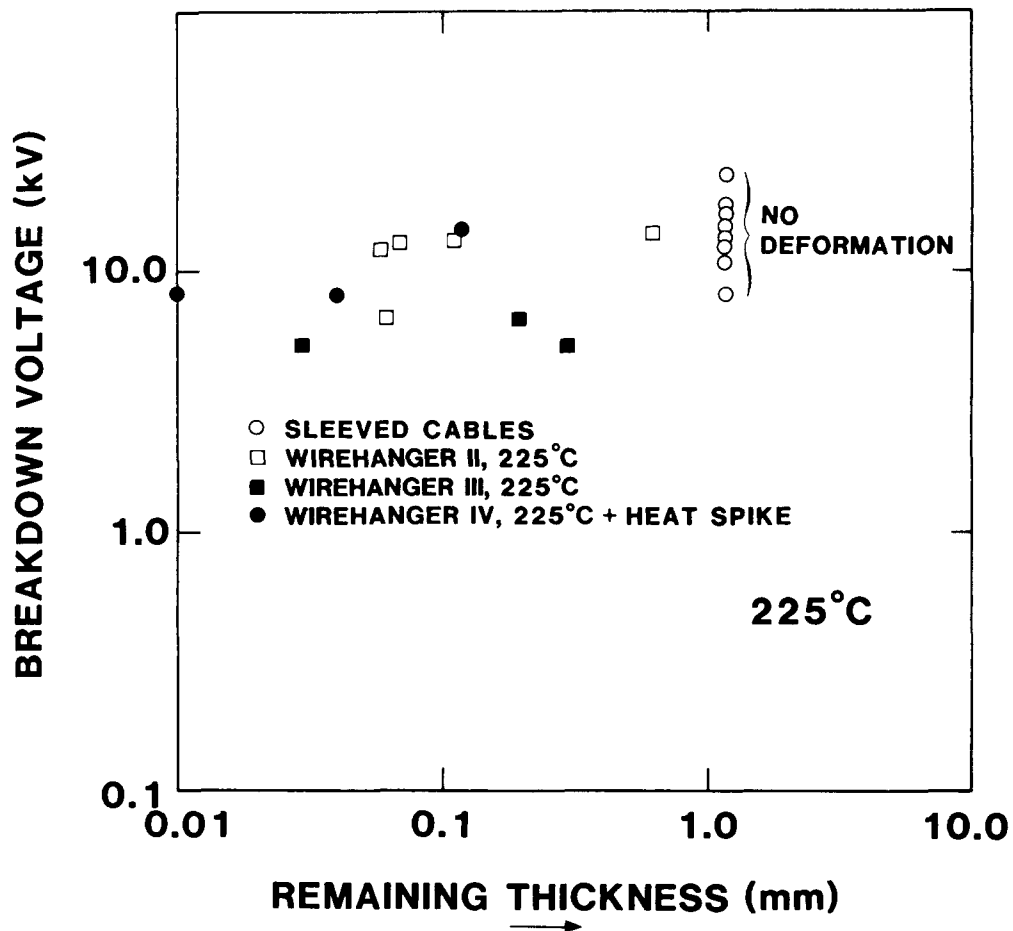
Figure 12: DC Breakdown Voltage vs. Remaining Polymer Thickness at 225°C

A third phenomenon further decreasing the breakdown probability has been observed. Over long times, and probably affected by vibrations, the "unfavorable" wire strand position (shown in Table II, [a]), appears to be unstable. The cable tends to twist towards the more stable position (b) indicated at the bottom of Table II. The wire now sinks in more slowly, and shortout at the support is delayed.

It is concluded that the phenomenon of concern in short observation times, e.g., under LOCA or circuit breaker failure conditions, is direct shortout between cable wire and metallic supports at high temperatures (>150°C) and high stresses (>600 lb./sq.in.) The 150°C value has been chosen conservatively. At 190°C a shortout under equivalent stress is practically certain.

2. Long-Term Tests

Using seven tensioners for 6 cables each, as shown in Figure 7, six coincident experiments were conducted in heat chambers maintained at 75°, 100°, 125°, 150°, 175°, and 225°C. A seventh experiment was conducted in the open at room temperature. In each test, creep versus time was measured by X-ray observation of the gradual reduction of insulator thickness in 6 cable samples. Each cable was hung over a 4.8-mm diameter steel rod and the cable-ends carried 0.45-kg or 0.9-kg lead weights. For three of the six cables in each test, an ac voltage of 480 V, between cable wire and support, generated an electrical field tending to pull cable wire and support together. The small mechanical stress of about 3 Pa (0.4 x 10^{-3} psi), which increases rapidly with decreasing distance, induced by the voltage also causes 120 Hz mechanical vibrations.

The task was to determine the closest approach between cable wire and support, the quantity marked y in Figure 8. Due to the stressing of the cable, and sometimes due to some movement of cable and support during many months of high temperature exposure, a number of calibration quantities had to be measured. They are indicated in Figure 13, a 38-times magnification of the original X-ray. The measuring and use of correction parameters is typified by the discussion of a sample data sheet, Table III.

The first nine rows of Table III contain raw data and the other rows are computer evaluations as follows.

- Rows 2, 3, and 4 show the thicknesses in mm for the EPR and Hypalon layers, and the independently determined total insulation thickness, measured on the negatives similar to Figure 8.

- Row 5 lists the tilt symmetry angle, α, introduced in Figure 8, for possible later use in correlation.

- Rows 6, 7, and 8 use the support width, d, defined in Figure 12, and the major and minor axes of the elliptical projection of the calibration hole, δ_0, δ. Support width is known to be 4.76 mm, and the major hole diameter is very close to 1 mm. The two quantities are therefore useful to obtain scaling factors. In row 6 the scaling factor is printed out directly.

- Row 9 gives the values for the measured tilt angle, α, versus the vertical, indicated in Figure 8.

- A computer program calculates corrections and averages of interest from the raw data. (The digit behind the decimal point in rows 10 through 14 is carried only for program convenience and is not significant.)

- Row 10 determines the support shadowing correction (i.e., the part of y hidden by the shadow of the not ideally aligned support) from the minor to major ellipse axis ratio, i.e., from the data in rows 6 and 7. The value is shown in microns.

- Row 11 improves the correction by taking the tilt angle (row 8) into account.

- Row 12 shows the actual thickness of the EPR layer in microns, calculated by dividing row 2 by row 6, the scaling factor.

- Rows 13 and 14 list the corrected apparent thicknesses for the Hypalon and for the total polymeric layers. As the lower part of these layers may be partially covered by the support, the correction calculated in row 11 is added.

- Row 15 provides averages for the 6 thickness measurements in rows 2 to 4 in microns. The EPR values are listed in column 2, Hypalon and total values in columns 4 and 6, respectively.

- Rows 16 and 17 contain the standard deviations for row 15, in microns and percent of the average value, respectively.

- In rows 18 to 23 are listed the normalized values for the data presented in rows 12 to 17; for each cable the total thickness before exposure is defined to be 100%.

- Finally, in rows 24 and 25, reduced group values are listed. These help in assessing differences between the three cables under voltage and the three nonenergized cables. Here the preexposure thickness for each of the layers is set at 100%.
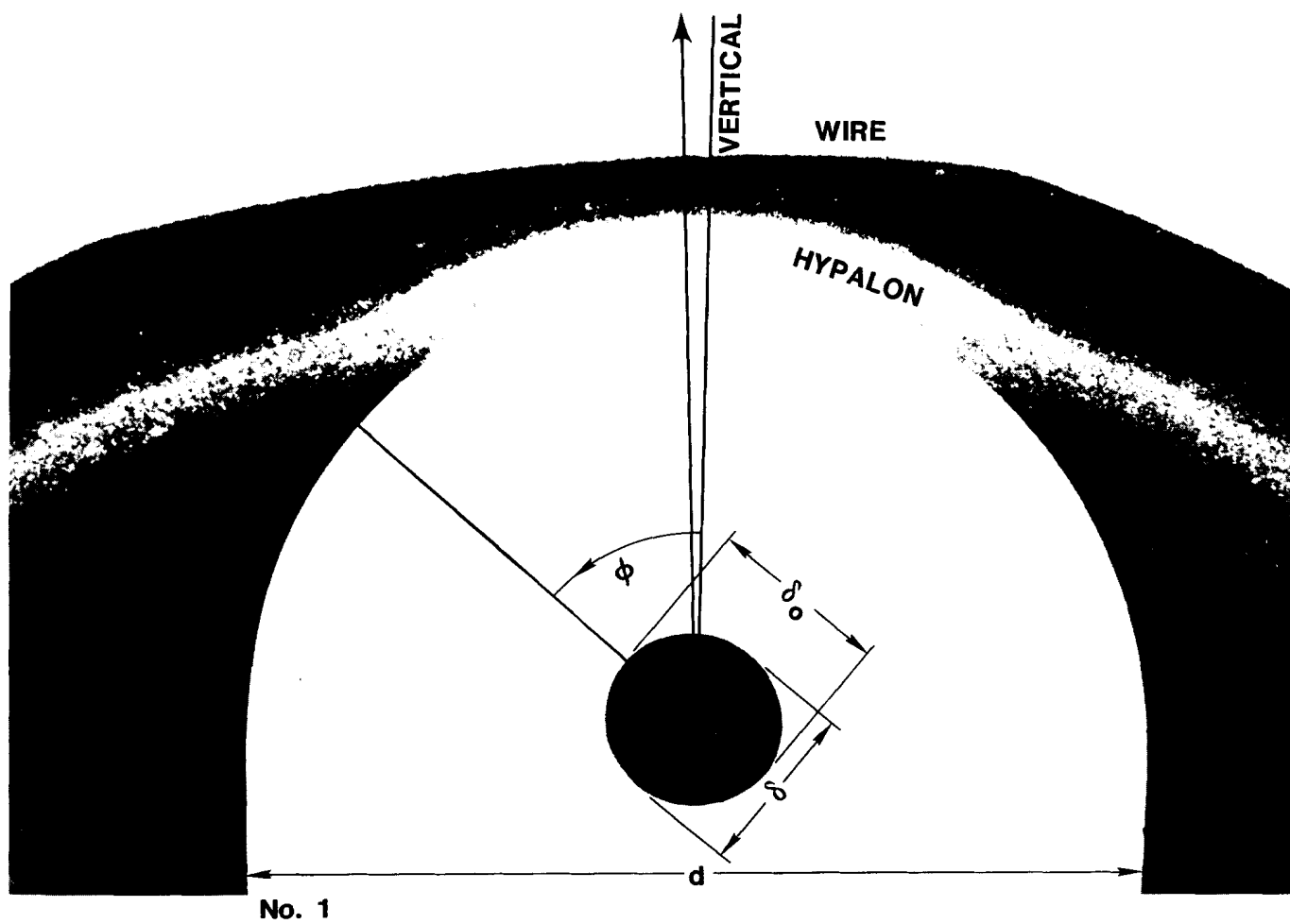
Figure 13: Measurement Parameters (38 x)

Table III

Example of Data Evaluation

Raw Data			175°C, 2-mo exposure			
1 Cable Number	1	2	3	4	5	6
2 EPR, measured (mm)	14.0	12.0	12.0	14.5	13.0	11.5
3 Hypalon, measured (mm)	9.0	10.0	10.0	10.5	10.5	9.0
4 Total, measured (mm)	23.0	22.0	22.0	25.0	23.5	20.5
5 Alpha, (degrees) (Fig.8)	9.0	1.0	1.0	1.0	1.0	0.0
6 Scaling factor	39.5	39.5	39.5	39.5	39.5	39.5
7 Large hole diameter (mm)	38.0	38.0	38.0	38.0	38.0	37.5
8 Small hole diameter (mm)	35.0	37.5	36.0	38.0	37.0	35.0
9 Phi, (degrees) (Fig.13)	15.0	35.0	20.0	0.0	50.0	55.0

Computer Evaluations

10 Kappa (μm)	23.7	3.9	15.8	0.0	7.9	20.0
11 K*sin(phi)	6.1	2.3	5.4	0.0	6.0	16.4
12 EPR (μm), corrected	354.4	303.8	303.8	367.1	329.1	291.1
13 Hypalon (μm),corrected	234.0	255.4	258.6	265.8	271.9	244.2
14 Total (μm),corrected	588.4	559.2	562.4	632.9	601.0	535.4

	EPR	Hypalon	TOTAL
15 Average (μm)over 6 cables	324.9	255.0	579.9
16 Std. dev. (μm)	28.0	12.7	31.7
17 Deviation (%)	8.6	5.0	5.5

18 Reduced, EPR (%)	44.9	38.7	36.3	39.7	39.4	34.2
19 Reduced, Hypalon (%)	29.7	32.5	30.9	28.8	32.5	28.7
20 Reduced, Total (%)	74.6	71.3	67.2	68.5	71.9	62.8

21 Average, E,H,T (%)	38.9	30.5	69.4
22 Std. dev., E,H,T (%)	3.3	1.6	3.8
23 Deviation (% of %)	8.6	5.3	5.4
Group Averages			
24 E,H,T, 1 to 3 (%)	67.9	75.3	70.9
25 E,H,T, 4 to 6 (%)	64.5	72.4	67.7

The reason for introduction of normalized values is that the original dimensions of the cable samples, although taken sequentially from the same reel, vary considerably. Bending the cables over support rods increases the variation. In Table IV, some statistical data of interest are shown. The first three groups of figures show before-exposure averages for 42 cable samples used in the seven creep experiments; thicknesses and standard deviations are measured in microns and the relative standard deviations in percent. For a population of 42, a relative standard deviation of 10% must be considered large. Normalization of the total thickness to 100% eliminates the standard preexposure deviation for this parameter; as the two bottom groups in Table IV show, the relative deviation for the EPR insulator is halved, and the relative deviation for the jacket improved. The original dimensions are therefore not reduced proportionally. This points to nonuniformity of composition or of processing and makes extrapolation more difficult. Further statistical facts will be analyzed below, after the exposure experiments have been discussed.

Measurements of the remaining thickness of the EPR layer (only) versus time are presented in Figure 14 (average values of the 6 cables in each test) and Figure 15 (worst cable of each lot of 6), with the exposure temperatures as parameters. The cables were not aligned as far as the position of the wire strands is concerned (see drawings in Table II); a random assembly was attempted.

In short-term measurements under load, such as depicted in Figure 10 above, it was observed that the reduction of the creep distance occurred the faster, the higher the temperature was. This is no longer the case for a few months exposure, as Figure 14 and 15 show. In Figure 16 the thickness reduction after 3 months is plotted versus the temperature of the experiments; it has a minimum around 100 to 125°C. The phenomenon is easy to explain. In the beginning the cable material is the softer, the higher the temperature is, and thus sinks in the faster. But at higher temperature the hardening of the polymers accelerates after a while compensating for the greater softness – the distance reduction curves then flatten out.

More surprising seems to be the observation that after a year or so the creep distance, y, becomes larger again. The effect is most pronounced between 100° and 150°C. The "lift-off" phenomenon is due to the plasticity of the wire and the subsequent redistribution of support stresses.

In Figure 17 the geometry of the cable is shown a) for the beginning of the creep process and b) for the time after which the cable wire has bent to a smaller radius. (The drawings exaggerate the effect.) On top of the Figure is the situation pertaining to the stretching arrangement of Figure 7, on the bottom the geometry for a corner. After the stress has moved to the outside, the center of symmetry lifts up and plastic is squeezed back. While the effect complicates

Table IV

Preexperiment Averages, 42 Cables

EPR Layer (microns)	552.8
Standard deviation, EPR, (microns)	55.3
Rel. Standard deviation (%)	10.0
Hypalon Layer (microns)	328.7
Standard deviation, Hyp., (microns)	35.2
Rel. Standard deviation (%)	10.7
All cable (microns)	881.6
Standard deviation, (microns)	69.4
Rel. Standard deviation (%)	7.9

Reduced thickness, EPR, (%)	62.7
Standard deviation (%)	3.4
Rel Standard deviation (% of %)	5.5
Reduced thickness, Hyp., (%)	37.3
Standard deviation (%)	3.2
Rel. Standard deviation (% of %)	8.6
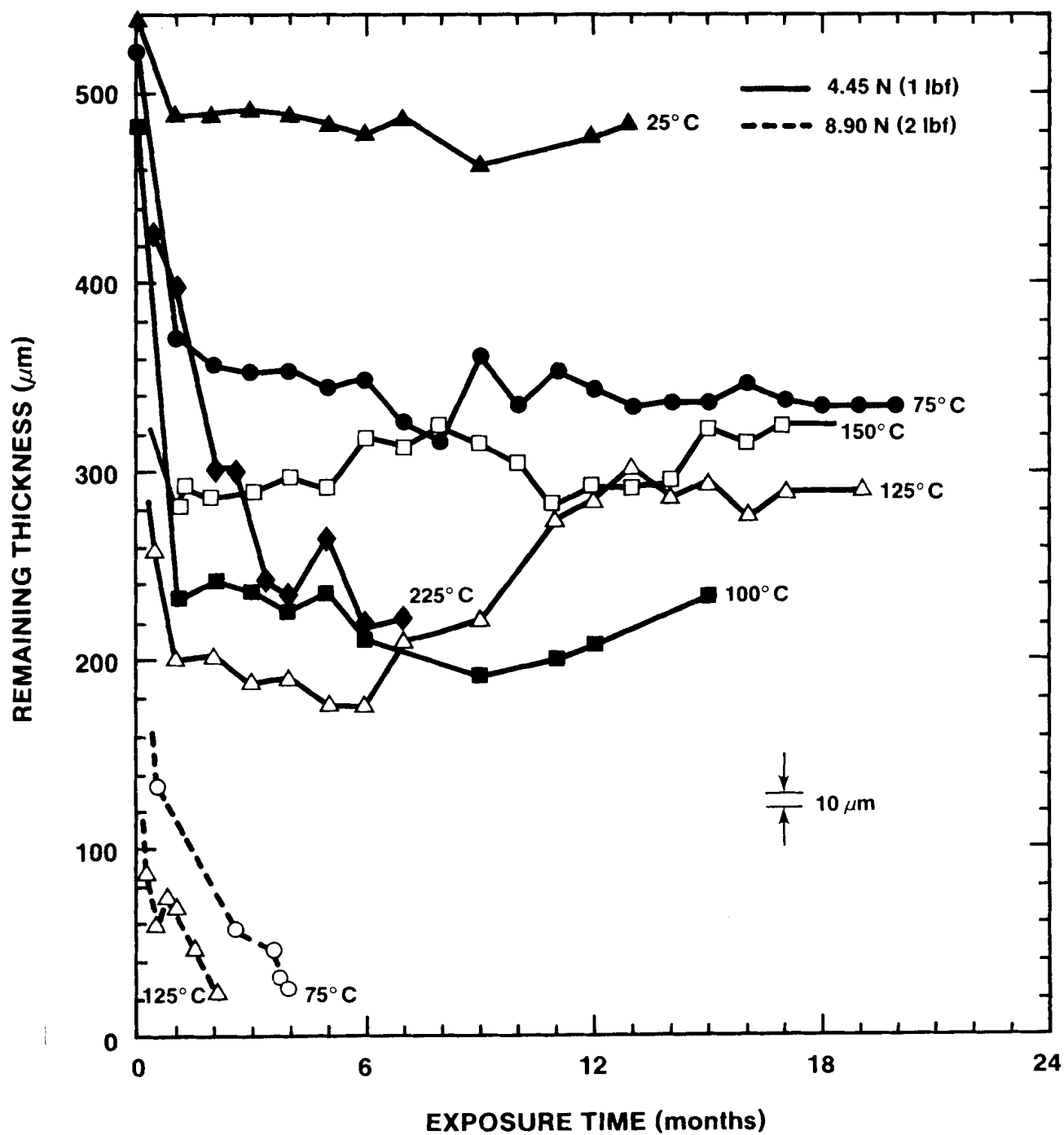
Figure 14: EPR Reduction (Average of Six Cables) vs. Time
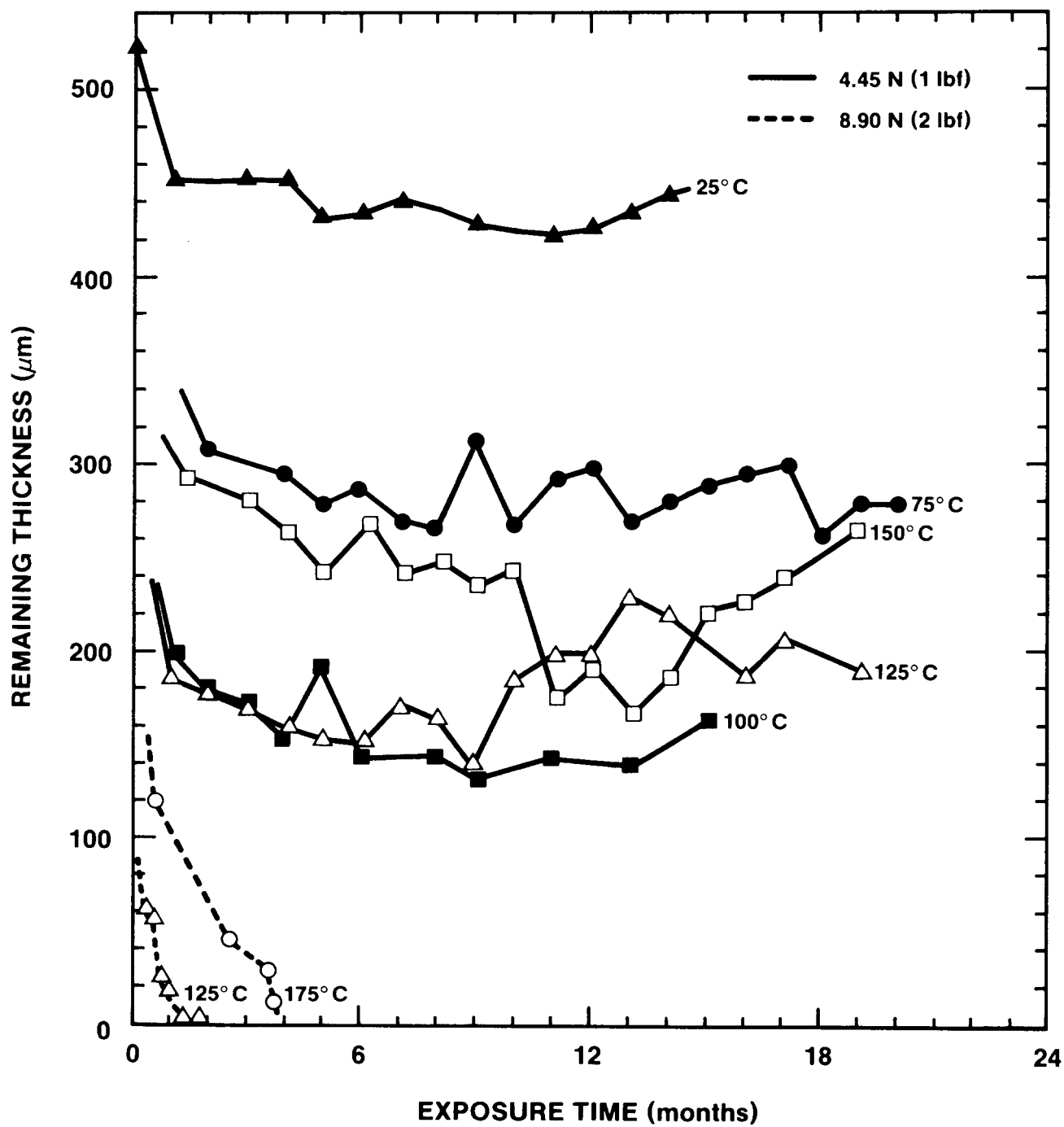
Figure 15: EPR Reduction (Worst Cable of 6) vs. Time

7 EXPERIMENTS, 3 MONTHS EXPOSURE

●━━● AVERAGE
■--■ WORST CASE
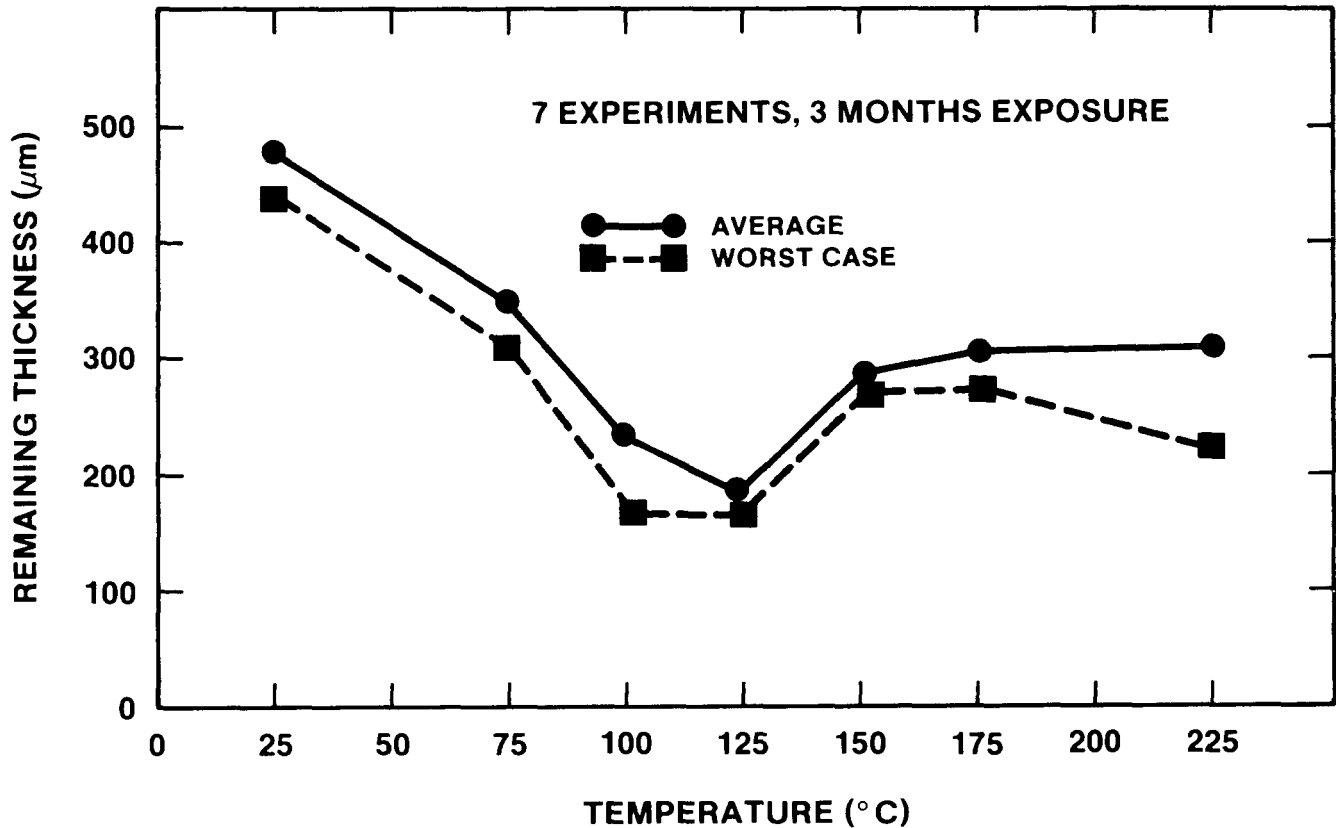
Figure 16: EPR Reduction After 3 months vs. Temperature

the test evaluation, it is beneficial as it increases the effective support area and therefore slows creep.

Another kind of lift-off effect is observed for cables for which the strands have a unfavorable lie, similar to Figure a) in Table II. This geometry, as stated above, is unstable. The strands therefore twist into position b) and for a while the distance, y, to the support will increase. It is believed that this phenomenon is responsible for some of the sudden upward "spikes" in the data of Figures 14 and 15.
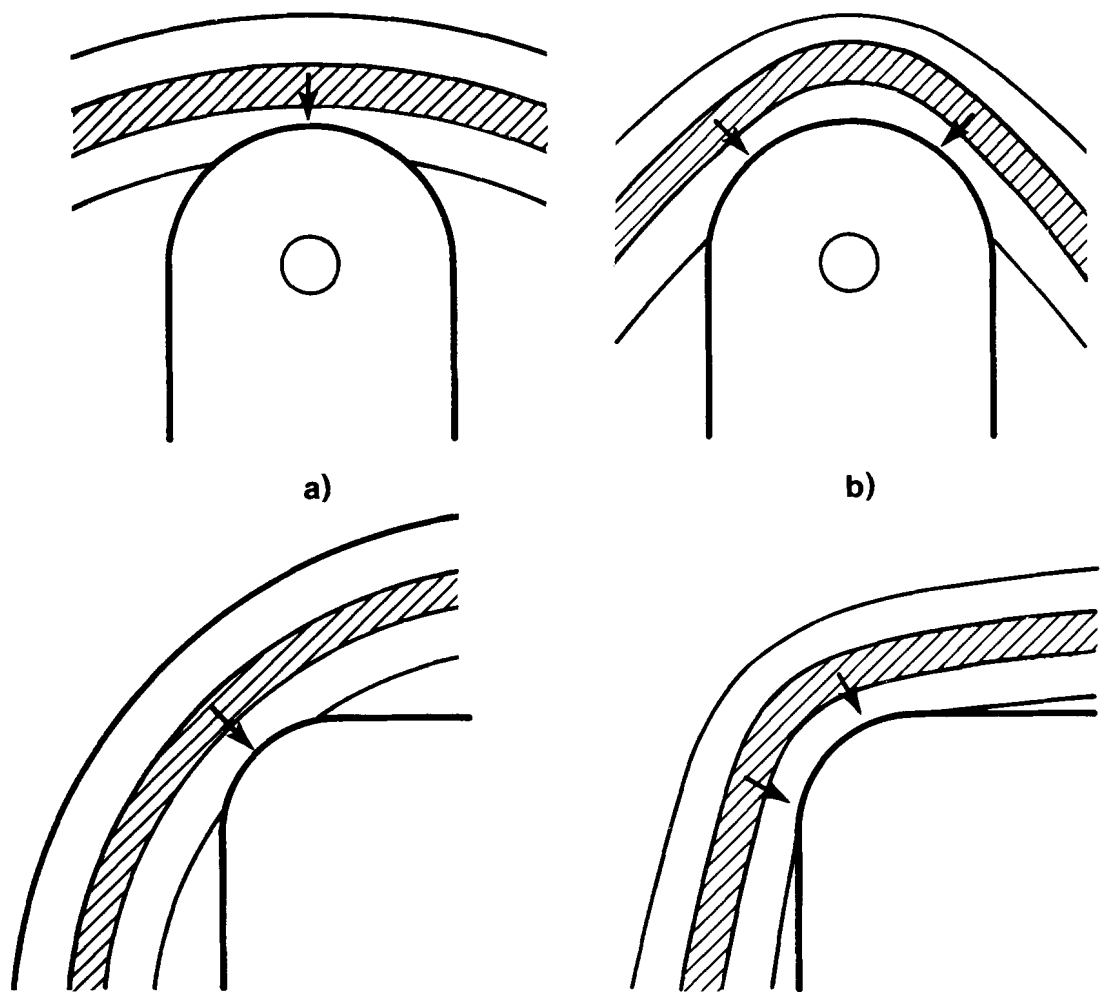
Figure 17: Original (a) and Later (b) Distribution of Support Forces

The above described phenomena, temperature nonlinearity and wire lift-off, are most strongly developed for the EPR layer. The Hypalon jacket, added for protection, consists of tougher and more stable material, and is expected to exhibit less average creep.

Figure 18 describes the Hypalon layer reduction for 1-lb. load weight, a nominal stress of about 220 lb./sq.in. A comparison with Figure 14 for EPR shows that the overall temperature dependence of creep is reduced by about a factor of 3. A nonlinear temperature dependence similar to Figure 16 is still recognizable, but it is noticeably smaller. Most important is the relatively low dependence on increased load. A few data points obtained with 2-lb. load weight are plotted in Figure 19. A squeeze-out such as for EPR, which would lead to shortout, as in Figure 14, is not to be expected; an almost 200 micron thick layer remained in all long-term experiments.

In Figure 20 a majority of the long-term data points pertaining to the composite thickness (EPR + Hypalon) are entered. A log-log scale is used to make long-time projections easier. Total thickness for the worst out of 6 cables is plotted in the right upper region for the groups of cables under 1-lb. and 2-lb. loads (nominal stresses 220 and 440 lb./sq.in. respectively).

At least for small strains the creep compliances (see Figure 9) for longer times can be represented by a power law; extrapolation has been discussed by Struik.[27] In Figure 20 a conservative power law extrapolation line is drawn, which assumes the average total thickness of polymer insulation (882 microns, see Table IV) still to exist after 8 hours of exposure, and which would decrease to a thickness of 1 micron in 40 years. All long-term measurements (upper right), 220 and 440 psi stay above this line and tend away from this "critical curve."

To describe the meaning more clearly, some data points for 880 lb./sq.in. (6 MPa) are drawn on the left side of Figure 20. At this nominal stress the 190°C measurements tends away from the critical curve, predicting the shortouts shown in Figure 10. (The 125°C values may cross the critical curve later. The 225°C measurements have shortouts at less than 8 hours, which are not shown.)

As a measure for the quality of the data, the relative deviation for our samples of 6 cables are plotted in Figure 21. The percent deviations increase essentially with increasing temperature and stress. Part of this is due to the fact that with increase of these parameters, the reference value, remaining thickness, becomes smaller. Otherwise, the measurements appear surprisingly well behaved and support the conclusion that the measurement methods do not have a systematic error.
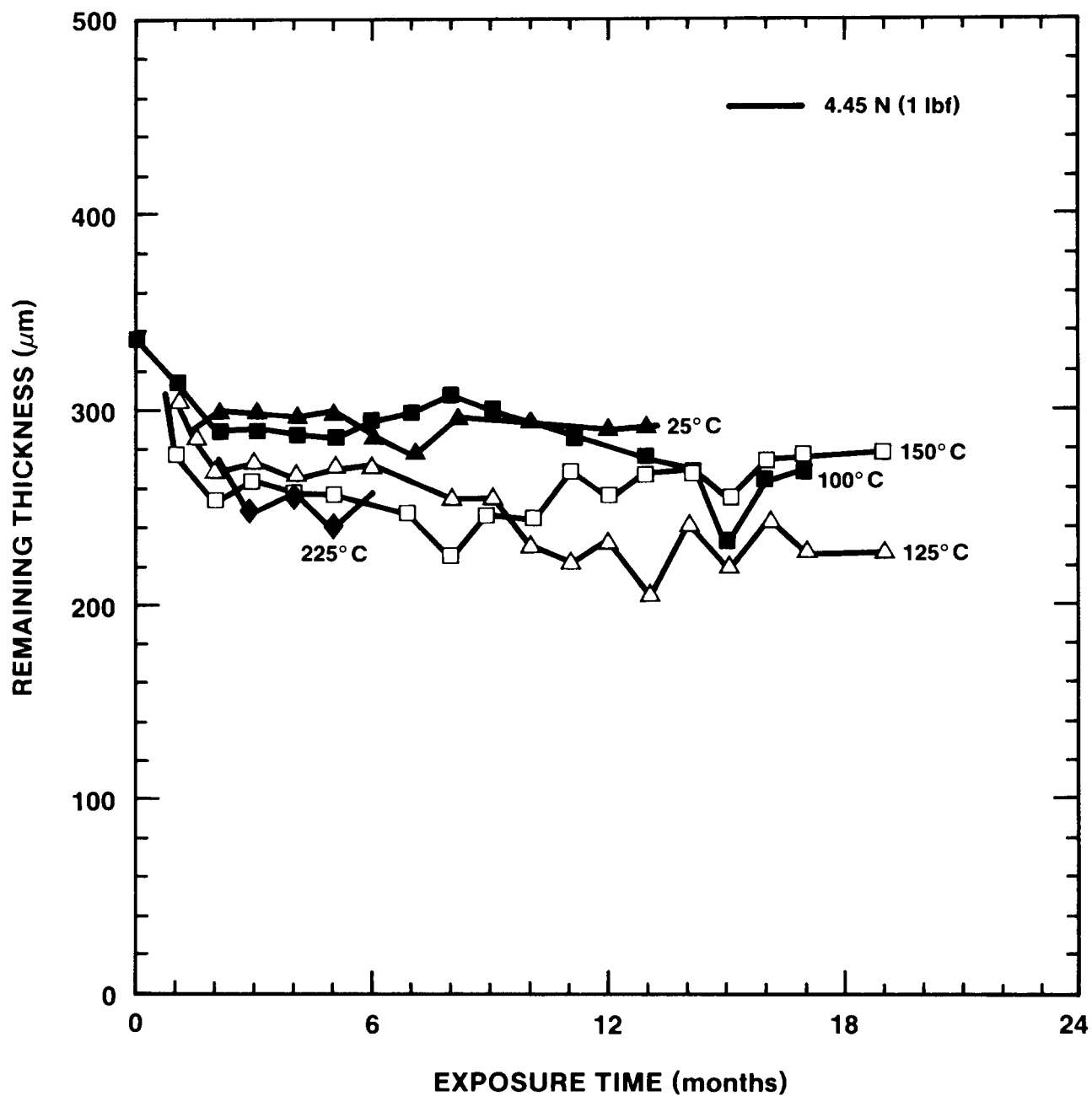
Figure 18: Hypalon Thickness Reduction, 1-lb. Load
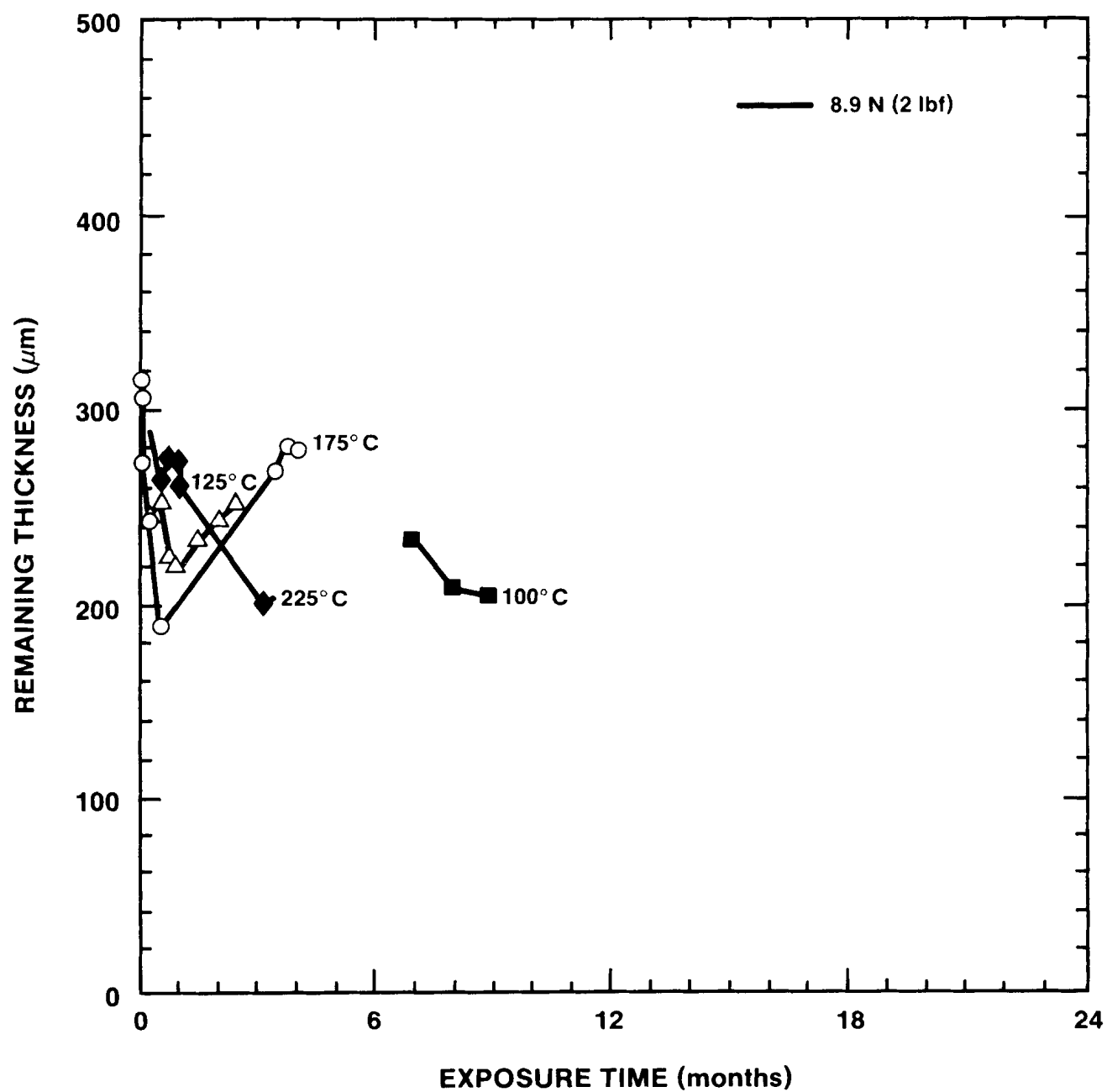
Figure 19: Hypalon Thickness Reduction, 2-lb. Load

TOTAL THICKNESS
(WORST CASE)
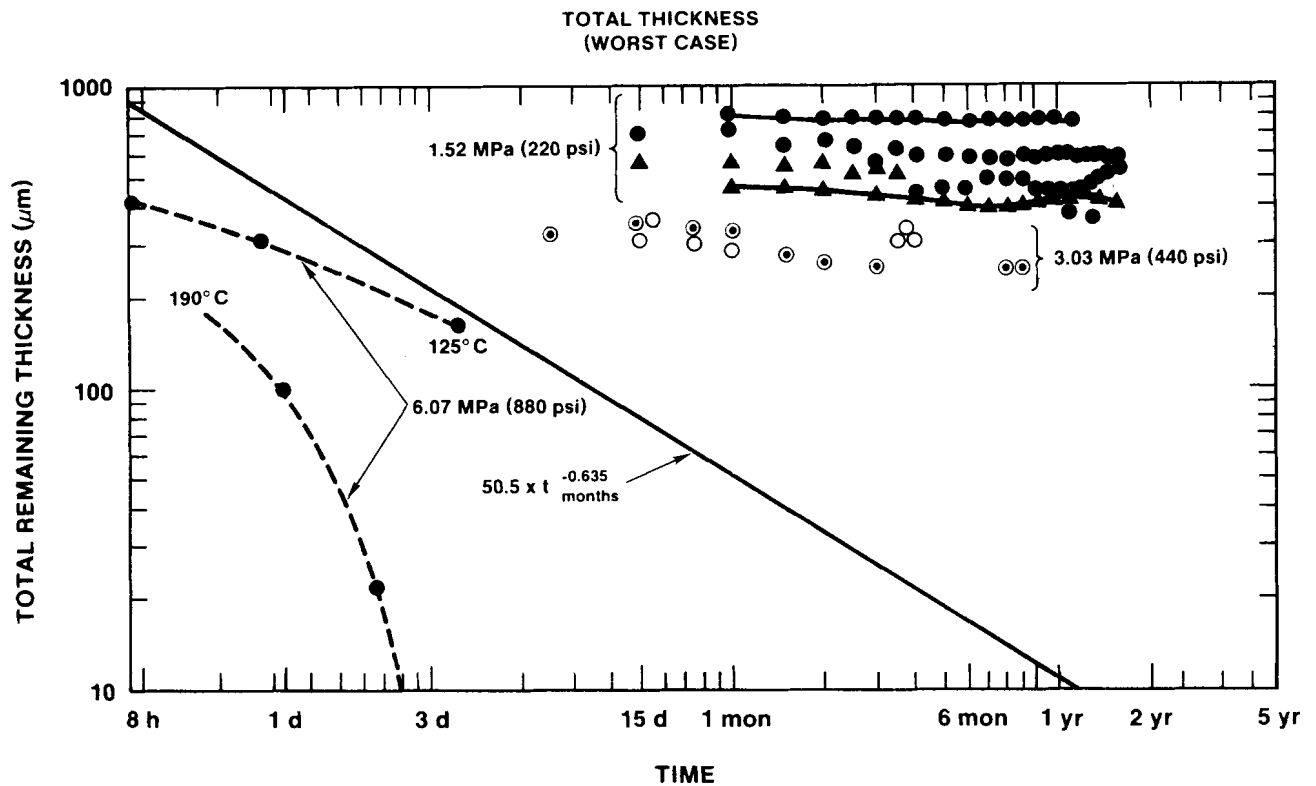
Figure 20: Comparison of Creep Data. Total remaining thickness vs. time measurements and stipulated power function decreasing to 1 micron in 40 years.
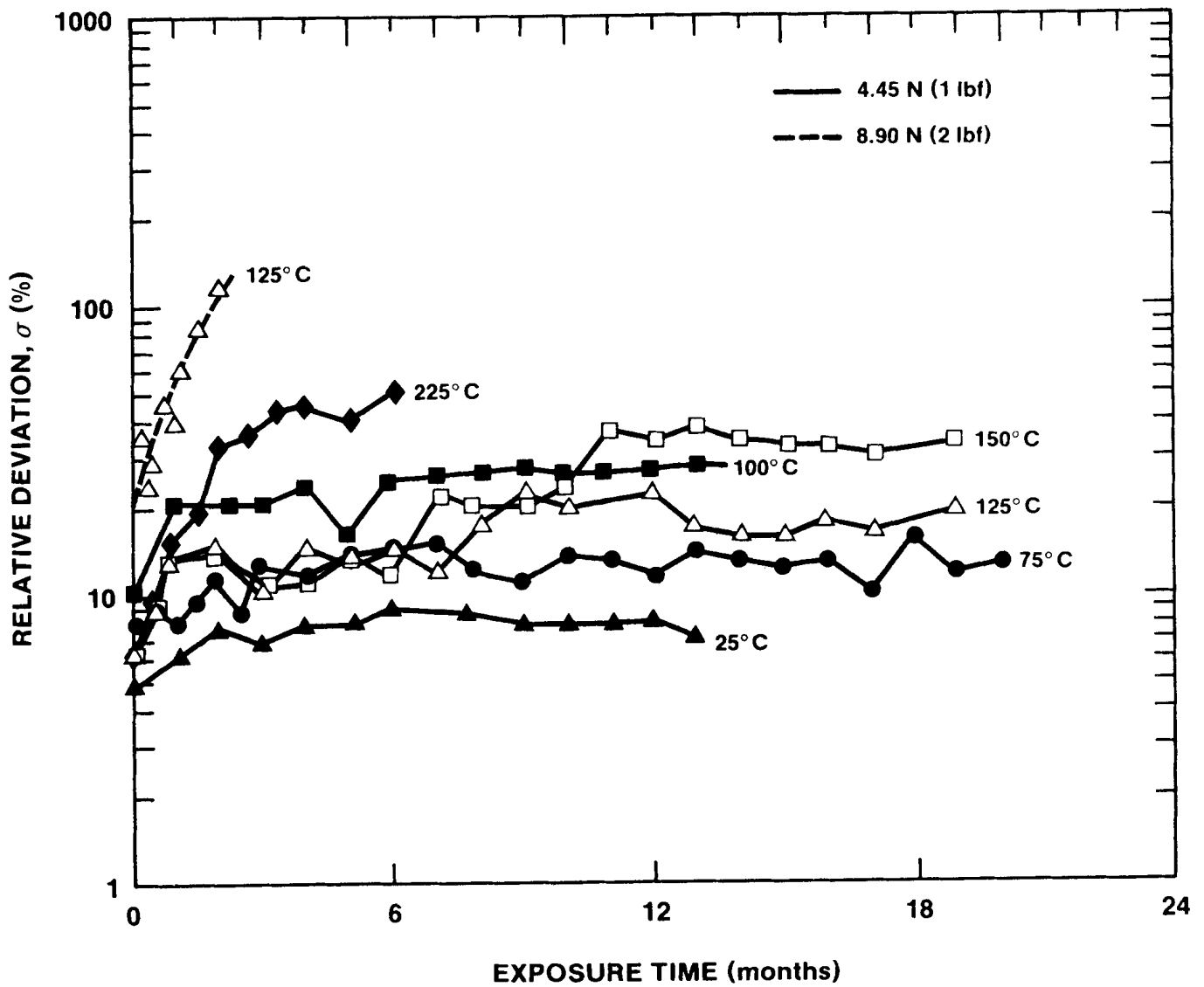
Figure 21:   Relative Deviation (%) for 6 Samples vs. Exposure Time

C. Temporary Electrical Breakdowns

In Figures 15 through 21, the 225°C data have not been plotted beyond 5 to 7 months. Around this time temporary electrical shortouts of the cables under voltage were noticed. Reduction of the EPR layer to zero was almost or fully completed at this time for 2-lbs. stress weight. The Hypalon layer thickness had not materially decreased (see Figure 22), but the Hypalon had been turned into a powdery substance and showed noticeable cracking. After removing the voltage and some cooling of the cable, the insulating properties were fully restored. Conservatively, however, temporary shortouts have to be considered failures.

The phenomenon will be brought up again in the next section, which deals with cracking.

IV. CRACKS IN CABLES

Cracks in the insulator-jacket protection of a cable may lead to electrical shortout, especially during an accident when the combination of humidity, contaminants, and spray may form conducting paths to ground or to another crack.

Experiments have been performed during this investigation that show that the existence of a crack through jacket and insulator does not always lead to an immediate shortout, even if the cable is immersed in a conducting liquid. The conditions under which a short does not occur, even though cracks are present, are very complex and not completely understood, but are clearly related to the surface breakdown phenomena which have been previously investigated for a reactor accident environment.[19]
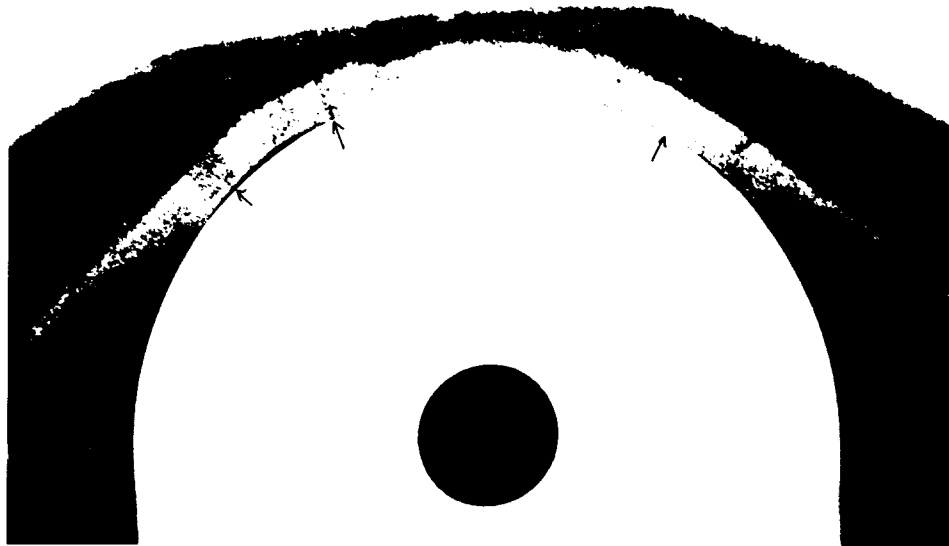
Figure 22:   Embrittlement Cracks at 225°C

For the present discussion the criterion will be that cracks penetrating to the inner conductor may cause a shortout and are considered as causing failure.

Three specific situations are of primary concern:

a) Long cables lying in conduits or trays, unstressed by outside forces, may develop cracks under thermal cycling or shrinkage.

b) Cables, sharply bent, (e.g., around conduit corners) may crack under the mechanical stress produced by temperature cycling or by overhang weighting. (This stress is tensile and perpendicular to the cable cross-section, in contrast to the compressional stress responsible for creep shortout.)

c) Cables, embrittled by aging, may be mechanically stressed and cracked by handling, e.g., during maintenance.

Variations and combinations of these characteristic situations may occur.

The investigation of cracks in cables is made difficult by two phenomena. First, a crack will originate at a flaw, and the distribution of nonuniformities is generally widely variable. (Once a crack starts enlarging, it relieves tensional stresses in its neighborhood and prevents further cracking there.) Second, cracks, especially small ones, can heal again.[28] (This phenomenon was clearly observed and witnessed only once during this investigation, but was quite conspicuous at the time.) For these reasons, measurements of number and size of cracks occurring for a certain temperature history and stress distribution will show large variations.

Extrapolations are difficult, too. Investigations at the Bell Telephone Laboratories[29] have shown that for low-density polyethylene (LDPE) cables the time needed to develop incipient cracking, plotted versus inverse temperature, exhibits non-Arrhenius behavior. It cannot be assumed that the present materials combination behaves more simply.

Ninety percent of all cracks observed are either (nearly) circumferential (i.e., perpendicular to the cable axis) or (nearly) axial (longitudinal). In order for a crack to occur, stresses perpendicular to the direction of the crack must be present. These are quite easily explainable for bending cracks, but require involved mechanisms for very long straight cables. It has been found that a combination of materials' volume changes, together with (nonuniform) sticking of the cable layers to each other and/or to the cable wire are mechanisms which occur and may suffice to explain the observations.

A. Volume Changes in Materials

When EPR or Hypalon are initially heated up, the materials first expand (see e.g., Reference 11, Figures 3-7). After a while (months at 75°C,

hours at 200°C) materials' changes and loss of additives come into play. At higher temperatures and in longer times, EPRs may expand or shrink,[30] Hypalon shrinks. (The EPR of the presently used cable most often shrinks.) Both shrinkage and expansion, together with localized sticking can lead to stresses which cause observed cracks. J. E. Reaugh of Science Applications, Inc., (Appendix A, Section 2) has discussed the stress distribution in strictly cylindric two-materials cable geometries; we will utilize his results below.

A number of methods were used to measure specific volume changes. The most reproducible method was a series of volumetric measurements made by dipping samples of the exposed whole cable into alcohol, where air bubbles adhering to the samples could be easily removed. Polymers and wire were then separated. It was observed that at certain times during exposure, EPR and Hypalon became vulcanized to each other, and later the EPR was fused to the wire.

In Figure 23a, long-term measurements of specific volume change are shown. In the beginning of the experiments Hypalon and EPR can still be separated; for the 75°C and 100°C exposures the (in this case swelling) values for both materials are first plotted. After some time the two polymers vulcanized together, indicated by the mark "V" for the 100°C and higher temperature curves; from then on only the combined volume change could be measured.

Figure 23a depicts measurements taken with about 1-year old material. Measurements with older cable of the same composition do not show a volume increase for low temperatures on the scale of drawing. In Figure 23a the end values (12 months) of $\Delta V/V$ for one of these measurements on older cables of the same make are indicated.

The figure shows that at low temperatures Hypalon expands more than EPR in the beginning of the experiments. At higher temperatures Hypalon also shrinks more. This is not shown in the graph, as it has to be measured before vulcanization sets in, i.e., at short times. In an early measurement Hypalon shrank about 1.8 times as fast and as much as EPR at temperatures above 125°C. (This factor is used for several examples in Appendix A.)

Some short-term measurements of shrinkage are presented in Figure 23b. Here the linear axial shrinkage has been shown versus temperature for various times. The linear shrinkage in the axial direction is of importance for the generation of circumferential cracks. For an isotropic material, linear shrinkage would be about 1/3 of volume shrinkage. It is seen from comparing Figure 23b with Figure 23a that for the highly anisotropic structure a cable with wire represents, the linear shrinkage is an order of magnitude lower than isotropic shrinkage would be. Shrinkage data will be used in Section G, below, to correlate observations with theory.
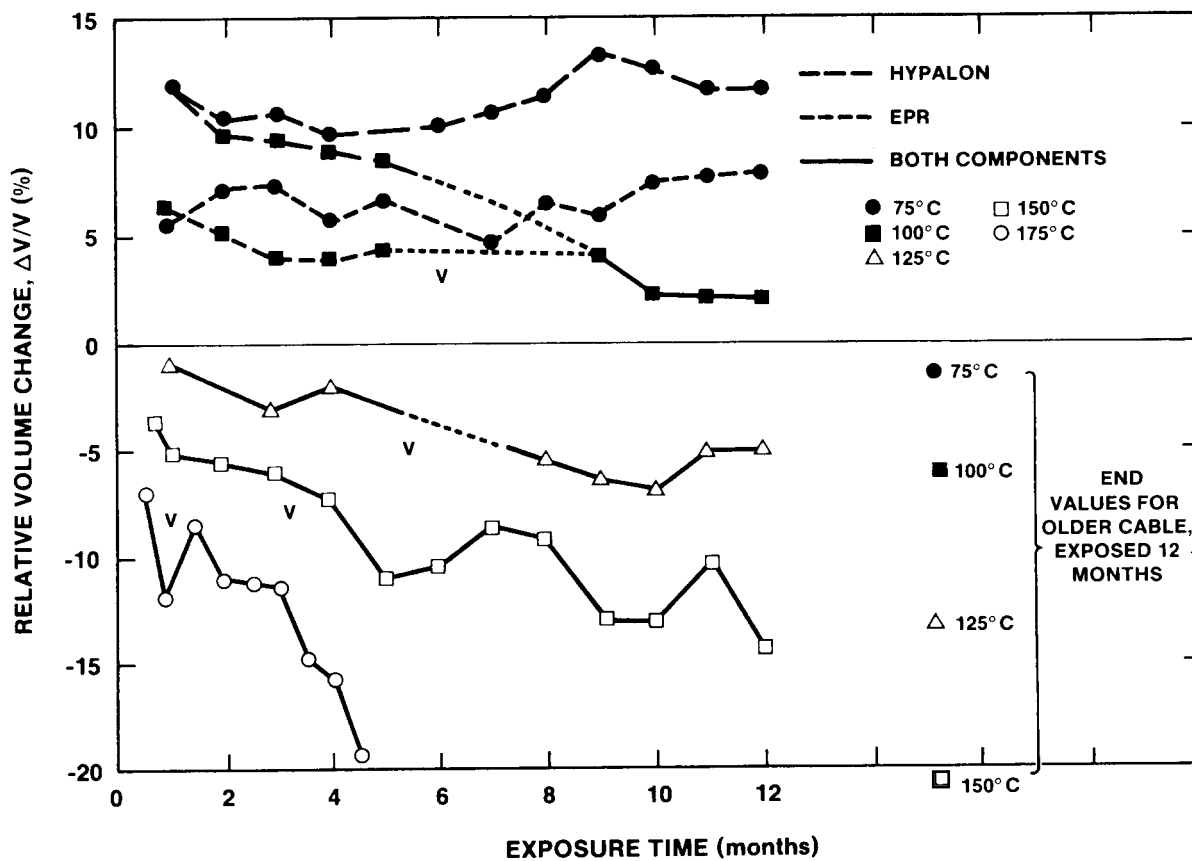
Figure 23a: Percent Volume Changes of EPR and Hypalon Layers with
Accelerated Aging
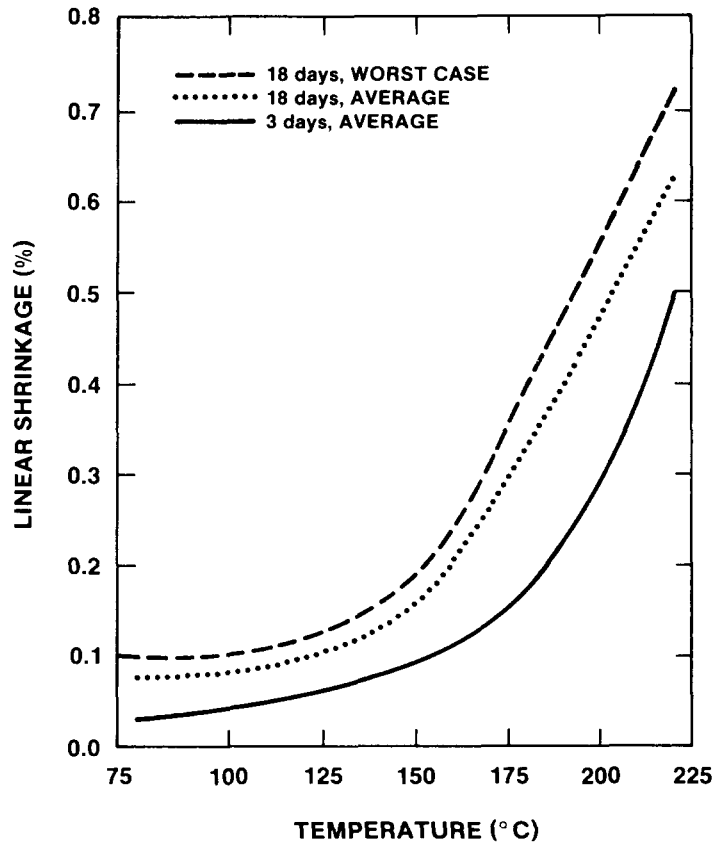
Figure 23b   Linear (composite) Shrinkage vs. Exposure Temperature
(Averages are for 3 Samples)

B. Cracks in Long Conduits
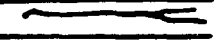
Cables lying horizontally in long conduits are essentially free of outside
applied stresses. Cracking phenomena for such conditions were studied in
three thirty-feet long iron pipes of 2-inches diameter, surrounded by
thick foam insulation. In each of the pipes, six long cables were heated
by passing from 20 to 30 amperes of dc current through the cable
conductors. Thermocouples were positioned at 1-m intervals on the inside
of each pipe. An upper third of pipe and insulation could be removed to
permit cable insertion, cable removal, and inspection. The arrangement
is described more fully in Reference 1, Section III.

The heat distribution along the pipe caused a fall-off of the temperature
by about 4% with reference to room temperature within one meter from each
end. The temperature across the pipe, measured outside the cables, was
constant within 2%.

A brief experiment demonstrated crack generation during a severe heat
spike, where temperature was permitted to rise to 320°C in two hours.
After cooling, the system was opened. The wires had warped and some had
crossed over others. Both perpendicular and longitudinal cracks were
present. The perpendicular cracks went through both jacket and insulator,
the longitudinal cracks occurred in the jacket only. The distribution of
the cracks is shown in Table V. It is of interest to note that one
cable, otherwise indistinguishable from the others, showed no cracks at
all. This demonstrates the nonuniformity of material and/or processing.

TABLE V

Perpendicular and Longitudinal Cracks in 10-m Long EPR/Hypalon Cable
after Severe Overload
(Temperature rise to 320°C in 2 hours)

CABLE	PERPENDICULAR	LONGITUDINAL
1	NONE	1 EACH 110 cm LONG 1 EACH 4 cm LONG
2	1 EACH 3.8 mm WIDE 1 EACH 4.9 mm WIDE	1 EACH 61 cm LONG
3	NONE	1 EACH 96 cm LONG
4	NONE	1 EACH 113 cm LONG
5	NONE	NONE
6	2 EACH 4.1 mm WIDE 1 EACH 3.2 mm WIDE	1 EACH 10 cm LONG 1 EACH 20 cm LONG 1 EACH 22 cm LONG 1 EACH 77 cm LONG

Long-term experiments were performed (with cable bundles of six each) at 95°C, 135°C, and 165°C. Every three months the test pipes were let cool down, opened, and the cracks were counted. Their direction and approximate widths and lengths were noted.

Two experiments were run at 95°C, a temperature slightly higher than the rated value. An early test lasted one year, a much more precisely controlled test had a duration of 2 1/2 years. No cracks developed.

Data from measurements at 135°C and 165°C are compiled in Table VI.

After 3 months at 165°C and after 6 months at 135°C, a rubbery, blackish effluent (which later hardened) was observed at three to five locations in the pipes. A chemical investigation showed that the effluent consisted of hydrocarbons and exhibited a high water content. No adverse influence on cracking or electrical breakdown could be discovered.

C. Other No-Stress Measurements

As opening and restarting the conduit experiments described above is cumbersome, the measurements were spaced 3 months apart. This is not enough to determine the onset of cracking - and especially that of through cracks - with desirable accuracy.

TABLE VI

CRACKING IN CONDUITS: Number of all cracks and/or through cracks

Experiment	Exposure (months)	Perpendicular All	Through	Longitudinal All	Through	Comments
12 gauge, 135°C	3	0	0	0	0	
	6	9	2	0	0	
	9					
	12	784	189	984	0	
10 gauge, 135°C	3	0	0	0	0	
	4	79	0	11	0	
12 gauge, 165°C	3	113	24	12	2	
	6	782	42	370	19	longitudinal
	9					cracks
	12	2757	756	948	6	combine

A special series of tests was undertaken with bundles of 60 cable pieces, each 1-ft. long, inserted into ovens in use for other experiments.   In intervals of days at high temperatures, and of half-months at low temperatures, three or six each of the cables were withdrawn and analyzed for cracks.   The resulting data are shown in Figure 24, where the number of cracks measured in 3 cables is plotted.   (I.e., at 225°C half the total number of observed cracks is shown.)

With increasing time, first cracks are observed in Hypalon.   After the time has about doubled, through-cracks appear.   The samples exposed to 100°C or lower temperature did not exhibit any cracking in 2 years – a result in agreement with the observations in long conduits.

D.   Hot Cracking in Stressed Bends

Especially in long-duration experiments, cracks may form during cooling; hence a test series was performed where cracking was evaluated before the specimens had opportunity to cool.
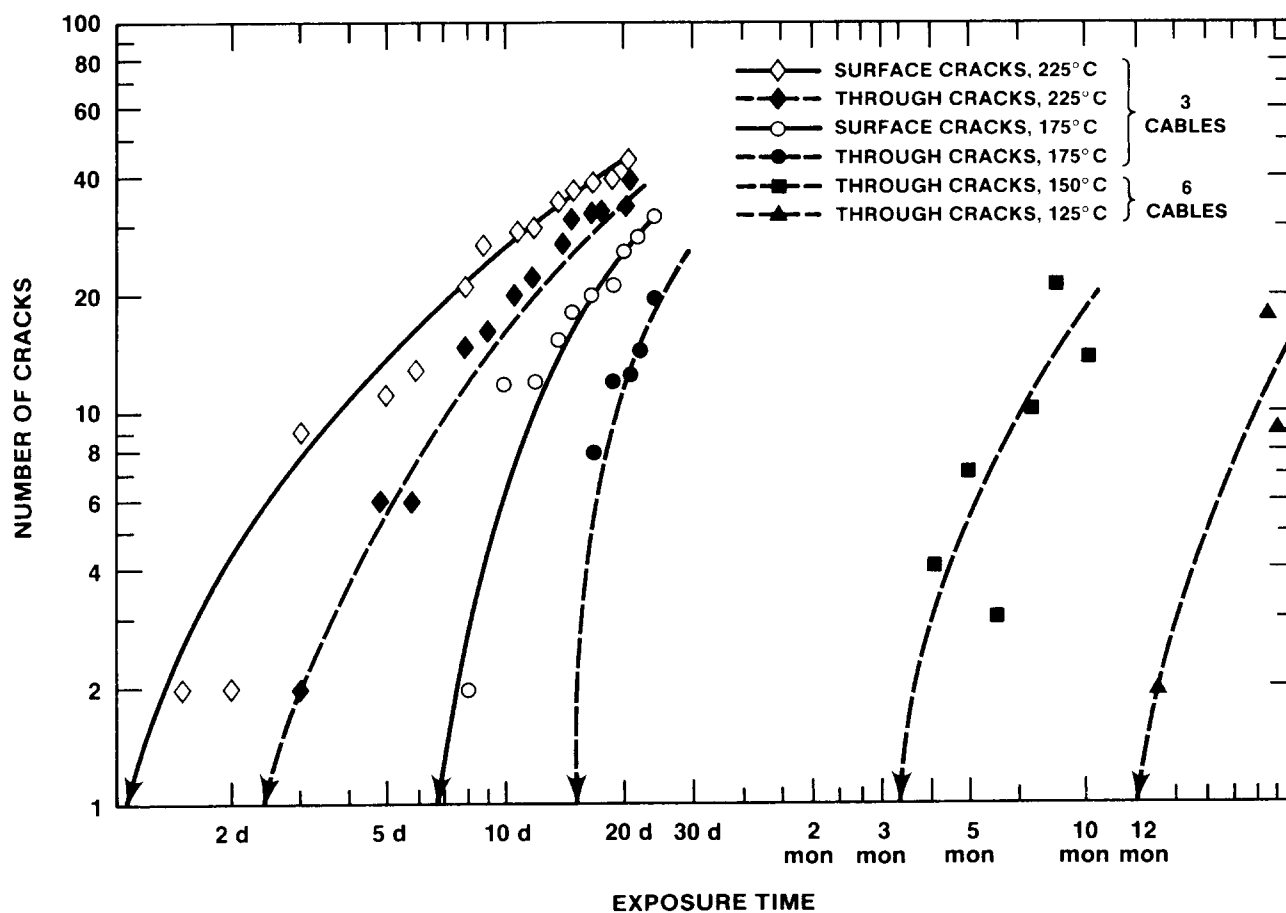
Figure 24: Unstressed Cracking: Number of Cracks Appearing During
            Exposure vs. Time

Thirty-five cable samples were exposed to a thermal treatment in which the temperature was slowly increased, over a period of 5 days, to 225°C in steps of 25°C. The cables were stretched over a sharp edge with weights of either 1.6 kg or 0.34 kg each. Half the experiments were performed in a dry atmosphere; for the other half, the humidity ranged between 95% and 100%. In the last experiment, a one-hour heat spike of 265°C was applied before the normal heating sequence.

Listed in Table VII is the average number of observed cracks, the average width of the cracks, and the integrated crack width per cable. Also given is the percentage of cracks which reached the conductor (through cracks). It was observed that the formation of cracks increased strongly between 200°C and 225°C. One crack in experiment III was found to have healed after cooling. All cracks, with the exception of 2 out of nearly 100, were perpendicular to the cable axis.

The most severely stretched cables, those in experiment I, clearly exhibited the largest number and the highest total width of cracks. The average crack width was very low in this experiment. The presence of humidity (during the relatively brief aging experiments) does not seem to have noticeable influence. The addition of a heat spike, simulating a temporary overload, had strong impact, however. It resulted in very tiny cracks (or crazing) which did not penetrate to the conductor. This inconsistency (and some of the observations above) may be related to the adhesion of the insulator to the center wire. In the first three experiments, the three cable components (jacket, insulator, wire) stuck inseparably to each other after cooling. The heat spike in test IV led to easy separability of the three components, however.

The experiments were designed to simulate severe accident conditions. Temperatures above 175°C and high mechanical stresses lead to substantial crack formation within days.

It was observed that occasionally cracks formed during cooling and even later. Such cracks were fewer than 10% of the total.

E. Cold Bending Cracks

To simulate damage from bending during maintenance handling, sample groups of 6 cables each were exposed to temperatures of 75°, 100°, 125°, 150°, 175° and 225°C and were allowed to cool completely, then bent around a mandrel. Care was taken to exert as little longitudinal stress as possible. The bending jig is described in Reference 1, and shown there in Figure 13. The cracks, most of which appeared in the bends or their immediate neighborhood, were counted.

The results of the test series are plotted in Figure 25. Of major interest are the "through" cracks which appear on the lower part of the Figure. It is seen, in comparison to the unstressed crack distribution
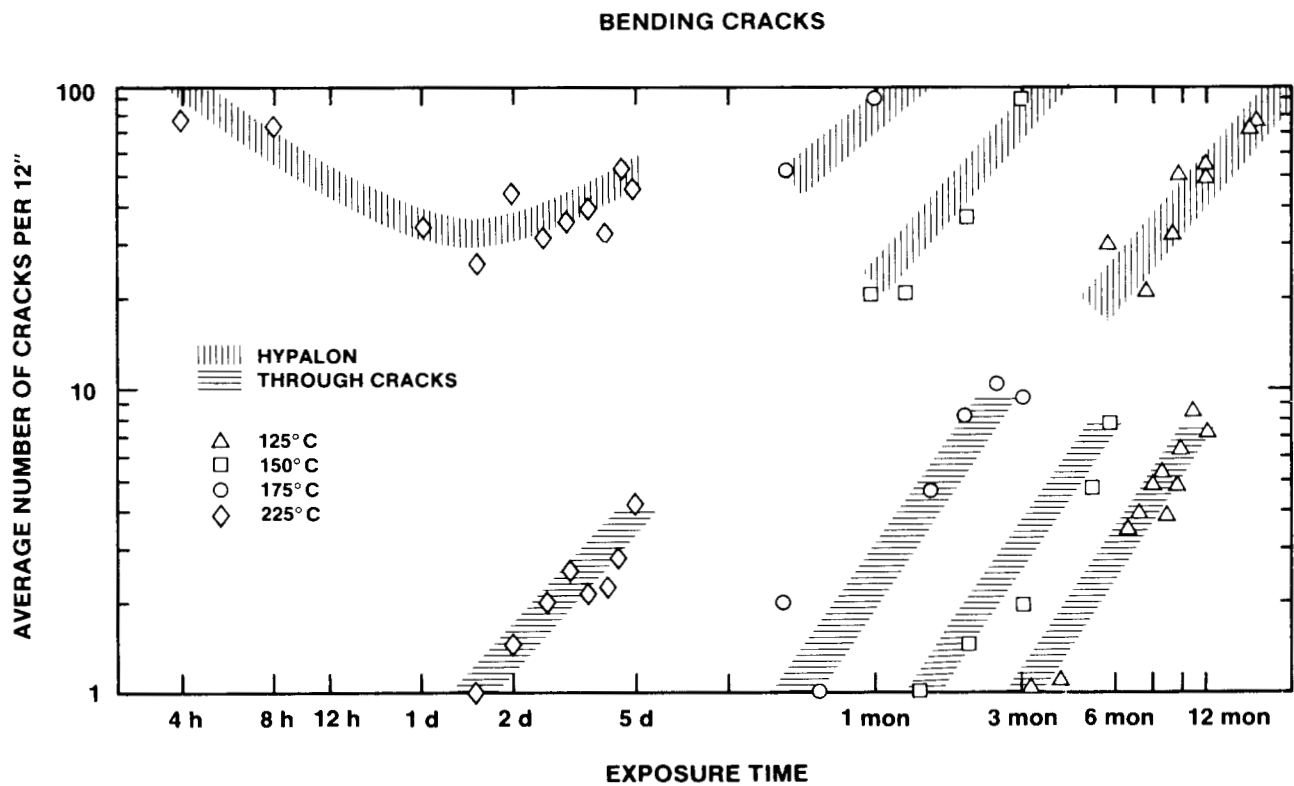
BENDING CRACKS

Figure 25: Cold-Bending Cracks vs. Exposure Time (Average Number of
Cracks per 12-Inch Sample; Six Samples per Plotted Value)

Table VII

Crack Statistics For Heating to 225°C Over 5 Days
Perpendicular Cracks

Experiment	I	II	III	IV
Number of cables	10	10	10	5
Load per cable (kg)	1.6	0.34	0.34	0.34
Environment	Dry	Dry	Humid	Humid (Heat Spike)
Average number of cracks per cable	4.6	1.9	2.3	1.6
Standard deviation	40%	34%	21%	154%
Average width of cracks (mm)	0.9	1.1	1.6	0.1
Standard deviation	27%	51%	42%	----
Integral crack width (mm)	4.2	2.1	3.7 (Est.)	0.16
Through cracks (percentage)	77%	35%	67%	0

of Figure 24, that through cracks appear earlier if the cable is bent. The Hypalon surface cracks, for clarity, have not been plotted to low numbers. They do, of course, appear much earlier yet than they do for nonstressed cables. As the data for 225° show, the Hypalon crack distribution has a minimum: with increasing temperature first very many small cracks appear, then fewer but larger cracks are generated by combination of small ones. After some time, a few of the larger cracks extend through the EPR insulator, forming the through cracks plotted in Figure 25.

It is noted, that with increasing time, the data points tend to show more scatter. The measurements still permit a reasonable estimate of the time, at which through cracks become probable.

A scaling experiment was performed to assess the cracking in thinner and thicker cables of the same composition as the standard cable used. Twelve batches five different gauge thickness cable samples, each sample consisting of six specimens, were exposed at the same temperature (125°C). Each month a batch was bend-tested. The bending mandrels were scaled approximately proportionally to the diameters of the cables. As pointed out below, this would produce an approximately constant bending strain. Gauge 6, 8, 10 and the standard gauge 12 cable samples were cut from freshly received rolls. Gauge 14 low power cables, from an earlier delivery, were added.

The "old" cable, gauge 14, started showing both surface and through cracks after 4.5 months of exposure, and developed worse cracks of either kind earlier than the others.

The four cable sizes of more recent manufacture (gauges 6, 8, 10, 12) started to exhibit surface (Hypalon) cracks between 5 and 5 1/2 months; the thicker the cable, the earlier the cracking occurred and the more cracks were formed in the 12 month measuring period.

Through crack formation was much more involved; however, it is shown in Figure 26. Here the total number of complete cracks appearing in 6 test samples is plotted for each gauge on log-linear graph paper; the bottom line marks signify one crack. The measurements are plotted for 125°C exposures, where in accordance with the observations above the scatter in the measurements had to be expected to be high. It is observed, that often fewer through cracks are found at a later date. An unexpected quirk is shown for the standard cable, gauge 12, where five batches of 6 specimens showed no through cracks; the sixth batch, tested at 9 1/2 month exposure, showed the first complete crack.

An argument can be made for the observed fact that thick cables – everything else equal – show cracks somewhat earlier and in larger numbers than thinner cables, even when the bending strain is (approximately) the same: The surface is now larger and more surface flaws are to be expected statistically.

F. Sticking

As stated, the fusing together of the three cable components has a marked influence on the generation of cracks. Fusing takes longer at low temperatures, as expected. The observations are difficult, as the separation of phases depends on the skill of the experimenter and starts first on a few locations, spreading gradually along the cables. The time where fusing has been observed is marked by the letter V (for vulcanization) in Figure 23a.

**COLD BENDING (MANDREL SCALED)
THROUGH CRACKS AT 125°C**

6 AWG
8 AWG
10 AWG
12 AWG
14 AWG

NUMBER OF THROUGH CRACKS
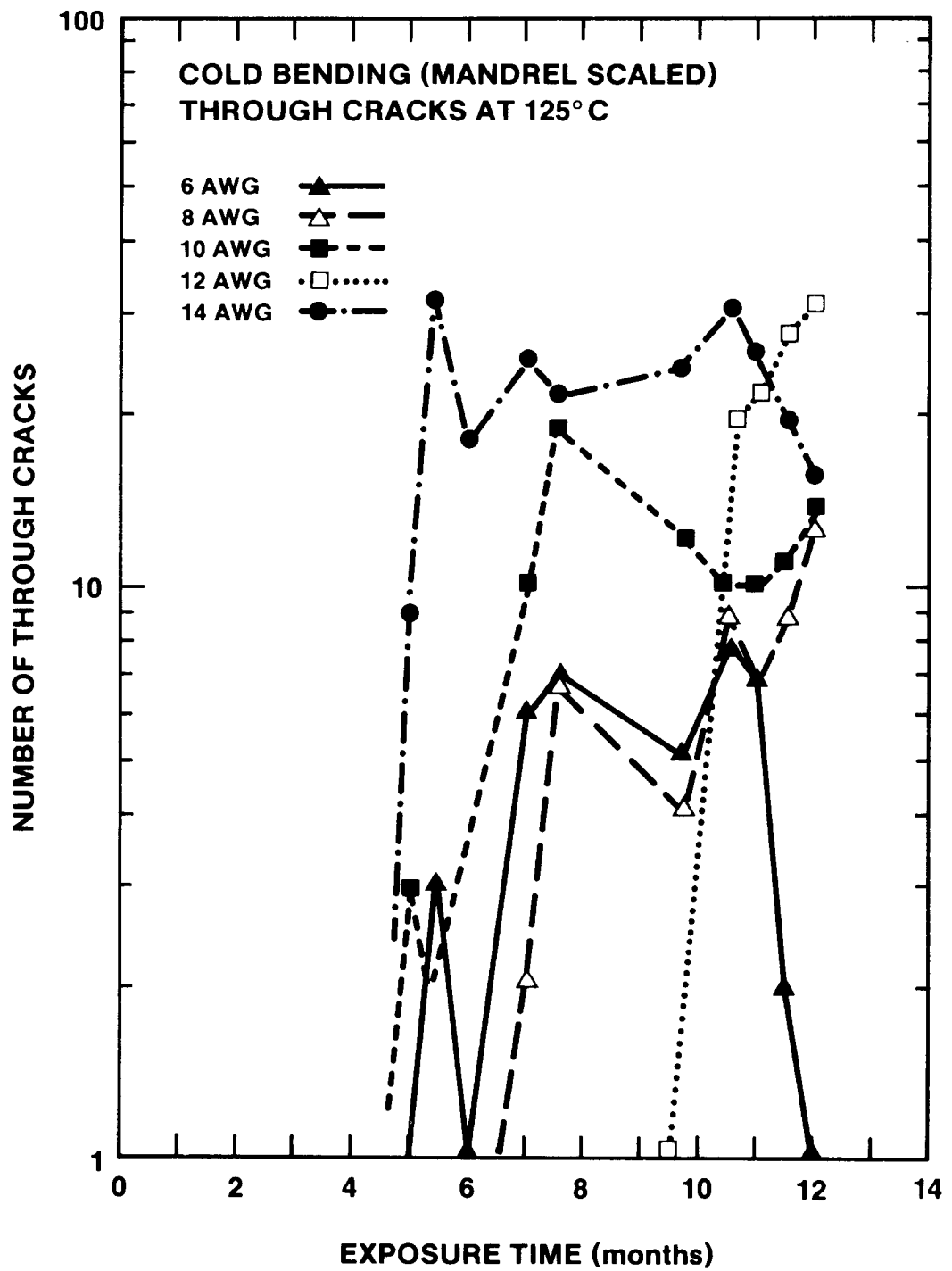
EXPOSURE TIME (months)

Figure 26: Cold Bending Test for Cables of Various Thickness

Sticking measurements (or rather observations) were also made in connection with nonstressed cracking, Figure 24, but are not marked in the plot. Observations were made on other occasions. In Figure 27 the acquired sticking data are shown in a log time versus inverse temperature plot. Error bars are estimated. Downward arrows are used to identify data points where only the upper limit is known. The time, at which Hypalon reaches a strain to break factor $e/e_o = 0.1$ is indicated as a reference line. If the fusion processes can be described by an activation energy, the respective energies for sticking are smaller than the activation energy for embrittlement of Hypalon (and of EPR).

G. Discussion

   1. Cracking Without Outside Stress

   A theoretical treatment of cable cracks generated without outside stress is available in J. Reaugh's report, Appendix A, Section II. Although the model is highly simplified, it explains many of the observed features reasonably well.

   In Figure 1, Appendix A, the theoretical stress distribution calculated for the model used is shown for a certain shrinkage situation. The axial stress, σ_z, is seen to be higher in Hypalon than in EPR. It is also higher than the circumferential stress in both materials. The material will, therefore, first show circumferential cracking in the Hypalon at the EPR-Hypalon boundary. A stress distribution instability will make the crack propagate to the surface.

   The various possible combinations of stress development are treated by Reaugh in Figures 4-6 of the referenced report; the maximum normalized stresses $\sigma/E = (\Delta \ell/\ell)/(\Delta V/V)$ are plotted versus Hypalon to EPR volume change. The location of maximum stress is indicated by the letters a (Wire-EPR boundary) and b (EPR Hypalon boundary). Where no location indicator is used, the stress is the same throughout the material which is always identified by superscript H or E.

   In Figure 28, which is basically identical to Reaugh's Figure 6, an example situation is marked. We choose a Hypalon to EPR volume change ratio of 1.6, and (e.g. from Figure 23) $\Delta V/V = .15$. According to Figure 28, the highest stress developed is σ_z in Hypalon; the Figure shows that $(\Delta \ell/\ell)/(\Delta V/V)$ is .64 for the present example. The strain $\Delta \ell/\ell$ is therefore .10. If this equals the breaking strain e, the material will crack. For a breaking strain $e_o = 3.5$ before aging, the critical value for $e/e_o = .03$. When the aging material reaches this embrittlement factor, perpendicular cracks will occur. The second highest stress is the circumferential stress in Hypalon, σ_θ^H at the
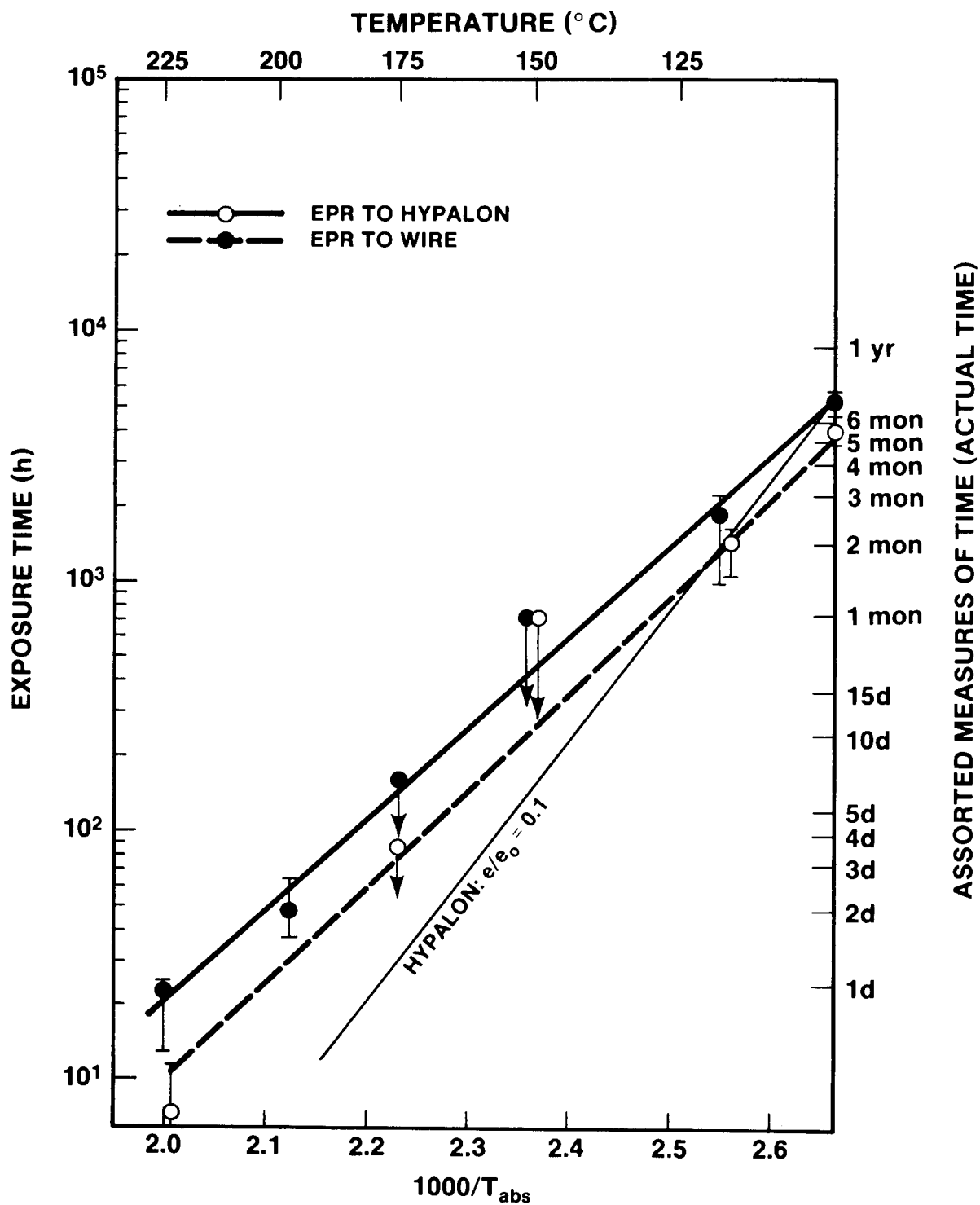
Figure 27: Arrhenius Plot of Sticking Data. (Hypalon $e/e_0 = 0.1$ line
furnished by K. T. Gillen, personal communication.)

EPR/Hypalon boundary. Here $\Delta\ell/\ell$ turns out to be .067 and the critical e/e_0 value is .02. At this value longitudinal cracks will occur.

The above example describes the behavior of the tested materials reasonably well. In all measurements made, perpendicular cracks occur earlier in the aging process than do longitudinal cracks. Below, the crack formation and the aging time at which the necessary values of e/e_0 are reached will be compared.

For materials where EPR expands instead of shrinking, Figure 28 predicts the occurrence of axial cracks first. The interesting feature is that comparable stress values and therefore comparable cracking are to be expected.

Figure 28 pertains to the "no slip" case; i.e., it is assumed that the three materials are fused together. From Figure 4 (all slip) and Figure 5 (sticking at conductor only), Appendix A, it is seen that the expected stresses are lower, often appreciably so. Cracking will therefore be inhibited at short aging times and low temperatures, where the cable materials are not fused.

2. Stress Cracking

For the assessment of bending cracks, a simple two-dimensional model can be developed with the help of Figure 29.

A strip of cable material of width 2ρ is bent (without deformation of the cross section) over a cylinder of radius r. At the outer side of the geometry, where cracks can start developing, the length of the plastic around a quarter bend is $\pi(r + 2\rho)/2$. At the neutral fiber, the corresponding length is $\pi(r + \rho)/2$. The resulting bending strain is then $\rho/(r + \rho)$. This strain is augmented by σ/M, if an applied stress, σ, exists, where M is the appropriate modulus. Cracks will develop if the sum of these strains exceeds or equals the breaking strain, e, that is, if

$$e \overset{\leq}{=} \frac{\rho}{r + \rho} + \frac{\sigma}{M} \tag{3}$$

The experiments, for cold bending described above in part (E) of this section, were of course performed with round cables and not with strips. Stress σ, as stated, was minimized. Lateral deformation of the geometry, usually less than 10%, was neglected. It was assumed that the effects of sticking between the three materials was small compared to the influence of the bending stress, Equation (3).

For the experiments described above, (e.g., the data in Figure 25), the bending radius, r, was 6.4 mm. The radius ρ extending to the surface (Figure 29) is 2.4 mm. The corresponding radius for the EPR Hypalon boundary is about 2 mm. According to Equation (3), cracking should occur for e/e_0 = .08 on the Hypalon surface; through cracks should start when e/e_0 = .06 for EPR.
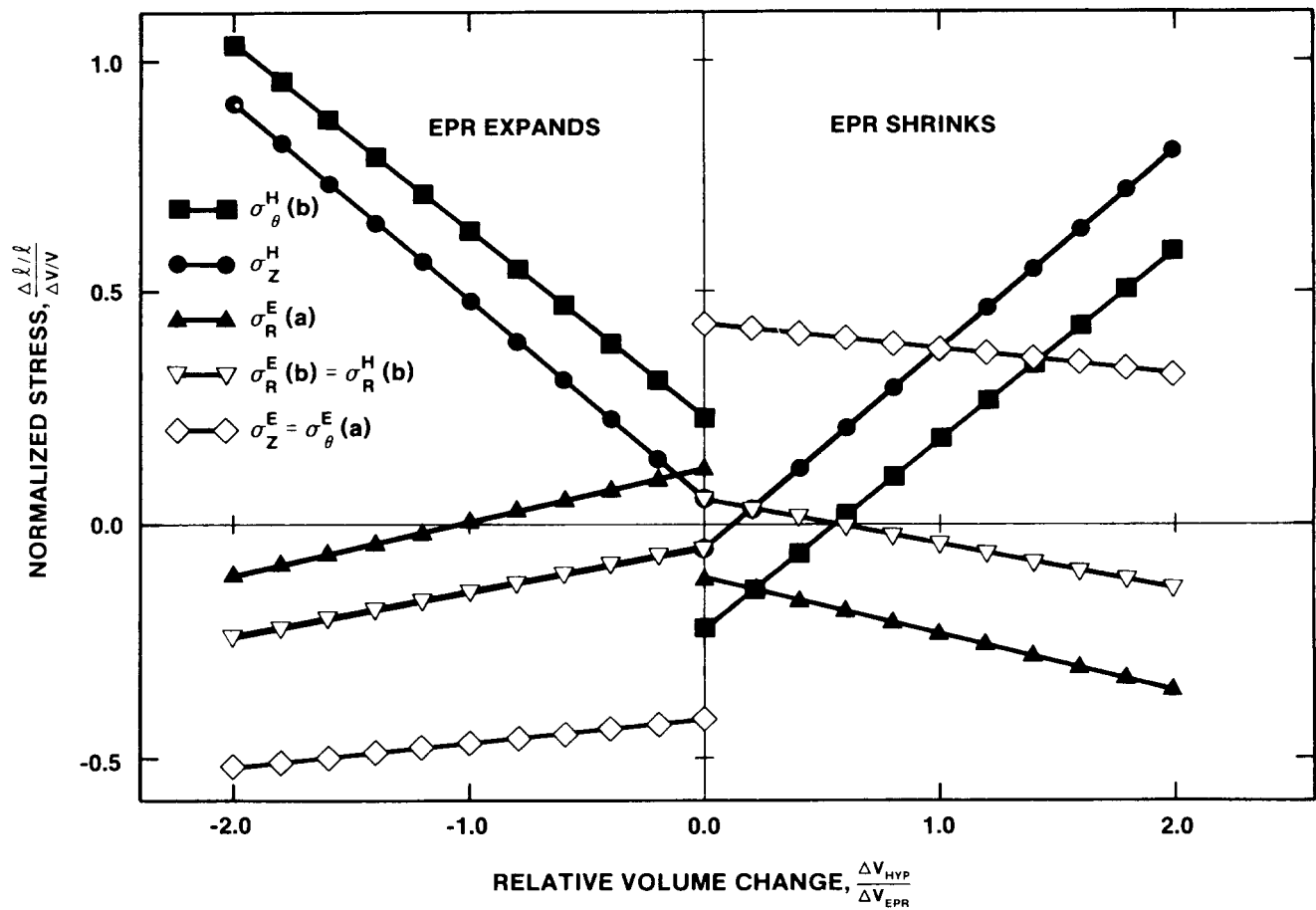
-58-

Figure 28: Maximum Normalized Stress as a Function of Relative Hypalon
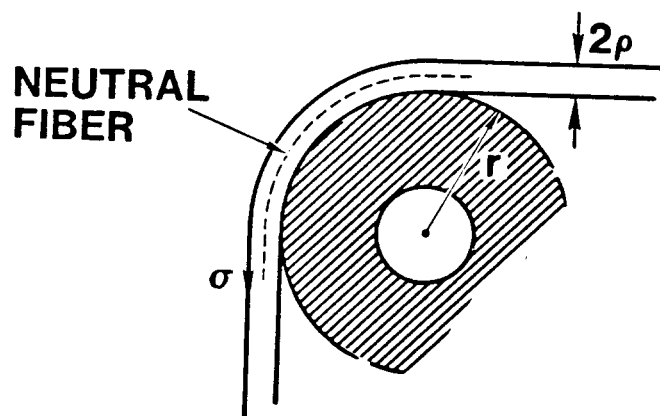Volume Change. All components stick together

Figure 29: Model for Derivation of Equation (4)

The model based on Equation 4 may be useful to estimate the embrittlement ratio e/e_0, above which no cold bending cracks will ever occur: For a very sharp bend (kink), the bending radius r will be very small and the ratio $\rho/(r + \rho)$ will tend towards unity. With e~1, the limiting value e/e_0 for the materials used in the experiments described above will be about 0.3. A very conservative working hypothesis would therefore demand that e/e_0 be kept above 0.4 to avoid any cold bending cracks. In the present experiments, no cracking has ever been observed above this value.

3. Time Dependence

The above discussions of both "unstressed" and of bending cracks links the occurrence of cracks quite simply to the strain to break ratio e/e_0. This is fortunate because this parameter is relatively well known for many materials.

In Figure 30 and Figure 31 our measurements are compared with updated e/e_0 measurements by Gillen.[22] In our Arrhenius type graphs his (average) straight lines for the time needed to reach e/e_0 = .1 for Hypalon and e/e_0 = .25 for EPR are entered. The smaller values for e/e_0 calculated above to imitate cracking will lie above these lines. We note that the activation energies for the two materials are practically identical. Our measured data are linked by lines parallel to the lines characterizing the materials.

Figure 30 shows the beginning of cracking versus temperature, where no outside stresses are applied. The data are from Figure 24, some additional not specifically reported measurements at 190°C, and from pipe experiments; for the latter only an upper limit of the cracking times could be determined. With increasing time, Hypalon cracks appear first. After the time has more than doubled, through cracks are formed.

In Figure 31 a corresponding plot is furnished for bending cracks. Most of the data pertain to the severe bending strains discussed above and lead to the data in Figure 25, for example. The data for different cross-section of Figure 26 are entered (at 125°C temperature) and marked by the cable gauge number. Very approximately, bending cracks occur at half the time of the corresponding unstressed cracks for the same aging treatment.

The error bars in Figure 30 are due to uncertainties in time measurements, and are the Gaussian deviations of the crack number distribution plotted on a linear scale. Instead of error bars, the influence of cable design (i.e., mostly gauge) is indicated in Figure 31. The uncertainties of the present measurements are larger than the ones observed by Gillen for his measurements of e/e_0. Nevertheless, the correlation of cracking with the embrittlement factor e/e_0 is convincing.
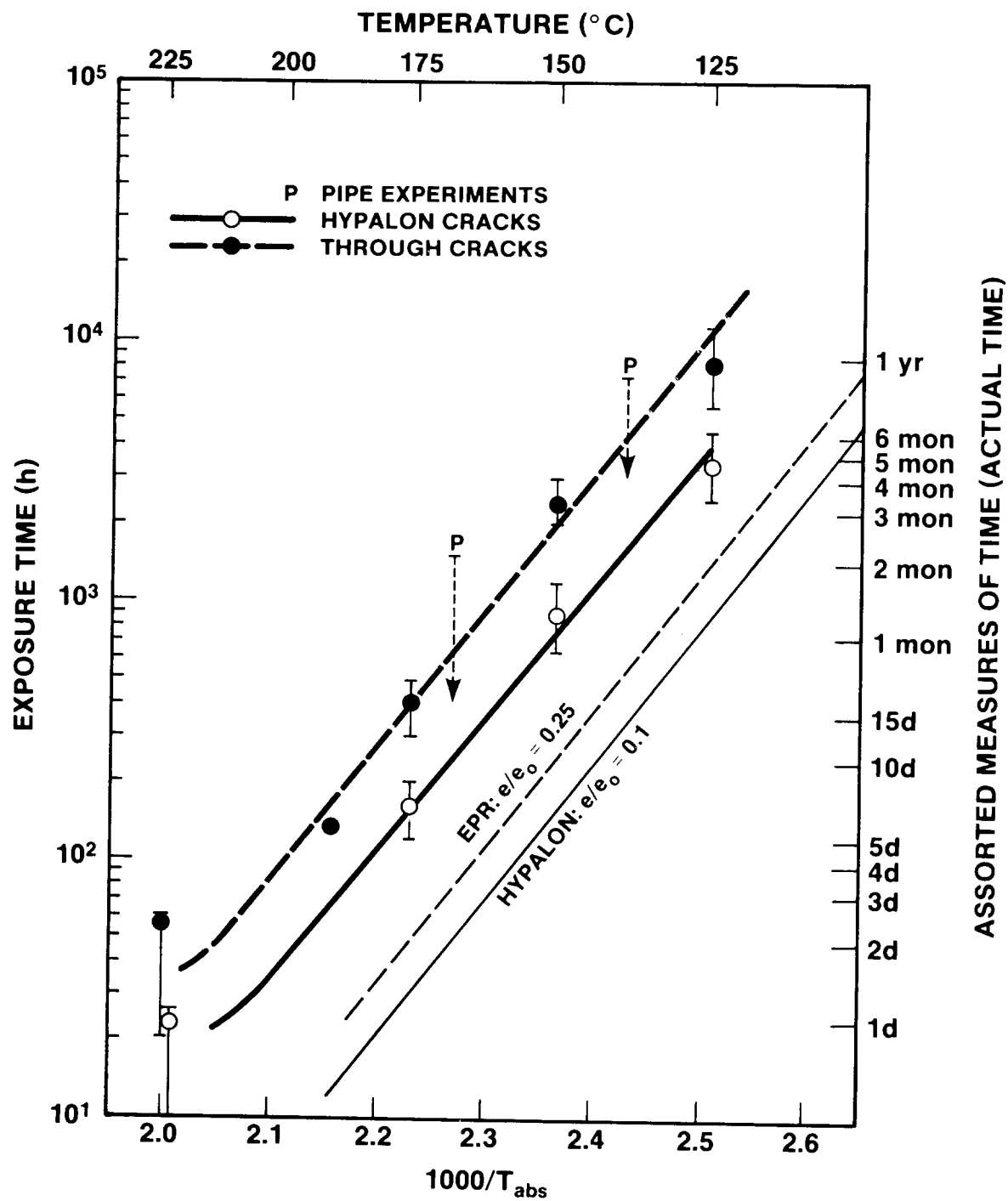
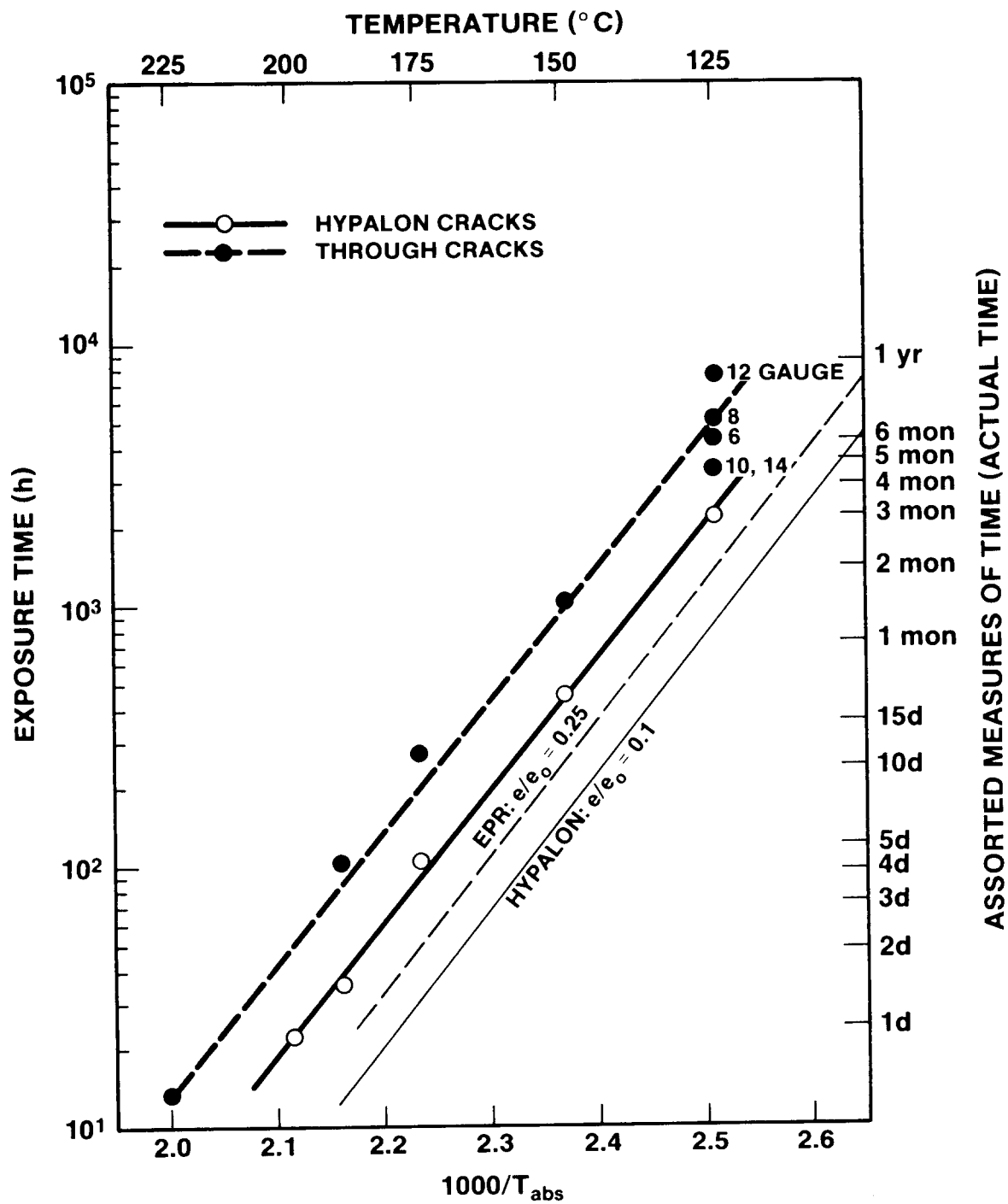Figure 30: First Occurrence of "No Outside Stress" Cracks

Figure 31: First Occurrence of Cold Bending Cracks

V. CONCLUSIONS AND PROJECTIONS

Circuit failure of EPR-Hypalon cables in a nuclear reactor plant
environment has been investigated, both for operating and for accident
conditions. Due to the complexity of the problem, the experimental work
had to be limited; one cable design and only thermal aging was used. It
is assumed that (a) the cables are operated within voltage and current
ratings and (b) no severe flaws (such as cuts through insulation) exist.
High statistical fluctuations exist in the measurements, caused by
nonuniformities in composition and in internal and external geometry.
The essential results of the investigation may be summarized as follows:

A. Short-Term Behavior

The observations extend over periods up to three years. A basic
understanding of deterioration processes and of some beneficial phenomena
has been obtained. It makes it possible to extrapolate the observations
to, say, twice the observation period, i.e., about five years. We find,
for total cable failure (i.e., a short circuit):

1. Purely electrical failure, i.e., internal field breakdown or
   thermal runaway in a cable, whose geometry has not changed (no
   bends, no cracks) is not of concern for signal cables. For
   standard EPR-Hypalon AWG 12 power cables the systems temperature
   must not exceed 200°C, where runaway becomes possible. Thicker
   cables (AWG 6 to 10) are relatively rare and will behave similarly
   at a medium voltage. High voltage cables are included in above
   statement except for very long (years) immersion in water, where
   treeing is not excluded by our experiments.

   Of concern are cable ends, which during high humidity periods of
   an accident may suffer surface contamination breakdown (tracking)
   for voltages between 100 and 1000 volts.

2. Creep shortout may occur in cables hanging over a corner and
   stressed by the weight of the overhanging part. Creep shortout is
   observed only at very high temperatures (> 175°C) in combination
   with very high stress (> 500 lb./sq.in.), where failure will occur
   in a short time (hours or days). Temperature and radiation
   hardening of the polymers (and other phenomena identified in
   Section III) slow down creeping with increasing exposure time.
   The critical stress observed (~500 psi) implies different
   lengths of critical overhang for different cable (and wire)
   sizes. The scaling can be done with the help of Equation (2),
   Section III.

3. Crack failure is, in principle, a phenomenon of lesser concern, as
   in addition to cracks extending through to the wire, considerable
   and long-term moisture is needed to permit or cause breakdown. In
   plants with sealed conduits and circuit boxes crack failure will
   not occur. If we consider the mere appearance of a through crack
   unacceptable, the phenomenon is important. Even in externally

unstressed cables lying horizontally in a conduit, cracking starts
fast at high temperatures. The first through cracks in our test
cables showed up in 12 days at 175°C and multiplied rapidly with
increasing time.

Crack appearance correlates well with the appearance of a certain
critical strain to break factor ($e/e_0 \simeq .03$), as indicated in
Figure 32, an extended composite of data presented in Figures 30
and 31. If the exposure temperature does not exceed 100°C,
complete cracks will not appear in 5 years.

It is of interest to note that at around half the exposure time
needed for "unstressed" complete cracks, the cable will, after
cooling, be prone to cracking during maintenance.

B. Radiation Influence

The data for the above work have been taken with temperature aging only.
In certain cases the results have to be adjusted, if substantial
radiation aging is present.

In Section II (purely electrical failures) it has been shown that the
presence of even large dose rates increases cable conductivity little, if
compared with temperature enhancement. Electrical runaway is therefore
not influenced. Radiation aging over long times is shown to have very
small and often beneficial effects on breakdown properties.

For creep assessment, additional radiation aging will enhance materials
hardening and is therefore beneficial.

The theoretical description of crack formation shows that only the strain
to break ratio e/e_0 is of importance, not how it is caused (i.e., by
thermal or by radiation aging or by both). But additional radiation will
shorten the time needed for a certain degree of embrittlement, and in the
graph of Figure 32 the "cracking lines" (e.g. a) have to be lowered (line
b). The distance a-b has to be experimentally determined; it should be
negligibly small for the normal radiation background in a reactor.

C. Extrapolation

It is impossible in principle to extrapolate statistical data from a few
years' observations to the expected reactor life of 40 years. We are,
however, mainly interested in the importance of the data for the safety
of the reactor. Two established facts are helpful for that assessment:
Firstly, a basic understanding of the deterioration phenomena of concern
has been developed, no indication of sudden increase in damage has been
found and is to be expected, and a reasonable extrapolation as well as an
assessment of damage changes with changes of the environmental parameters
is possible and justifiable. Secondly, real situations of concern have
been found to occur fast only at high environmental stress, viz.
high-temperature. During the life of a reactor these situations
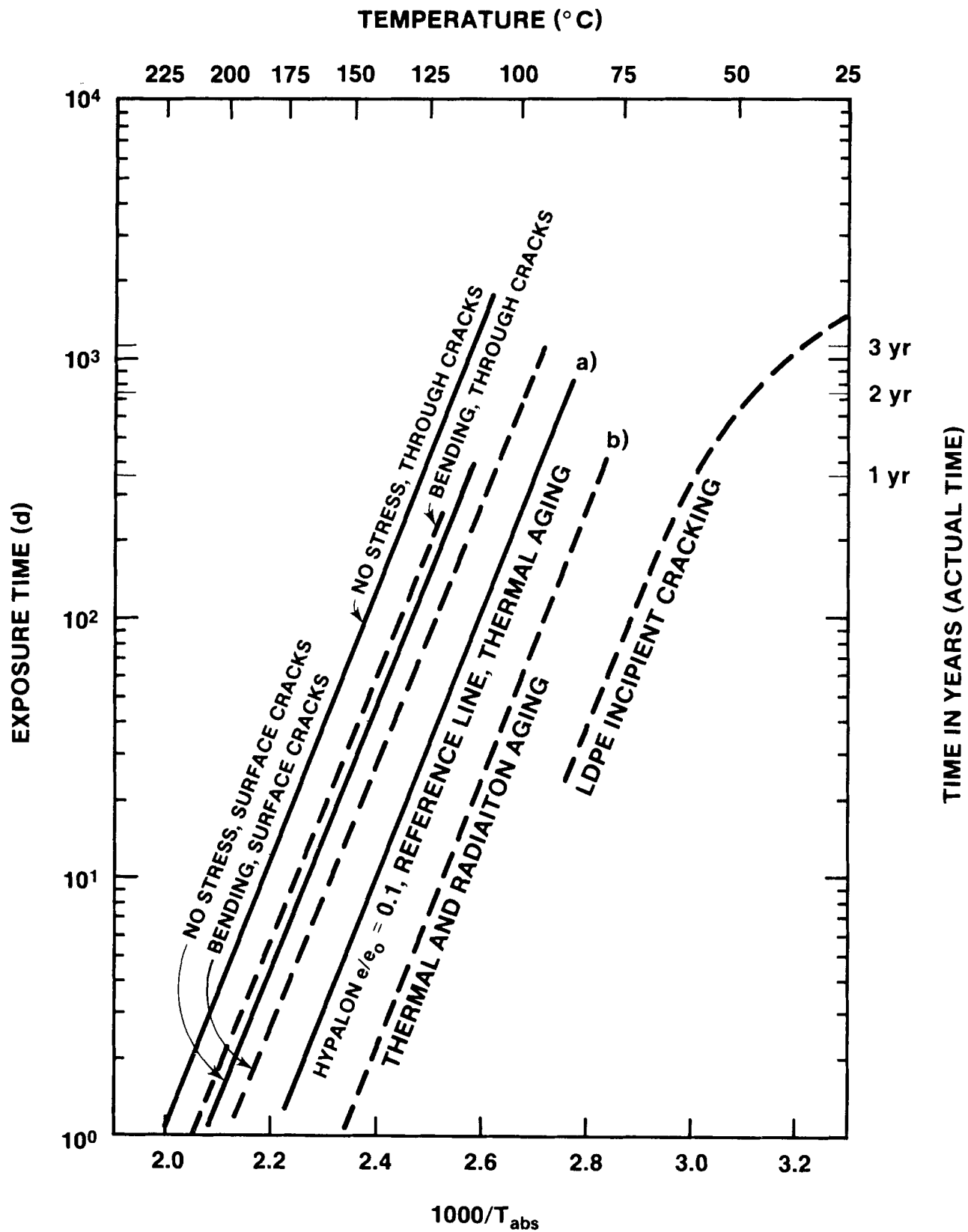
Figure 32: Crack Statistics Summary

occur only rarely and for times of days (accident, circuit breaker failure). Normally the temperature is below 80°C, and radiation flux is at worst of the order of 200 mR/hr.

It follows that what is of interest for long times are actually low temperature and low radiation deterioration data. Our experiments (e.g., Figure 14, 75°C data points, Figures 30 and 31, and room temperature measurements not specifically reported) show that deterioration is far too small to be of concern or that no deterioration could be detected in 3 years. Some evaluations by Gillen and Salazar[28] extend to 15 years: Cables, aged at low temperature (e.g., 48°C) and low radiation (120 mR/hr) were taken from a reactor, which had not operated (no radiation) for half the exposure time. No mechanical deterioration (e.g., in e/e_0) had occurred.

Theoretically one now has to worry about a kind of synergistic time effect: The long-term, low environmental stress aging may cause the polymer system to respond more severely to sudden high stress (heat spike) than our measurements for a non-preaged system show. Our understanding of the phenomena certainly predicts the opposite for creep shortout, but may have some effect on cracking.

Actually, preaging may diminish the generation of surface cracks. In Table VII cracks under stress are listed. In Column IV of this table five measurements with cables exposed to a brief heat spike before aging are compared to 30 measurements taken under steady rising temperatures. Average crack width and number were much lower than for the other test samples, and no through cracks were observed.

The cracking data presented appear to be challenged in literature: Gilroy[29], at the Bell Telephone Laboratories, has measured the incipient occurrence of microscopic surface cracks (not through cracks) for low density polyethylene (not the much tougher Hypalon). His data are entered on the right side of Figure 32; the measurements extended through 4 years. The curve shows bending in the unfavorable direction. The data are not applicable to the present system; however, the 15-year measurements referred to above would have had to show a measurable decrease in e/e_0.

With the above argument, it is justifiable to state that the shortout criteria presented in paragraph A are not materially changed – and sometimes mitigated – by long term exposure.

D. Conclusion

EPR-Hypalon reactor cables, and those of similar polymeric composition are highly reliable components. At low temperatures and low continuous radiation, no failures are to be expected if current and voltage ratings are not exceeded. High temperatures may cause creep shortout, but only for very large overhangs, not compensated for by tieing. For

unsealed conduits, high temperature-high humidity conditions may lead to crack shortouts.

VI. RECOMMENDATIONS

The admitted variation of cable properties both for the EPR-Hypalon family, and particularly for other cable compositions, may change the parameters we have identified above for safety assessment. As was discussed, there is little concern for the purely electrical parameters, in this area present cabling is specified and used very conservatively. It is, however, recommended to add a determination of the critical stress, above which creep shortout may occur, to present qualification tests. As evident from Section III discussions, critical stress can be found in relatively short time and with tolerable effort. As mentioned (and already generally being done), it is also necessary to determine the strain to break ratio (for each design and radiation environment) to assess cracking.

Other recommendations resulting pertain to circuit and systems layout and are often self-evident and occasionally already implemented: The avoidance of overloads, generally required, should be specially mentioned as (long) heat spikes may have severe secondary effects. The conduit/connection box system should be sealed to prevent malfunction caused by cable cracks. Sharp bends, already forbidden by many installation codes, have to be avoided even more carefully in the light of our results. Long vertical overhangs, if unavoidable, should be tied back for stress relief, and/or the curvature radii for overhang supports should be made large.

REFERENCES

1. O. M. Stuetzer, Status Report: Correlation of Electrical Cable Failure with Mechanical Degradation, Sandia National Laboratories, Albuquerque, New Mexico, NUREG/CR-3623, SAND83-2622, April 1984

2. O. M. Stuetzer, Status Report on Reactor Cable Breakdown Correlation Study, Internally published, Sandia National Laboratories, Albuquerque, New Mexico, January 1983.

3. L. D. Bustard, et al, The Effect of Alternative Aging and Accident Simulations on Polymer Properties, Sandia National Laboratories, Albuquerque, New Mexico, NUREG/CR-4091, SAND84-2291, May 1985.

4. E. W. Bennet, ITT Suprenant Division, personal communication.

5. F. V. Thome, Testing to Evaluate Synergistic Effects from LOCA Environments, SAND78-0718, April 1978.

6. C. Hosticka, et al, Qualification of Cables to IEEE Standards, IEEE Transactions on Nuclear Science, NS-27, Vol. 1, February 1980.

7. IEEE Standard 383-1974, "Standard for Type Test of Class 1E Electrical Cables, Field Splices, and Connections for Nuclear Power Generating Stations."

8. R. Grüb and B. Langeset, "Voltage Capability of EPR Power Cables," CERN/EF/Beam Tech. 82-1, January 1982.

9. M. Asaka, et al, "Radiation Resistance of Plastic Materials for Cables, Part 2," Fujikura Densen Giho, Vol. 48, 1973.

10. L. Corbelli and F. Tonioli, "Ethylene-Propylene Elastomers as Insulators in Electrical Technology," Kunststoffe, Vol. 30, Nr. 2/1977. (In German).

11. H. St. Onge, et al, "Research to Determine the Acceptable Emergency Operating Temperature of Extruded Dielectric Cable," EPRI Report EL 983, November 1978.

12. I. Kuriyama, et al, "Effect of Dose Rate on Degradation Behavior of Insulating Polymer Materials," IEEE Trans. on Electrical Insulation, EI-14, October 1878.

13. L. D. Bustard, The Effect of LOCA Simulation Procedures on EPR Electrical and Mechanical Properties, Sandia National Laboratories, Albuquerque, New Mexico, NUREG/CR-3538, SAND83-1258, October 1983.

14. T. Seguchi, et al, "Dose Rate Effects on Chemical and Mechanical Properties," Takasaki Radiation Chemistry Research Establishment, JAERI, undated.

15. Y. Murata, et al, "Electrical Properties Under Radiation and Steam Environment," Sumitomo Electric Industries, EIM-79-91, NE-79-13, 1979.

16. R. W. Sillars, "Electrical Insulating Materials," Peregrinus, London, p. 65 ff, (1973).

17. G. C. Derringer, et al, "Basic Study of the Aging Process," (Review Report), Batelle Institute, Columbus, November 1979.

18a. S. Kronenberg, et al, "Gamma Ray Induced Charge Buildup in Insulators," Army Electronics Command, Fort Monmouth, AD 786655, September 1974.

18b. W. H. Buckalew, F. J. Wyant, G. J. Lockwood, Response of Rubber Insulation to Monoenergetic Electron Irradiation, Sandia National Laboratories, Albuquerque, New Mexico, NUREG/CR-3532, SAND83-2098, November 1983.

19. O. M. Stuetzer, <u>Electrical Insulators in a Reactor Accident Environment</u>, Sandia National Laboratories, Albuquerque, New Mexico, NUREG/CR-1682, SAND80-1957, January 1981.

20. J. D. Ferry, "Viscoelastic Properties of Polymers," Wiley, New York (1970).

21. L. C. E. Struik, "Physical Aging in Amorphous Polymers," Elsevier, Amsterdam (1978).

22. K. T. Gillen, personal communication.

23. C. J. Aloisio and G. S. Brockway, "Thermomechanical Reliability of Plastics," International Conference on Plastics in Telecommunications 2, London, September 1978.

24. J. Reaugh, Science Applications, Inc., personal communication.

25. J. F. Colwell, et al, "Evaluation of Radiation Damage Mechanisms in a Reactor Power Cable", IRT Corporation Report IRT0056-002A, August 1978.

26. K. T. Gillen, R. L. Clough and N. J. Dhooge, <u>Density Profiling of Polymers</u>, "Polymer," in press.

27. L. C. E. Struik, "Physical Aging in Amorphous Polymers," Elsevier, Amsterdam (1978). (See pg. 157.)

28. K. T. Gillen and E. A. Salazar, letter to United Nuclear Industries, Inc., January 23, 1979.

29. H. M. Gilroy, "Thermal Oxidative Cracking of Polyethylene Insulation," Bell Telephone Labs, 1974.

APPENDIX

ANALYSES OF MECHANICAL FAILURE OF ELECTRICAL CABLES

REPORT OF ACTIVITIES UNDER SNLA CONTRACT 50-9536

24 September 1984

Submitted by
J. E. Reaugh
Science Applications, Inc.
4615 Hawkins St. NE
Albuquerque, NM 87109
(505) 345-8444

TABLE OF CONTENTS

LIST OF FIGURES

ANALYSES OF MECHANICAL FAILURE OF ELECTRICAL CABLES

1. INTRODUCTION

This report describes the analyses of two modes of electrical cable failure — insulator cracking and creep short-out. Reports of an ongoing companion experimental program (Ref. 1) describe the test methods and results. In this report, we discuss analysis methods suited to describing the two kinds of experiments, and results that have been obtained.

The approach taken in these analyses is to use simplified constitutive descriptions of the materials to identify and illuminate trends in the experimental results, rather than to develop the complex constitutive models that would be required to describe the detailed behavior of cable insulation and jacket materials during the aging process. Thus the analyses are not intended to be computer simulations of the experiments, but rather analyses of simplified material behavior in simplified geometry under similar loading conditions.

The results of this approach have succeeded in illuminating several of the experimental trends. We present these results with substantial emphasis on the methods used, their limitations, and suggested efforts for further development.

2. STRESS ANALYSIS OF INSULATOR AND JACKET CRACKING

2.1 INTRODUCTION

A sequence of experiments (Ref. 1) was performed on bundles of 10-m long cables. The horizontal layout and mechanical connections were such that the cables were under no mechanical load. The cable bundles were placed in insulated pipes, and held at a steady temperature. After a waiting period that depends on the temperature of the specific experiment, both perpendicular cracks (which run completely around the circumference) and longitudinal cracks (which are parallel to the cable axis) are observed.

It was separately observed that unstressed cables heated for a time-temperature combination exhibit permanent, volumetric shrinkage. Gillen (Ref. 2) has shown that for typical cable insulation materials, the volume change can be positive (swelling) or negative (shrinking). Hypalon, used for the jacket of these cables, always shrinks. For the cables used in the experiments (Ref. 1) both EPR, the insulation material, and Hypalon shrink, although the Hypalon shrinkage is about 1.8 times the EPR shrinkage.

It is also observed in Ref. 1 that there is an ordered sequence of changes with time at all temperatures:

1. There is free slip between Hypalon and EPR, and between EPR and the center conductor.

2. The EPR sticks to the conductor.

3. Hypalon sticks to the EPR.

We performed a stress analysis of a single long cable with permanent volume change to illuminate these results.

2.2 STRESS ANALYSIS

For the stress analysis we make the following simplifying assumptions:

1. Cylindrical symmetry, with the multi-strand center conductor represented as a cylindrical, rigid body.

2. Isotropic elastic materials, although EPR and Hypalon may have different properties.

3. Volume shrinkage or swelling is geometrically uniform, although EPR and Hypalon may have different values.

A-2

4. Thermal expansion strains, which are on the order of
    0.001 are ignored in comparison with permanent volume change
    strains, which may be as large as 0.1.

    The geometry for the stress analysis is a hollow, composite
cylinder. The inner radius (which is the boundry between the
central conductor and the EPR) is denoted a, the Hypalon-EPR
boundary is b, and the outer boundary is denoted c. In the
equations that follow, the radial direction is r, the hoop
direction is Θ, and the axial direction is z.

    Hooke's law for the stress components S is given by

$$S_r = Be_r + \lambda e_\Theta + \lambda e_z - KV$$

$$S_\Theta = \lambda e_r + Be_\Theta + \lambda e_z - KV \tag{1}$$

$$S_z = \lambda e_r + \lambda e_\Theta + Be_z - KV$$

where

$$\lambda = \frac{Ev}{(1+v)(1-2v)} \ ,$$

$$B = \frac{E(1-v)}{(1+v)(1-2v)} \ ,$$

$$K = \frac{E}{3(1-2v)} \ ,$$

and E is Young's modulus, v is Poisson's ratio, and V is the
permanent volume change.

    In this geometry,

$$e_r = \frac{du}{dr} \ ,$$

$$\tag{2}$$

$$e_\Theta = \frac{u}{r} \ ,$$

where u is the radial displacement, and e_z is a constant for each
material determined by the boundary conditions.

The equation of stress equilibrium is

$$\frac{dS_r}{dr} + \frac{S_r - S_\theta}{r} = 0.$$ (3)

Combining (1) and (2), and substituting into (3),

$$\frac{d^2u}{dr^2} + \frac{1}{r}\frac{du}{dr} - \frac{u}{r^2} = 0.$$ (4)

The solution of equation (4) is

$$u = Cr + D/r,$$ (5)

where C and D are in general different in the two materials. Thus there are six unknown parameters — C, D, and e_z for materials 1 (EPR) and 2 (Hypalon). The six equations are developed from the boundary conditions.

Condition (1) Free slip:

$$u_1(a) = 0, \quad \text{when } S_{r1} \text{ is compressive}$$

$$S_{r1}(a) = 0 \quad \text{otherwise}$$ (6.1)

$$S_{r1}(b) = S_{r2}(b)$$ (7.1)

$$u_1(b) = u_2(b), \quad \text{when } S_{r1}(b) \text{ is compressive}$$

$$S_{r1}(b) = 0 \quad \text{otherwise}$$ (8.1)

$$S_{r2}(c) = 0$$ (9.1)

$$S_{z1} = 0$$ (10.1)

$$S_{z2} = 0$$ (11.1)

Condition (2) EPR sticks to the conductor:

Equation (6.1) becomes

$$u_{1(a)} = 0 \qquad (6.2)$$

so that tension is allowed at the sticking interface. Other altered equations are

$$e_{z1} = 0 \qquad (10.2)$$

$$S_{z2} = 0 \qquad (11.2)$$

and the other equations are unchanged.

Condition (3) All boundaries stick together:

The altered equations are

$$u_1(a) = 0 \qquad (6.3)$$

$$u_1(b) = u_2(b) \qquad (8.3)$$

$$e_{z1} = 0 \qquad (10.3)$$

$$e_{z2} = 0 \qquad (11.3)$$

and the remainder are unchanged.

The six equations in six unknowns are then solved. A computer program written in BASIC that assembles and solves these equations is presented in the appendix.

For the present example, the baseline properties are taken to be that the elastic properties of EPR and Hypalon are the same, and that the Hypalon volume shrinkage is 1.8 times the EPR volume shrinkage. The geometry, corresponding to the dimensions of the cables tested in Ref. 1 is specified by a=1.15 mm, b=1.89 mm, and c=2.4 mm. For condition (3), EPR sticks to the conductor and Hypalon jacket, the stress components normalized to Young's modulus times the EPR volume change are shown in Fig. 1. In that figure, positive stress is tensile. The equivalent stress, used in mechanics to compare the approach to failure in an arbitrary stress state with failure in uniaxial tension, is given by

$$S_{eq} = \sqrt{1.5(s_r^2 + s_\theta^2 + s_z^2)} \qquad (12)$$

where the stress deviators, e.g. s_r are given by

$$s_r = S_r - (S_r + S_\theta + S_z)/3, \ldots \qquad (13)$$
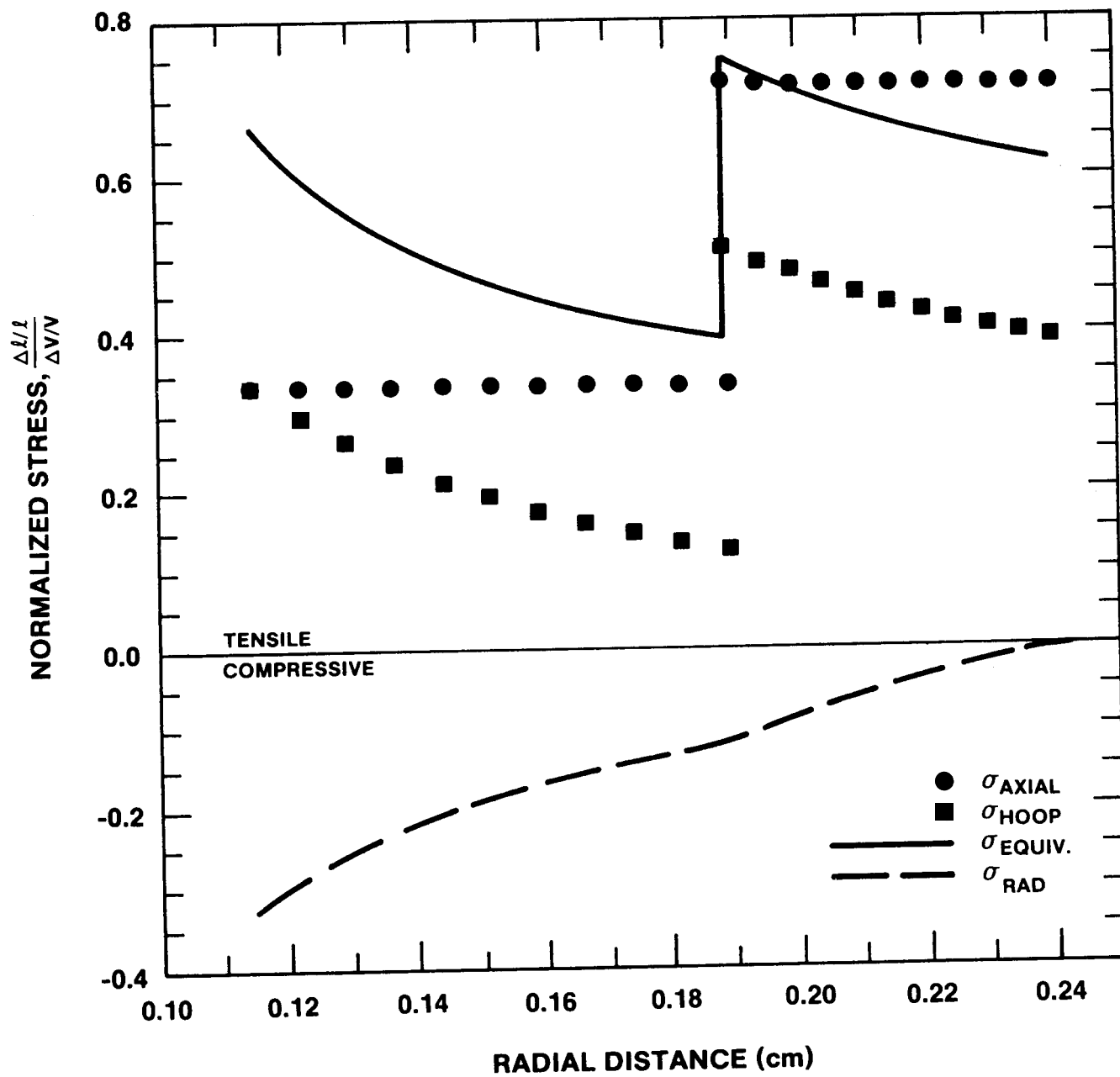
1. Normalized radial stress distribution. Dimensions are in cm. The copper conductor occupies the volume 0. < r < 0.115, EPR occupies 0.115 < r < 0.189, and Hypalon occupies 0.189 < r < 0.24

In a simple tension test, $S_{eq} = S_z$, and $S_{eq}/E = e_z$. Thus the normalized equivalent stress is identical with the equivalent strain normalized by the EPR volume shrinkage.

It is not uncommon that the strain-to-fracture is influenced by the state of stress — the strain is largest when two of the three principal stresses are zero, and smallest when all three are equal (hydrostatic tension). The strain-to-fracture of aged, embrittled EPR and Hypalon under the state of stress indicated in Fig. 1 is unknown. From experience with other materials, it is likely that the the strain-to-fracture, e_f, under these conditions is such that

$$e_f < e$$

where e is the measured strain to fracture in simple tension when aged by the same time-at-temperature condition. Aging curves for these and similar insulation and jacket materials are frequently presented as the ratio e/e_o vs. time, where e_o is the strain-to-fracture in uniaxial tension of the unaged material. For EPR and Hypalon, e_o is about 3.5. Although we present the results of these analyses as the ratio e/e_o for comparison with aging curves, it should be noted that the discussion above suggests that failure may occur sooner than the ageing time corresponding to that ratio.

Taking the EPR volume shrinkage to be 20%, perpendicular cracks would appear in Hypalon when it has aged enough that $e/e_o = 0.04$, longitudinal cracks when $e/e_o = 0.03$. Perpendicular and longitudinal cracks would appear in EPR when $e/e_o = 0.02$.

Although, as Fig. 1 shows, the maximum tensile stresses are at the inside radii of the two materials, elastic fracture mechanics analysis shows that in this geometry for these stress distributions, both kinds of cracks are unstable. That is, if a crack starts, it will propagate to a boundary without requiring additional stress or aging.

If, as seems to be the case experimentally, the Hypalon cracks first, we argue that perpendicular cracks, which are driven by the highest tensile stress in EPR at the Hypalon boundary, are more likely to be cracked through to the center conductor than are longitudinal cracks. A detailed analysis of the influence of a crack in Hypalon on the stress state in EPR has not been performed.

We additionally performed a sequence of calculations to vary Hypalon properties relative to EPR. Figure 2 shows the relatively minor effect of Hypalon's Poisson's ratio, and Figure 3 shows the relatively minor effect of Hypalon's Young's modulus. Finally, Figures 4-6 show normalized stress at the interfaces as a function of the ratio of Hypalon volume change to EPR volume change for EPR expanding as well as shrinking. These facts make the present analysis more generally useful.

Although essentially all stress in EPR is compressive when the EPR expands, one cannot conclude that through-cracks are impossible. A more detailed analysis of the stress redistribution caused by Hypalon cracks should be performed to determine if there are conditions that would permit through-cracking.


2.3 SUMMARY

When both EPR and Hypalon shrink, tensile stress is developed that will promote cracking provided that the materials have embrittled sufficiently. Assuming 20% volume shrinkage for EPR, 36% volume shrinkage for Hypalon, and the unaged strain-to-fracture of both materials, $e_o = 3.5$, then the cable will show perpendicular cracks in Hypalon when the Hypalon has aged enough that $e/e_o = 0.04$, longitudinal cracks in Hypalon when $e/e_o = 0.03$, and both perpendicular and longitudinal cracks in EPR when $e/e_o = 0.02$. We note that the state of stress may produce cracking somewhat sooner than the values given. For through-cracks to develop (if Hypalon cracks first) the stress redistribution caused by Hypalon cracks must show a sufficient stress riser that EPR cracking is promoted, thereby continuing the Hypalon crack. Since the EPR axial stress at the Hypalon boundary is much larger than the hoop stress, perpendicular through-cracks are favored over longitudinal through-cracks.

2.4 RECOMMENDATIONS FOR FURTHER RESEARCH

We have not included consideration of the ordered sequence of changing boundary conditions, and the corresponding history of permanent volume change in these materials. A more accurate analysis would take this sequence into account, and compare with e/e_o aging curves for these materials.

We have noted that the presence of a crack redistributes the stress in the uncracked section. The methods of linear elastic fracture mechanics can be used to obtain the stress redistribution. Since the estimated nominal strain-to-fracture is on the order of 15%, however, the inherent small-strain assumption of that discipline is only marginally met. The alternative is numerical simulation. The redistribution of stress is perhaps of even greater importance for assessing the likelyhood of through-
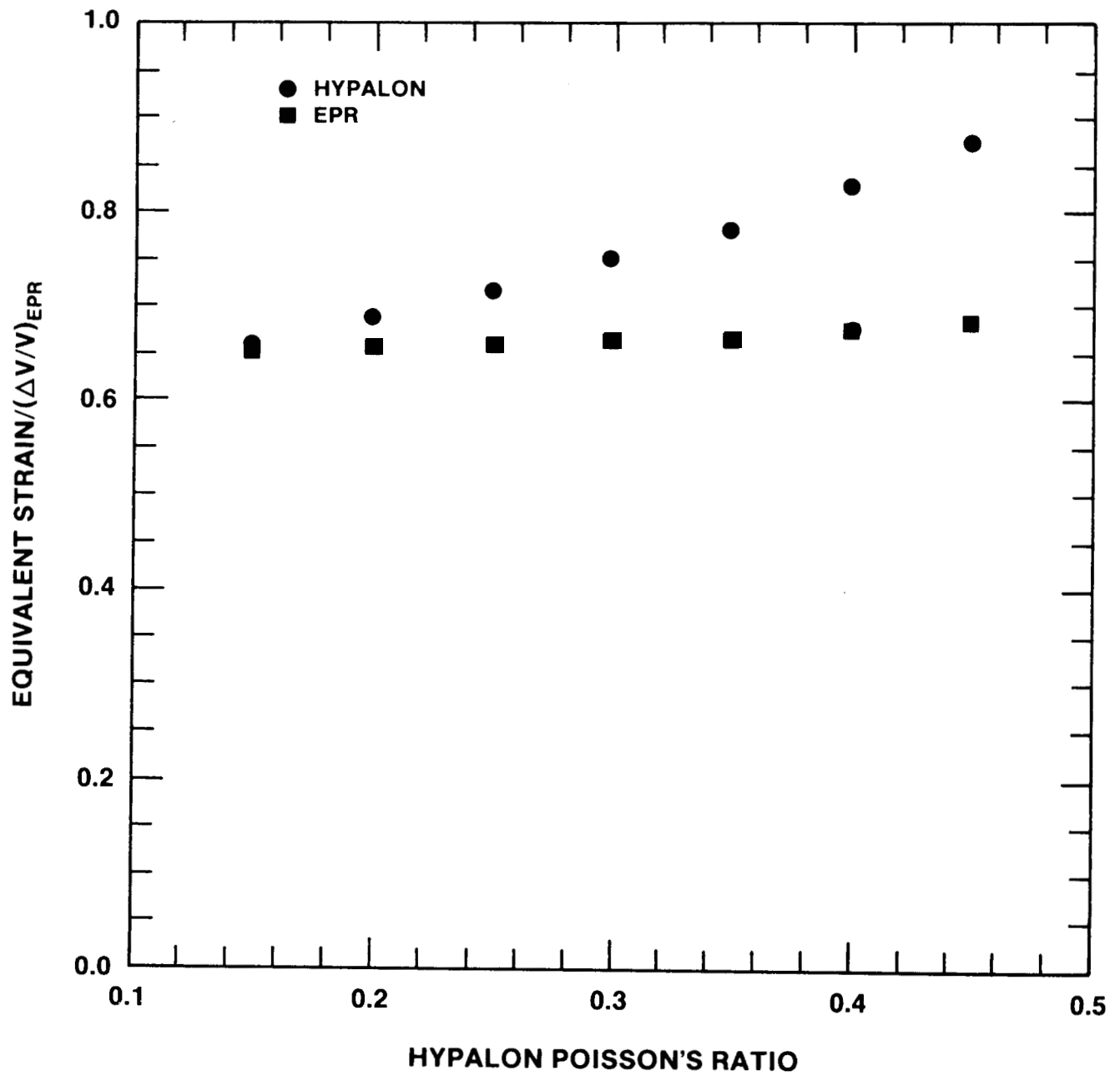
2. Normalized EPR and Hypalon equivalent strain as a function of Hypalon's Poisson's ratio
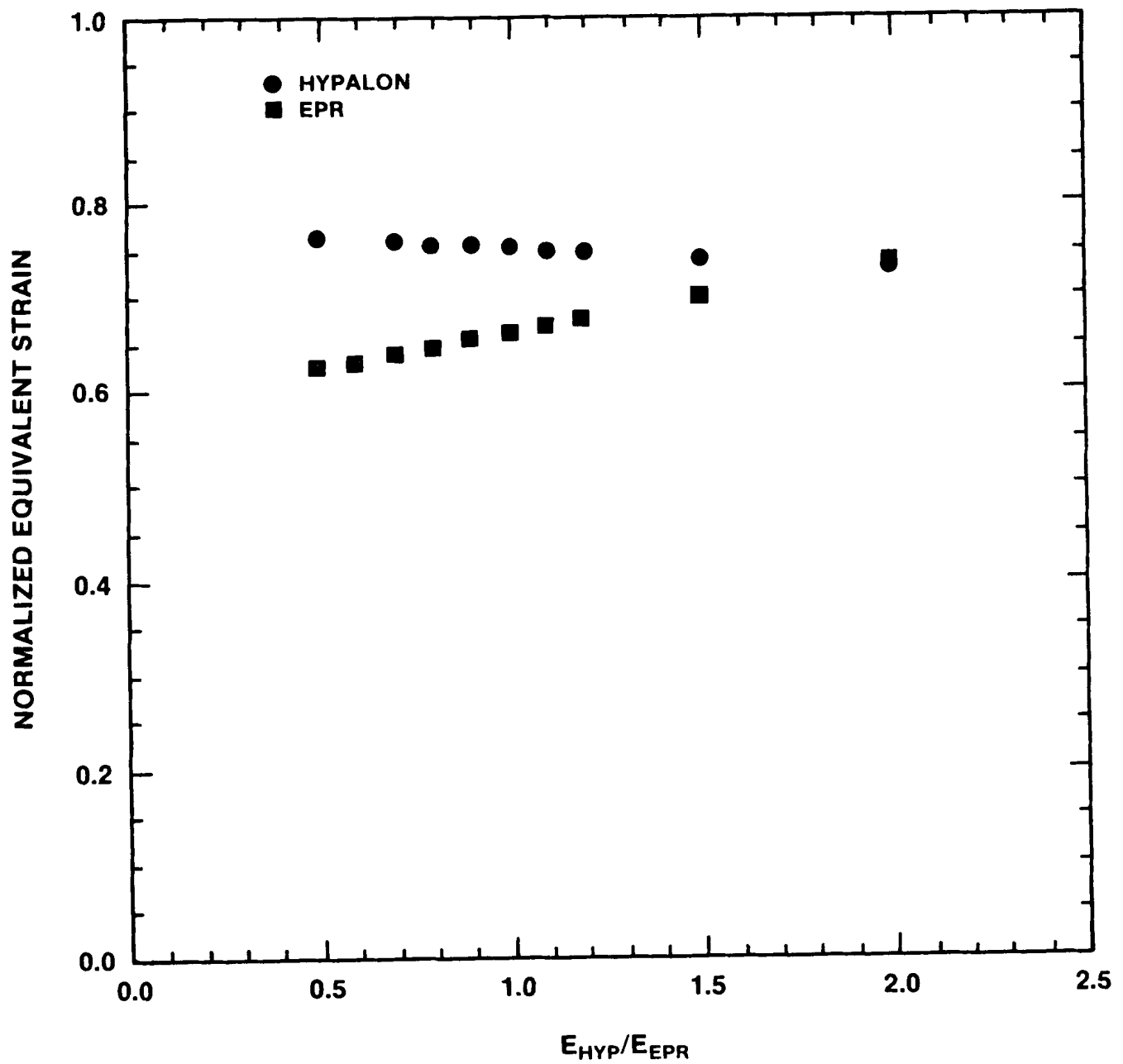
3. Normalized EPR and Hypalon equivalent strain as
   a function of Hypalon's Young's modulus
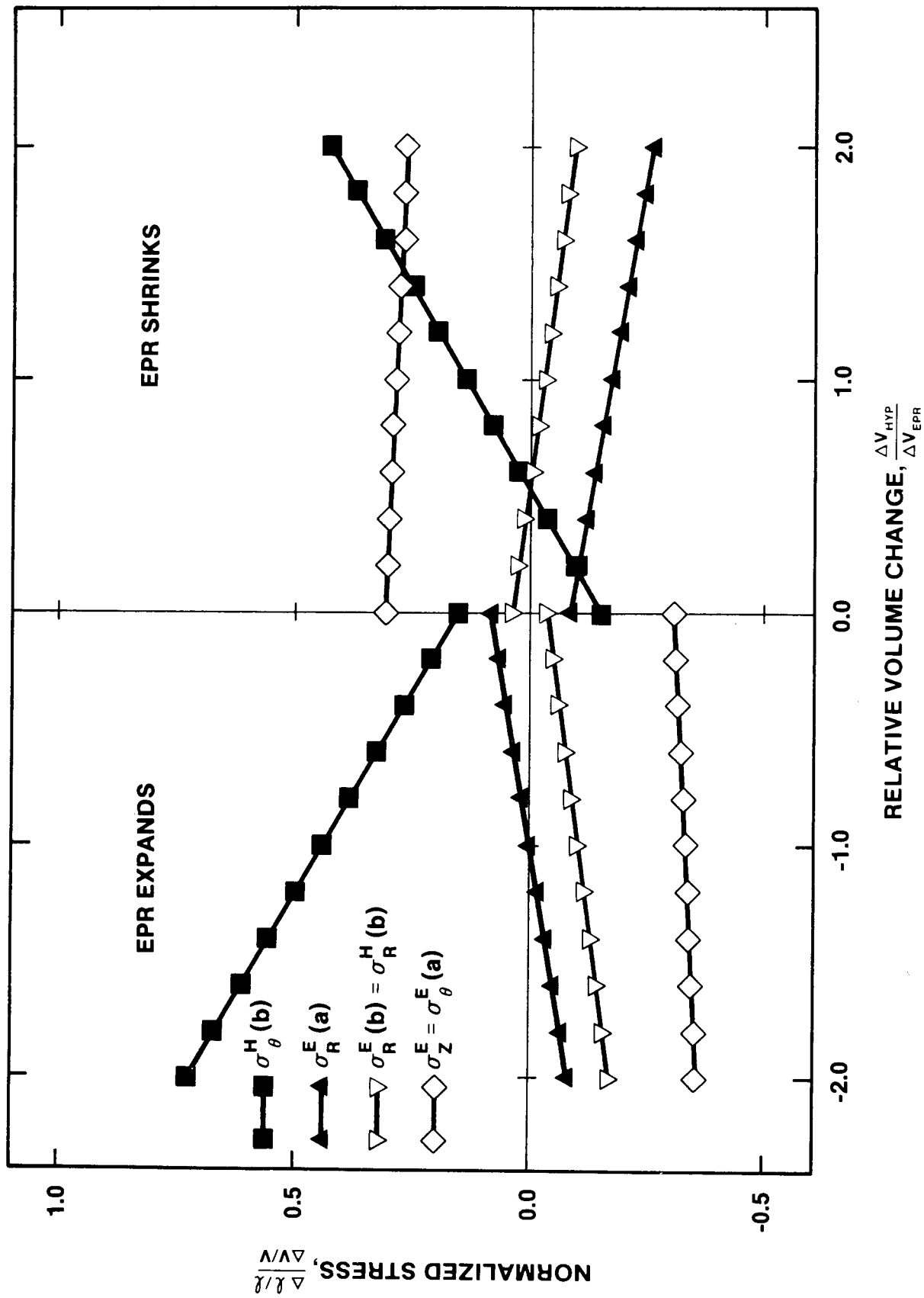
4. Maximum normalized stress as a function of relative Hypalon volume change — Condition (1) All Slip

A-11

RELATIVE VOLUME CHANGE, $\frac{\Delta V_{HYP}}{\Delta V_{EPR}}$

NORMALIZED STRESS, $\frac{\Delta \ell / \ell}{\Delta V / V}$

EPR SHRINKS

EPR EXPANDS

$\sigma_{\theta}^{H}(b)$

$\sigma_{R}^{E}(a)$

$\sigma_{R}^{E}(b) = \sigma_{R}^{H}(b)$

$\sigma_{Z}^{E} = \sigma_{\theta}^{E}(a)$
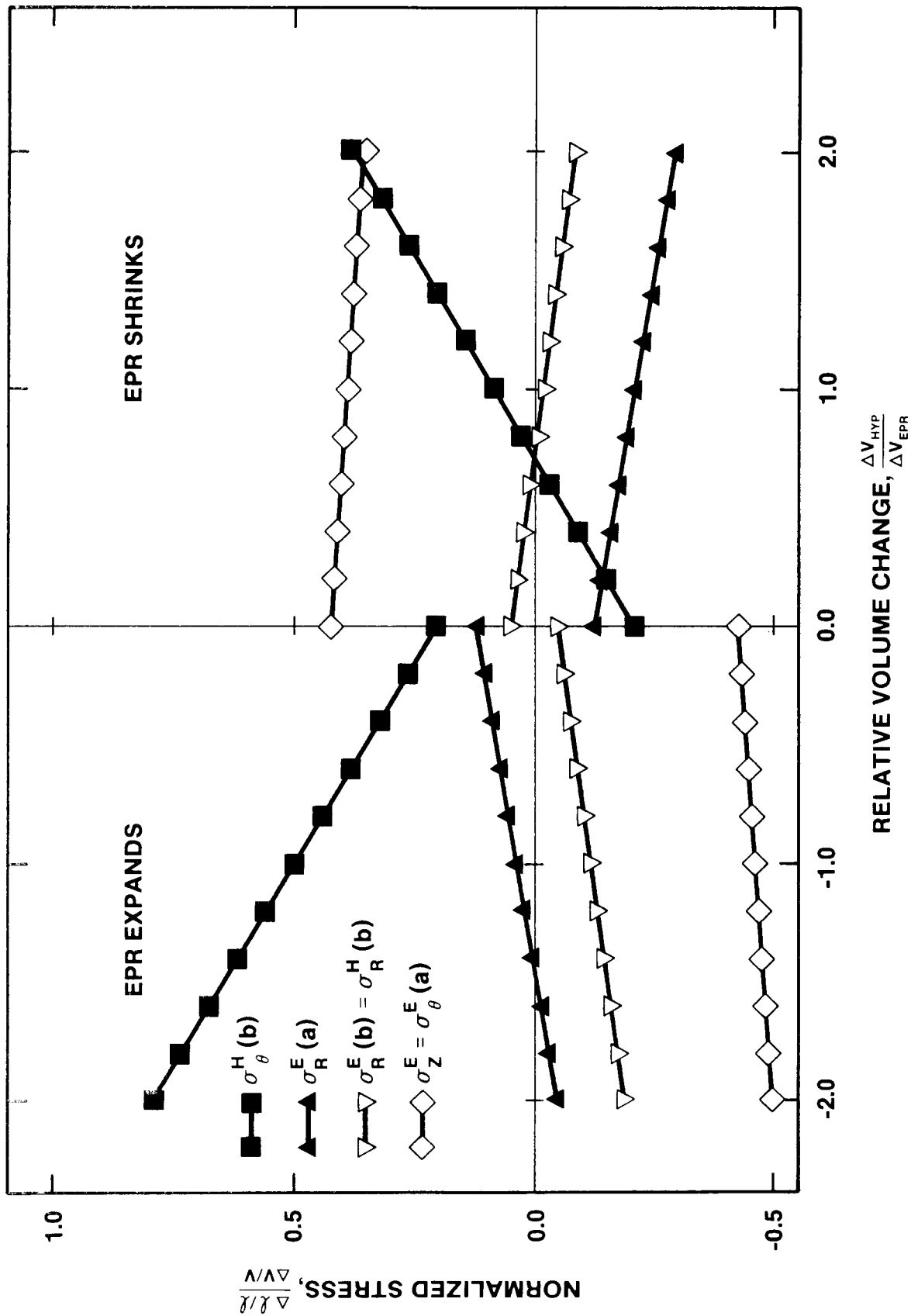
5. Maximum normalized stress as a function of relative
   Hypalon volume change – Condition (2) EPR sticks
   to the conductor.
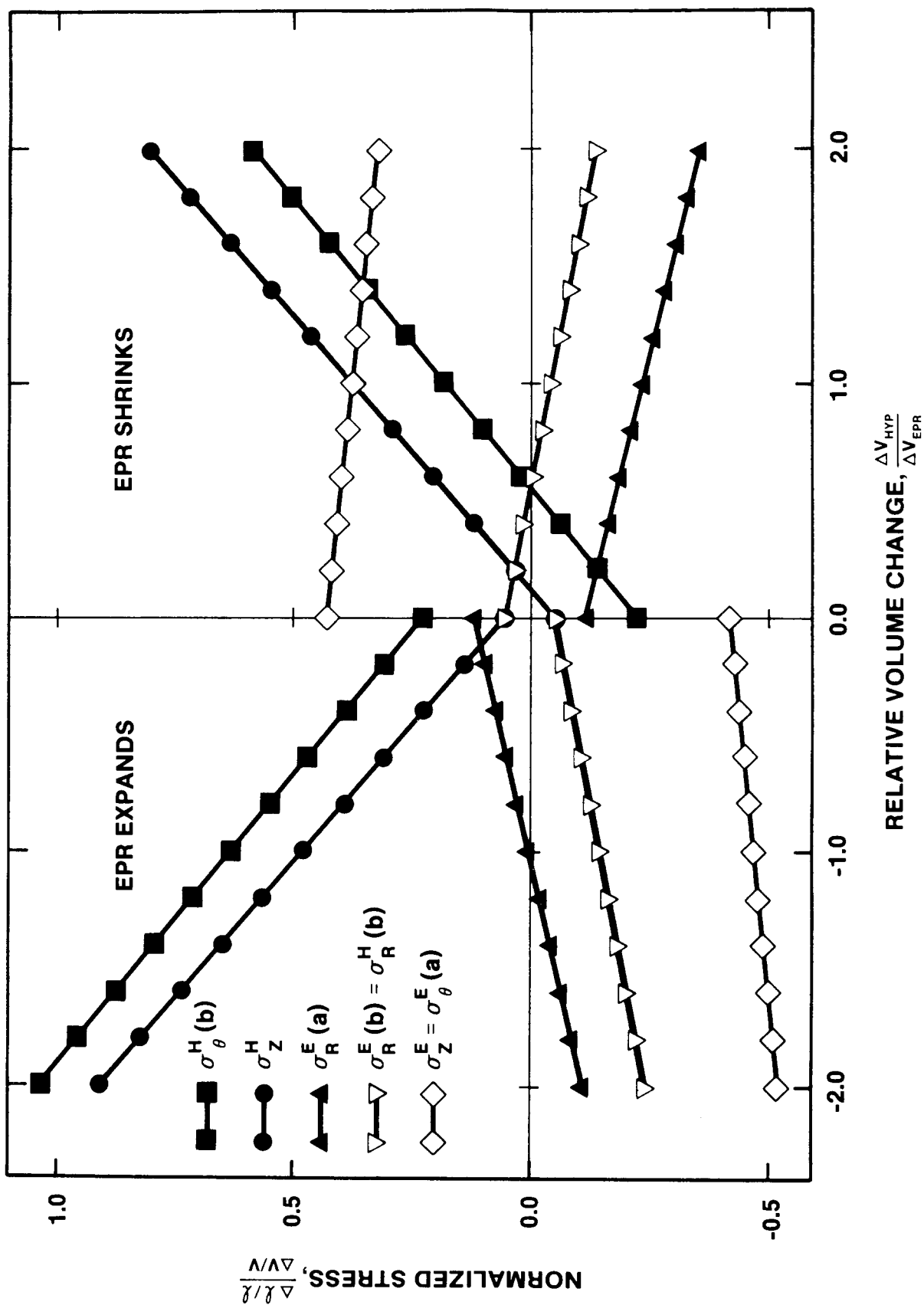
6. Maximum normalized stress as a function of relative Hypalon volume change – Condition (3) All stick

A-13

cracks when the EPR or other insulating material swells instead of shrinks. We note that two-dimensional analyses would be adequate to obtain this stress redistribution for both perpendicular and longitudinal cracks.

All of the preceeding (performed and recommended) analyses have postulated that the volumetric shrinkage is uniform and isotropic. It is clear from these analyses that nonuniform but isotropic volume change would tend to promote cracking earlier in the aging process (provided that the excess shrinkage were in the region of high stress), and that certain (but not all) anisotropies would also promote earlier cracking. Since there has been evidence and theory that both aging and densification are not uniform with radius, the expected time of crack appearance based on aging curves, is only approximate. We would recommend that the stress analysis presented here be generalized to incorporate best-available information on the non-uniformity of volume shrinkage so that quantitative, although approximate, estimates of the aging at which cracks appear can be obtained.

Finally, the unknown property in these analyses is the strain-to-fracture for these materials under multiaxial states of stress. Without independent measurement, we can only present approximate values of e/e_o for comparison with aging curves. Cracking may occur sooner than the indicated time.

3. STRESS AND DEFORMATION ANALYSIS OF CREEP SHORT-OUT

3.1 INTRODUCTION

In the creep short-out tests (Ref. 1) electrical cables are bent into an inverted U, hung over rods of various diameters, weighted, and held at temperature. The cable tensioner is shown in Figure 7, taken from Ref 1. Gradually, with a velocity that depends on temperature, the center conductor moves through the insulation toward the support. See Figure 8, also taken from Ref. 1.

Quasi-static analysis, Ref. 3, had indicated three trends that were both apparently amenable to and required more detailed analysis:

1. The support stress was inversely proportional to the support radius.

2. The support stress was proportional to the square-root of the applied load.

3. The drift of the center conductor was a power-law function of time. For a given support geometry and load, the drift velocity depends on the creep compliance.

Although three non-linear computer simulation programs were thought to be capable of doing these analyses, none was entirely successful. We report both the difficulties we encountered with applying these programs to the problem, as well as the results, for the benefit of further analyses.

3.2 COMPUTER SIMULATIONS

We simplified both the geometry and the material description of the electrical cable. The first geometry, Figure 9, shows the cable cross-section. Only half of the cross-section is calculated, as shown - the other half is represented by a symmetry condition. In Figure 9, the central portion (the conductor) is represented as a rigid body; a vertical downward force is applied through the center of masss. Since the calculation is performed in plane strain, that force is actually a force per unit out-of-plane length.

The actual value of that force was to be determined by a second calculation. In Figure 10 we show the pre-bent cable hanging over a rigid cylindrical bar. Here, too, the calculation is plane-strain, with half the geometry inferred from a symmetry condition. An enlargement near the contact surface of the cable
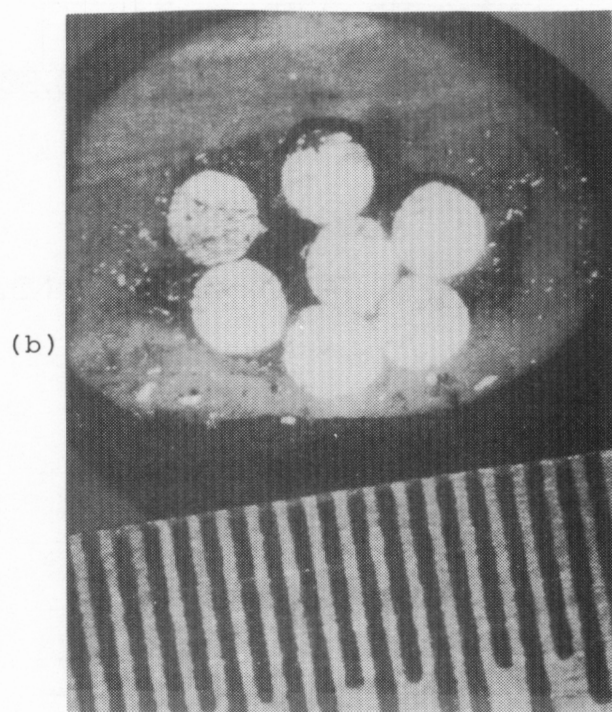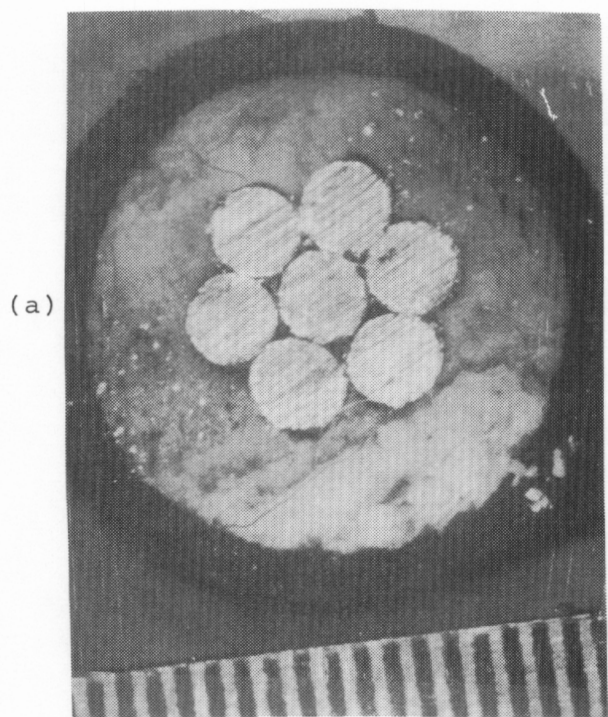
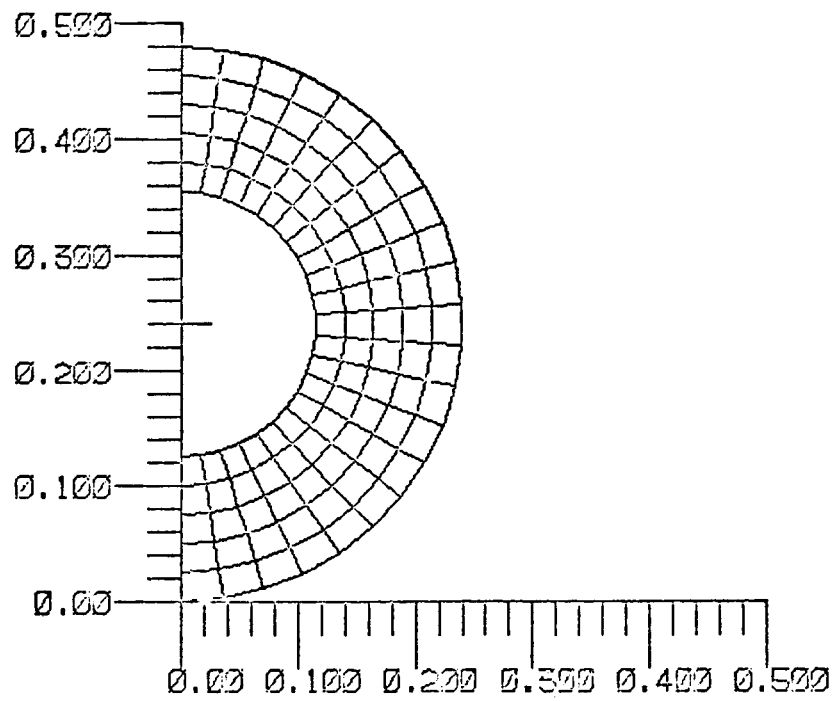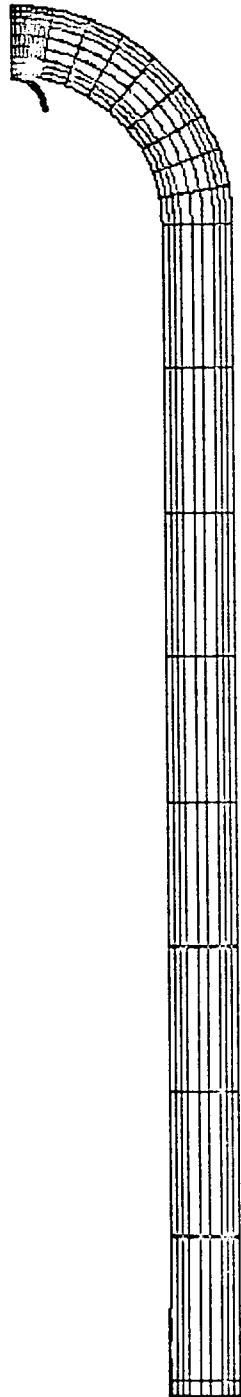Figure 7. Photograph of the Tensioner

(a)

(b)

Figure 8.   Cut Through a New Cable (a) and a Cable Stretched
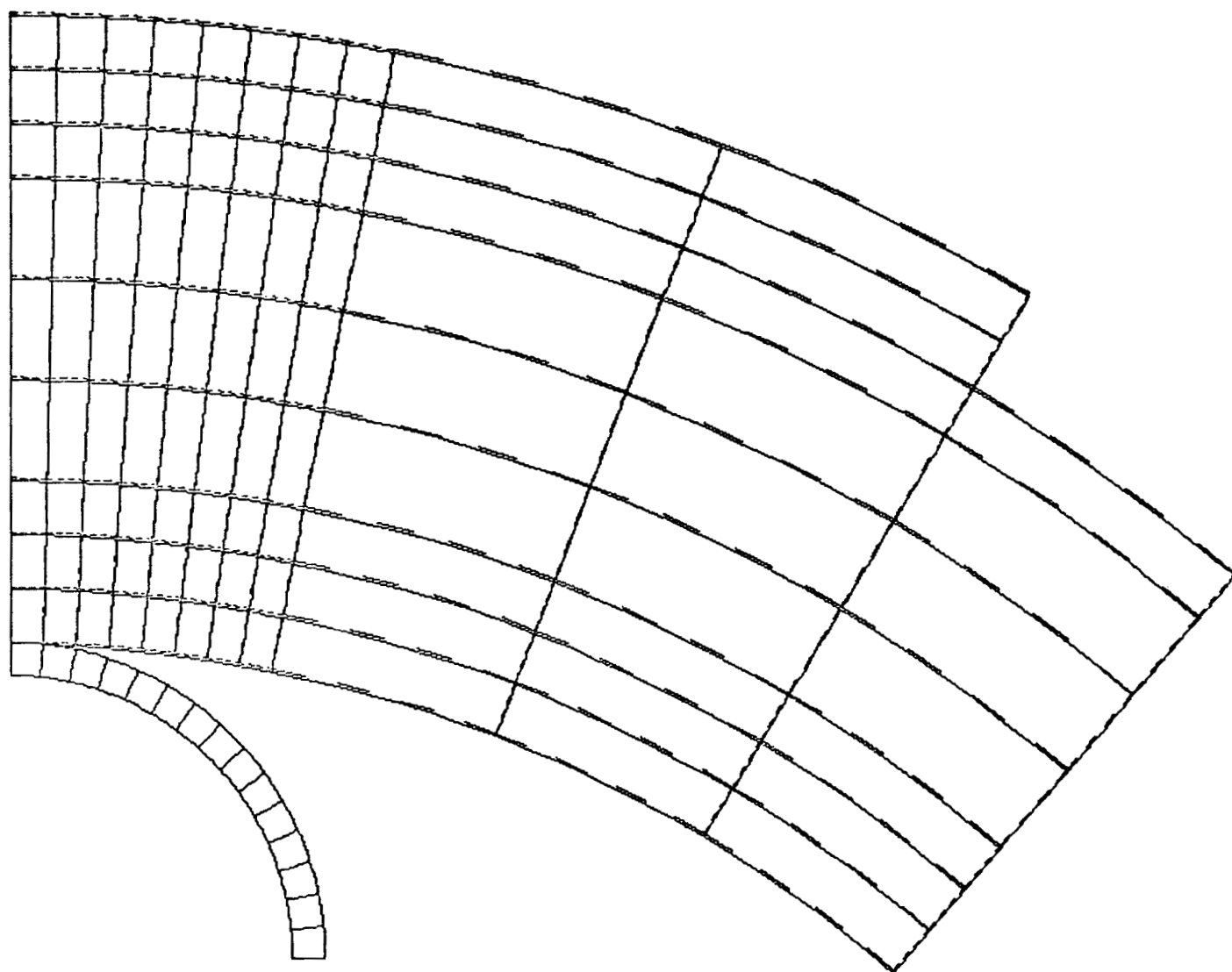by 0.9 kg at 125°C for 1 Day (b)

A-17

INITIAL REPRESENTATION OF GRID NO. 1

9. Geometry of cable cross-section

10.   Geometry of cable in tensioner

11.   Enlargement of cable tensioner geometry

and support rod are shown in Figure 11. The vertical stress at
the plane of symmetry, multiplied by the out-of-plane thickness,
from this calculation was to be used as the vertical force per
unit out-of-plane thickness in the first geometry.

We attempted first to calculate the geometry of Figure 9,
using the force estimated from a previous, analytic calculation
(Ref. 3), assuming that it would be a straight-forward applica-
tion of the computer simulation programs. We found that assump-
tion to be incorrect.

3.2.1 STEALTH Analysis

Although the STEALTH finite-difference code (Ref. 4), writ-
ten by SAI for the Electric Power Research Institute, is an
explicit, time-marching code, it incorporated the features re-
quired for the analysis - creep model formulation, rigid-body
interaction including void opening and closing, and formulated
for large displacements and rotations. It had been previously
used at SNLA for salt creep analyses of the Waste Isolation Pilot
Project, and showed reasonable performance in the Benchmark Pro-
gram.

For creep applications, the Courant condition, which re-
quires that the time step for each computational cycle is less
than the time required for sound to travel across the narrowest
zone, must be sidestepped. The method used is to modify the
inertia term in the equation of motion. More pragmatically, the
mass density is increased, thereby decreasing the soundspeed,
until the total deformation takes place in a large, but computa-
tinally feasible number of cycles, on the order of 10,000 for
this analysis. This method has been used in explicit codes for
many years, eg. Ref. 5.

We were unable to successfully complete the analysis beyond
a total time of a few days. The goal, of course, was 40 years.
The major problem seemed to be involved with the motion of compu-
tational zones adjacent to the rigid body as they slip around and
are effectively extruded from underneath the conductor-insulator
interface. Once an extrusion (sideways) velocity was set up, the
artifically large inertia of the computational cells were arti-
ficially difficult to stop. The resulting severe mesh deforma-
tions resulted in an effective program halt. After several
unsuccessful attempts to continue, the attempt to use STEALTH was
abandoned.

In retrospect, the STEALTH calculation required an artifi-
cial drag to retard the extrusion velocity. Were further anal-
yses attempted with STEALTH, we would recommend that the resolu-
tion be increased, with twice as many zones around the circumfe-
rence (at least near the conductor-insulator interface) and a

velocity-dependent drag on the computational nodes that slip on
the conductor. An alternative to the latter would be an addi-
tional control on the time-step to limit the slip motion in any
cycle to approximately a zone dimension. Although the develop-
ment of an appropriate artifice would be somewhat time-consuming,
as it requires some trial-and-error, we feel that it does have a
reasonable chance of success.

3.2.2   NIKE Analysis

        The NIKE finite-element code (Ref. 6) also has the required
features for these analyses. It was also available on the SNLA
computer system. We were unable to even start the analysis
however. Debug print statements introduced into the code helped
to isolate the difficulty as an apparent bug in the random I/O
package used at SNLA to allow I/O compatability with computer
codes developed at LLNL. Simple attempts to fix the bug were
unsuccessful. The attempt to use NIKE was abandoned.

        It is plausible that with a concerted effort, the NIKE code
could be made to run on the SNLA computer system. Indeed, chan-
ges to the Cray Operating System made subsequent to our attempts
(in the Spring of 1983) may permit the code to run in these
applications without further effort. Since the NIKE code has
been formulated for large-displacement slip on interfaces, in
contrast to ABAQUS, discussed subsequently, the effort required
to set up the analyses and to make the required modifications to
allow for compatability with the ABAQUS creep model would seem to
be worthwhile. We recommend that such an effort be pursued.

3.2.3   ABAQUS Analyses

        The ABAQUS finite-element code (Ref. 7) is liscenced to the
SNLA computer facility. We thought we were successful in analy-
zing both geometries with ABAQUS. We subsequently discovered,
however, that the small displacement assumption inherent to the
interface-slip description of ABAQUS Version 4.4 had compromised
the accuracy of our results. Attempts to use the rigid-body slip
formulation in the development version (Version 5), were unsuc-
cessful.

        We performed two calculations in the first geometry (Figure
9) with 300,000 dyne/cm force to 40 years, and with 600,000
dynes/cm to 10 years. Figure 12 shows the deformation due to the
smaller load at 40 years, and Figure 13 shows the deformation due
to the larger load at 10 years. In those figures, the original
configuration (dashed lines) overlays the deformed configuration
(solid lines).

Gap
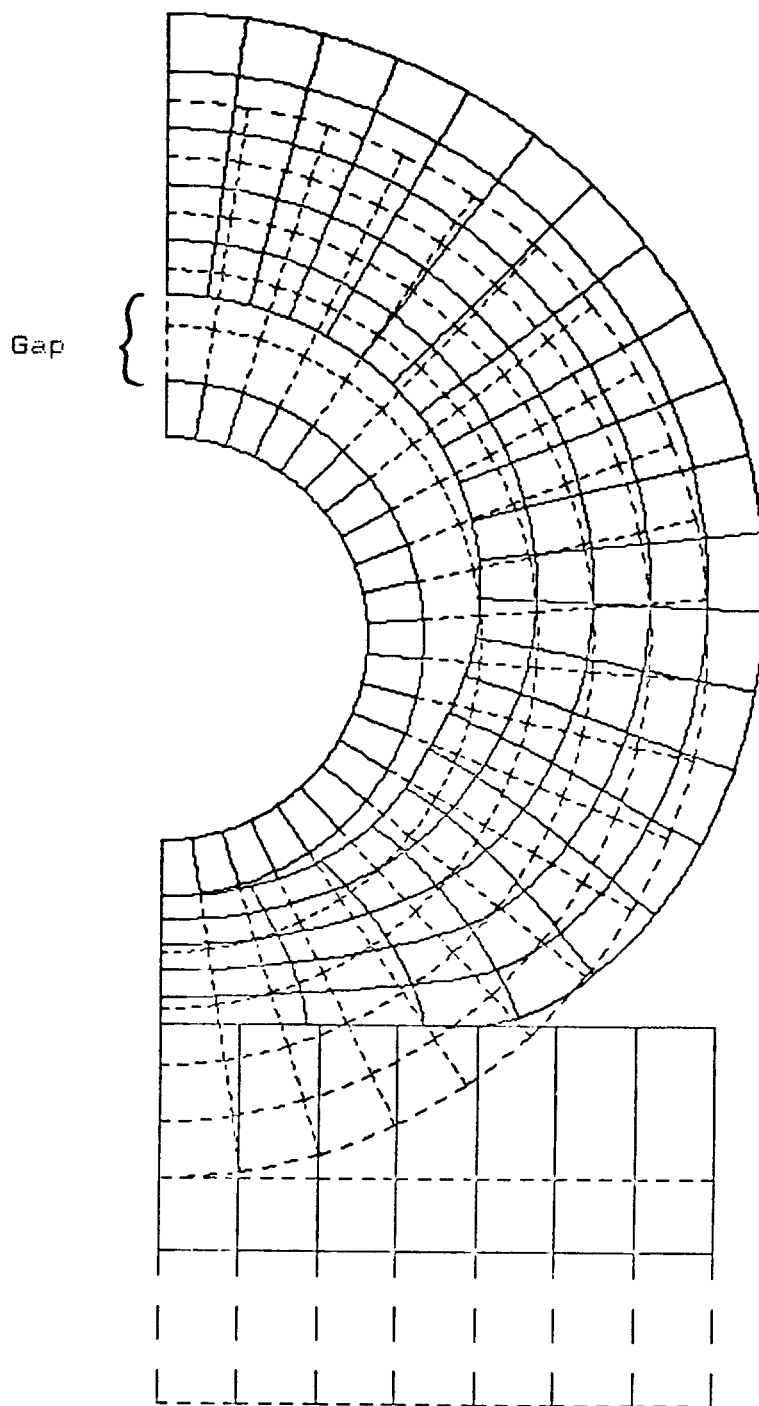
12. 40-year deformation, 300,000 dynes/cm. Note that
     a gap has developed between the conductor and
     insulator, as in the experiments shown in
     Fig. 8

Gap
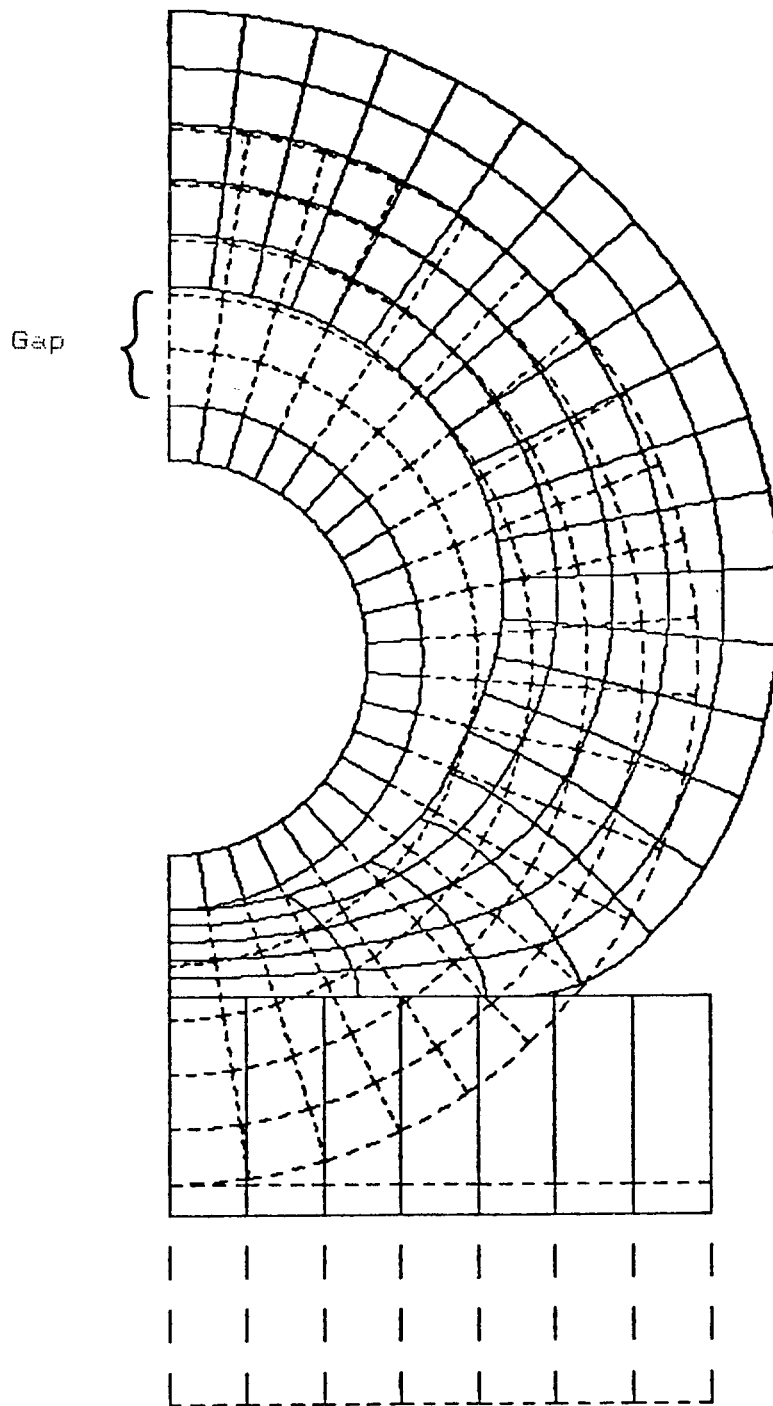
13. 10-year deformation, 600,000 dynes/cm

The creep law used is strain-hardening (as opposed to time-hardening). The creep-strain rate is given by

$$\overset{\cdot}{e}_{ceq} = 9.2 \times 10^{-10} \ S_{eq} \ t^{-0.8188} \tag{14}$$

in cgs units. Here e_{ceq} is the equivalent creep strain, and t is time (sec). This law is consistent with the creep compliance inferred in Ref. 3 from analysis of experiments on these cables. Note that in this analysis, no distinction has been made between the properties of EPR and of Hypalon, and no interface between the two materials has been specified.

The migration of the center conductor for those two analyses is shown in Figure 14 using the same choice of plotted variables as in Ref. 1 (solid lines) and a modified set used in Ref. 3 (dashed lines) that apparently permits straight-line extrapolation. Qualitatively, higher loads produce more severe deformation. Both these calculations use the assumptions of constant force per unit out-of-plane distance, i.e. a two-dimensional geometry, and a constant creep law.

We have to admit that the results are inaccurate. In Figure 12, for example, we note that the element adjacent to and in contact with the center conductor is severely deformed. The algorithm used in ABAQUS for interface-slip/void-opening employs a small displacement approximation. Thus although the insulator appears to have separated from the conductor, there are interference (gap) forces being applied to some of the apparently separated nodes. A development version of ABAQUS (Version 5) does contain rigid-body interaction that relaxes the small-slip assumption. We attempted to use that version to perform these calculations. That attempt failed. The time-step required to permit solution convergence with the rigid-body interaction became prohibitavely small. Apparently the difficulties we encountered with STEALTH are also apparent in ABAQUS, although manifested somewhat differently.

We also performed analyses of the second geometry (Figure 10) to determine the appropriate force. During creep deformation, an increasing area of the bent cable is in contact with the cylindrical rod. As a consequence, the contact stress at the plane of symmetry decreases with time. (See Figure 15 for a close-up picture of the cable at 40 years under a 1-lb. load.) For that 1-lb load, the (vertical) contact stress, S_y, can be well-represented as

$$S_y = 5.11 \times 10^6 \ t^{-0.041} \ dynes/cm^2 \tag{15}$$
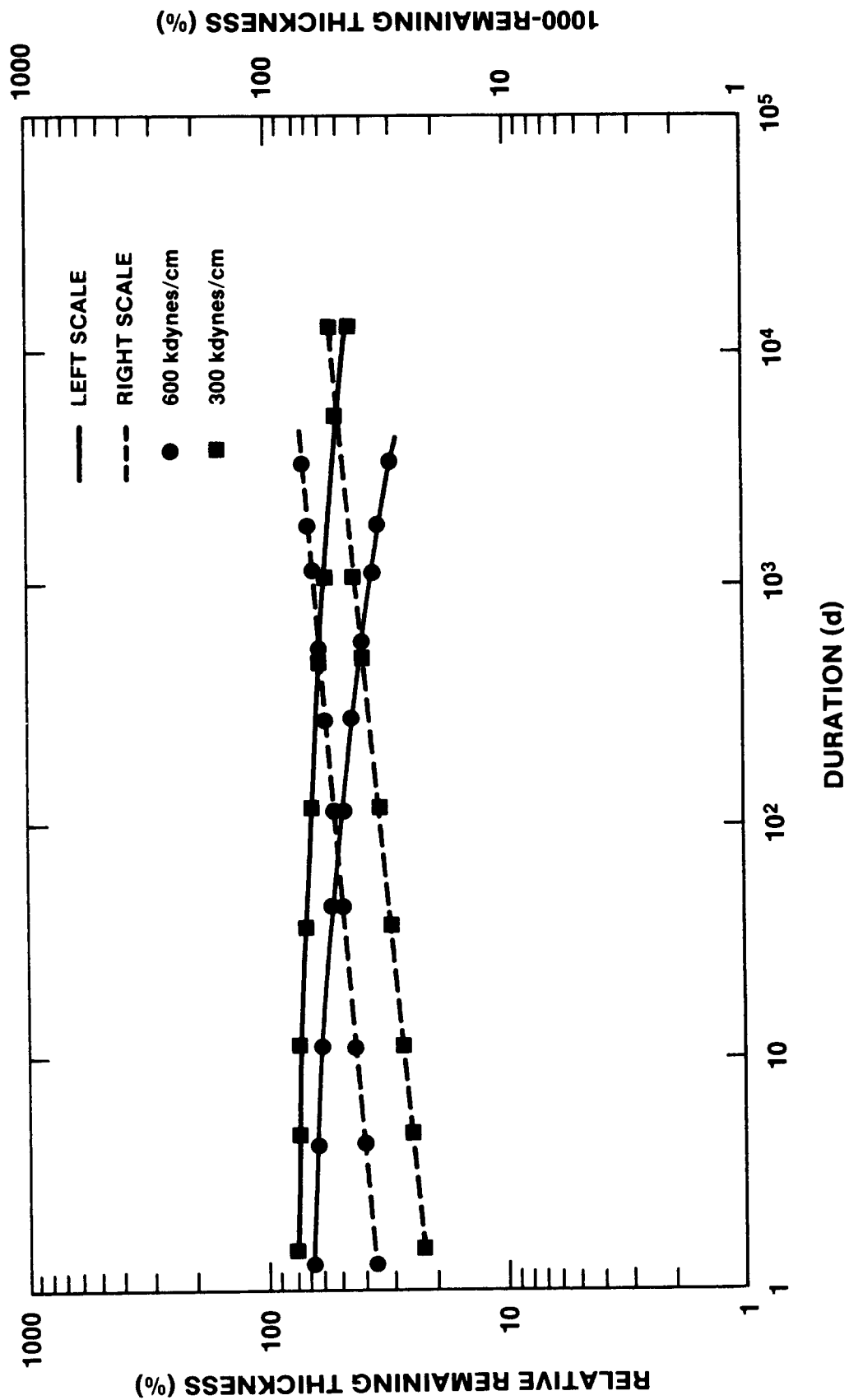
14. Center Conductor Migration
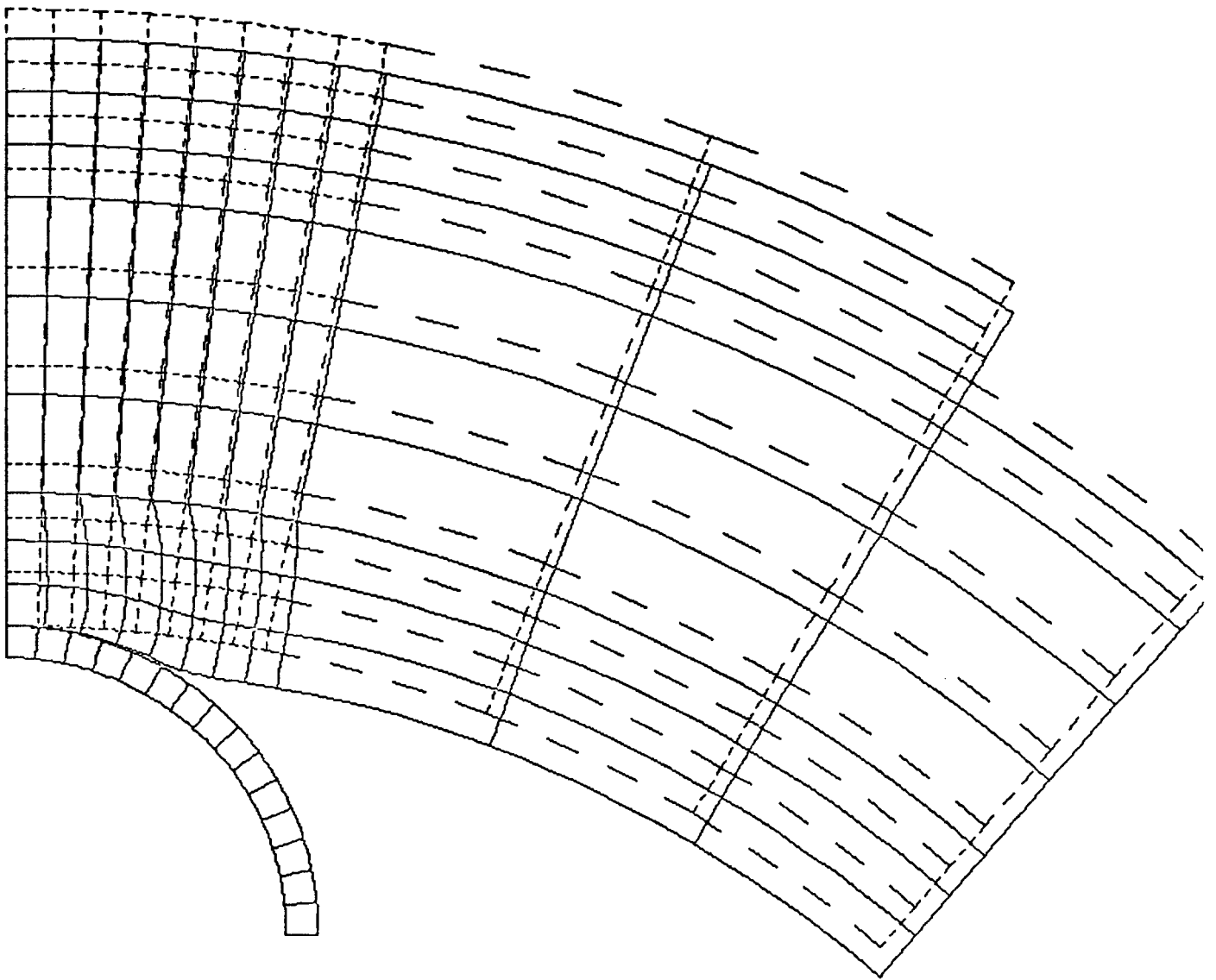
15.　40-year wire tensioner geometry - 1-lb weight

For the 2-lb load,

$$S_y = 7.68 \times 10^6 \, t^{-0.034} \, dynes/cm^2 \tag{16}$$

Roughly, the contact stress is proportional to the square-root of the load. However, as can be seen by examining Figure 15, these calculations are also inaccurate due to the small displacement approximation of the contact forces.

3.3 DISCUSSION OF THE ANALYSES

The results of these analyses are consistent with the approximate analytical results of Ref. 3. There are two significant simplifications that have potential impact on the results:

1. The EPR insulation and Hypalon jacket are not differentiated.

2. The creep law does not explicitly incorporate any effects of material aging. The strain-hardening law used describes materials that do not exhibit aging.

Experiment seems to indicate a significant difference between the deformation of EPR and of Hypalon. The process appears to be that first the entire insulation is extruded from beneath the conductor. Then the Hypalon jacket is subsequently extruded. Secondly, we anticipate that as aging and embrittlement become significant, the creep rates would diminish with time even more rapidly than the simple power-law dependence would indicate.

The difficulties associated with obtaining constitutive properties for the separate materials have been discussed before. Among the several roadblocks are

1. The materials used in electrical cable manufacture are neither simple nor well-defined.

2. Cable insulation in a cable ages differently than the same material isolated from the cable configuration, apparently due (in part) to copper diffusion.

3. Long-term experiments, durations of even 10% of the 40-year life-cycle are not feasible.

Despite these roadblocks to numerical simulation of creep short-out, the analyses are a valuable adjunct to the experiments. When the creep law can be represented by a power law in time, the parameter 1-f, where f is the remaining fractional thickness of insulation and jacket, is also a power law in time.

The power is nearly independent of the load. Both decreasing
contact stress and material aging will tend to reduce creep
short-out compared to the power-law extrapolation of 1-f. Thus
it is tempting to conclude that straight-line extrapolation of
the measured 1-f results on a log-log plot is conservative with
respect to creep short-out.

3.4 RECOMMENDATIONS FOR FURTHER RESEARCH

Before relaxing any of the simplifying assumptions used in
the analyses to date, it is imperative that an accurate solution
for creep short-out deformation be found. None of the computer
codes used to date could be used for the analyses without modifi-
cation, and none has an SNLA support group. We recommend the
following proceedure as the minimum-cost method to obtain a code
capable of performing the analyses:

1. Request assistance from Hibbett & Carlson in obtaining a
computationally efficient boundary treatment for ABAQUS.

2. Try a simple test problem with NIKE to determine whether
the I/O package is currently working.

3. If all else fails, fund a (1-2 month) development effort
for modifying the boundary treatment of STEALTH.

Only after a code has been obtained would we recommend
relaxing the simplifying assumptions we used. We recommend then
that first the changing force per unit out-of-plane thickness be
applied to the geometry of Figure 9. Second, modify the creep
law to reflect the embrittlement with age. Third, provide sepa-
rate treatment of jacket material and Hypalon, with appropriate
slip or stick interface conditions as determined by experiment.
Finally, significant improvement of the contact stress vs. time
distribution can be obtained with three-dimensional analysis.

4. REFERENCES

1. Otmar Stuetzer, "Status Report: Correlation of Electrical Cable Failure with Mechanical Degradation", SNLA, NUREG/CR-3263 (SAND83-2622), April 1984.

2. O. M. Stuetzer, personal communication.

3. J. E. Reaugh, "Analysis of Insulator Cracking and Creep Shortout", Report of activities under Sandia Contract, SAI, November 1982.

4. "STEALTH", A Lagrange Explicit Finite-difference Code for Solids, Structural, and Thermohydraulic Analysis, EPRI, NP-176-1, Revised April 1978.

5. John E. Reaugh, "Calculation of Quasistatic Elastic-Plastic Deformation with Heat Conduction", ANS Trans. vol 18, TANSAO 18 1-401 (1974), June 1974.

6. J. O. Hallquist, "NIKE2D: An Implicit, Finite-deformation, Finite-element Code for Analyzing the Static and Dynamic Response of Two-Dimensional Solids, LLNL, UCRL-52678, March 3, 1979.

7. ABACUS User Information Manual, Hibbett & Carlson, Inc., 1981 et. seq.

5. APPENDIX

PROGRAM LISTING OF SHRINK

The computer program SHRINK was written to assemble and solve the equations developed in Section 2.2 of this report. It is written in a dialect of BASIC developed by Microsoft for use with the CP/M operating system, BASIC-80 Release 5.0, termed MBASIC. As written, the program runs on an Osborne I microcomputer with an Epson MX-80 printer.

This dialect of BASIC is similar to that used on TRS-80 and compatable microcomputers, and also similar to Microsoft's BASIC-86, which is available for the IBM-PC and compatable microcomputers.

```
510 A(5,5)=1
520 A(6,6)=1
540 GOTO 1000
600 REM ----- ALL SLIP
610 A(5,1)=2*EL
620 A(5,5)=EM
630 A(5,7)=BULK*D
640 A(6,3)=2*ELP
650 A(6,6)=EMP
660 A(6,7)=BULKP*DP
665 IF EFLAG=4 THEN A(1,1)=EM+EL: A(1,2)=-(EM-EL)/(ALC^2): A(1,5)=EL: A(
1,7)=BULK*D
670 GOTO 1000
700 REM ---- SLIP AT CONDUCTOR
710 A(5,5)=1: A(5,6)=-1
720 A(6,1)=2*EL*(BLC^2-ALC^2)
730 A(6,3)=2*ELP*(CLC^2-BLC^2)
740 A(6,5)=EM*(BLC^2-ALC^2)
750 A(6,6)=EMP*(CLC^2-BLC^2)
760 A(6,7)=BULK*D*(BLC^2-ALC^2)+BULKP*DP*(CLC^2-BLC^2)
765 IF EFLAG=5 THEN A(1,1)=EM+EL: A(1,2)=-(EM-EL)/(ALC^2): A(1,5)=EL: A(
1,7)=BULK*D
770 GOTO 1000
800 REM ----- STICK AT CONDUCTOR, SLIP AT JACKET
810 A(5,5)=1
820 A(6,3)=2*ELP
830 A(6,6)=EMP
840 A(6,7)=BULKP*DP
845 IF EFLAG=6 THEN A(2,1)=EM+EL: A(2,2)=-(EM-EL)/(BLC^2): A(2,3)=0: A(2
,4)=0: A(2,5)=EL: A(2,7)=BULK*D
850 GOTO 1000
1000 REM
1110 N=6
1120 GOSUB 10000
1130 AA=A(1,7): BB=A(2,7): DEL=D: SM1=EM: SM2=EL: SM3=BULK: EZ=A(5,7)
1140 LPRINT CHR$(15): LPRINT
1150 LPRINT "      ","INNER","OUTER"
1160 LPRINT "YOUNGS",E,EP
1170 LPRINT "POISSON",GNU,GNUP
1180 LPRINT "DEL",D,DP,"      ",LAB$(EFLAG)
1182 LPRINT "EZ",A(5,7),A(6,7)
1183 LPRINT "AA",A(1,7),A(3,7)
1184 LPRINT "BB",A(2,7),A(4,7)
1190 LPRINT: LPRINT "  R"," SIGR"," SIGTH"," SIGZ"," P"," SIGEO","
  DISPL"
1200 R=ALC: GOSUB 5000
1210 R=(ALC+BLC)/2: GOSUB 5000
1220 R=BLC: GOSUB 5000
1230 AA=A(3,7): BB=A(4,7): DEL=DP: SM1=EMP: SM2=ELP: SM3=BULKP: EZ=A(6,7
)
1240 R=BLC: GOSUB 5000
1250 R=.5*(BLC+CLC): GOSUB 5000
```

```
10 REM ------ SHRINK
20 REM
30 REM ------ CALCULATE STRESSES
40 REM           IN TWO-LAYER CABLE INSULATION
50 REM           DUE TO SHRINKAGE
60 DEF FNAT$(I)=CHR$(27)+"="+CHR$(I+31)+CHR$(32)
100 DIM A(6,7),NFIL(6)
110 DEFINT I-N
115 LAB$(0)="NO SLIP": LAB$(1)="ALL SLIP": LAB$(2)="SLIP AT CONDUCTOR":
LAB$(3)="STICK AT CONDUCTOR, SLIP AT JACKET": LAB$(4)="ALL SLIP - CONDUC
TOR STRESS=0": LAB$(5)="SLIP AT CONDUCTOR - SIGR(A)=0": LAB$(6)=LAB$(3)+
" - SIGR(B)=0"
120 N=6
122 D=-1!: E=1!: GNU=.3: GNUP=.3
123 FOR DP=-1.8 TO -1.8
124 FOR EP=.5 TO 2.05 STEP .1
125 FOR EFLAG=0 TO 6
130 FOR I=1 TO N
135 NFIL(I)=0
140 FOR J=1 TO N+1
150 A(I,J)=0
160 NEXT
170 NEXT
175 NFILT=0
180 ALC=.115
190 BLC=.189
200 CLC=.24
210 A(1,1)=ALC
220 A(1,2)=1/ALC
230 A(2,1)=BLC
240 A(2,2)=1/BLC
250 A(2,3)=-BLC
260 A(2,4)=-1/BLC
270 PRINT: PRINT "INNER MATERIAL PROPERTIES"
280 REM INPUT "YOUNGS";E
290 REM INPUT "POISSON";GNU
300 BULK=E/(3*(1-2*GNU))
310 SHEAR=E/(2!*(1+GNU))
320 EM=BULK+4*SHEAR/3
330 EL=BULK-2*SHEAR/3
340 PRINT: PRINT "OUTER MATERIAL PROPERTIES"
350 REM INPUT "YOUNGS";EP
360 REM INPUT "POISSON";GNUP
370 BULKP=EP/(3!*(1-2*GNUP))
380 SHEARP=EP/(2*(1+GNUP))
390 EMP=BULKP+4*SHEARP/3
400 ELP=BULKP-2*SHEARP/3
402 GOSUB 2000
410 PRINT: FOR J=0 TO 6: PRINT J;"...";LAB$(J): NEXT
420 REM INPUT EFLAG
430 ON EFLAG+1 GOTO 500,600,700,800,600,700,800
500 REM ------ NO SLIP
```

```
1260 R=CLC: GOSUB 5000
1300 REM GOTO 120
1310 NEXT: NEXT: NEXT
2000 REM PRINT: INPUT "DEL";D: INPUT "DELP";DP
2010 A(3,1)=EM+EL
2020 A(3,2)=-(EM-EL)/(BLC^2)
2030 A(3,3)=-(EMP+ELP)
2040 A(3,4)= (EMP-ELP)/(BLC^2)
2050 A(3,5)=EL
2060 A(3,6)=-ELP
2070 A(3,7)=BULK*D-BULKP*DP
2080 A(4,3)=EMP+ELP
2090 A(4,4)=-(EMP-ELP)/(CLC^2)
2100 A(4,6)=ELP
2110 A(4,7)=BULKP*DP
2120 RETURN
5000 REM ------ CALCULATE STRESSES
5010 SIGR=(SM1+SM2)*AA-(SM1-SM2)*BB/R/R-SM3*DEL+SM2*EZ
5020 SIGT=(SM1+SM2)*AA+(SM1-SM2)*BB/R/R-SM3*DEL+SM2*EZ
5030 SIGZ=2*SM2*AA-SM3*DEL+SM1*EZ
5035 P=-(SIGR+SIGZ+SIGT)/3: SIGEQ=SQR(1.5*((SIGR+P)^2+(SIGZ+P)^2+(SIGT+P
)^2))
5040 LPRINT USING "##.#####        ";R,SIGR,SIGT,SIGZ,P,SIGEQ,AA*R+BB/R
5050 RETURN
10000 FOR K=1 TO N
10002 IF K=1 THEN FOR I=1 TO N: GOSUB 11000: NEXT I
10010 OOS=1/A(K,K)
10020 A(K,K)=1
10030 FOR J=K+1 TO N+1
10040 A(K,J)=OOS*A(K,J)
10050 NEXT J
10055 IF K=N THEN 10120
10060 FOR I= K+1 TO N
10070 S=A(I,K)
10080 A(I,K)=0
10090 FOR J=K+1 TO N+1
10100 A(I,J)=A(I,J)-S*A(K,J)
10110 NEXT J
10112 GOSUB 11000
10115 NEXT I
10120 NEXT K
10190 FOR K=2 TO N
10200 I=N+1-K
10210 FOR J=I+1  TO N
10220 A(I,N+1)=A(I,N+1)-A(I,J)*A(J,N+1)
10230 NEXT J
10240 NEXT K
10250 RETURN
11000 REM ------ pun matrix on screen
11020 WIDTH 255
11030 IF I>31 THEN 11140
11035 IF I>1 THEN 11050
```

```
11040 PRINT CHR$(26);: FOR IP=1 TO N: FOR JP=1 TO N: IF A(IP,JP)<>0 THEN
 NFIL(IP)=NFIL(IP)+1: NFILT=NFILT+1
11042 NEXT: NEXT: PRINT CHR$(27)+"="+CHR$(39)+CHR$(72);"Orig =";NFILT;
11050 PRINT FNAT$(I);
11055 NFILJ=0
11060 FOR JP=1 TO N
11070 IF A(I,JP)=0 THEN PRINT ".";: ELSE PRINT "X";: NFILJ=NFILJ+1
11080 NEXT JP
11090 IF NFILJ<>NFIL(I) THEN NFILT=NFILT-NFIL(I)+NFILJ: NFIL(I)=NFILJ
11100 PRINT "   ";NFIL(I);CHR$(27)+"="+CHR$(41)+CHR$(72);"Total=";NFILT;
11110 IF NFILTM<NFILT THEN NFILTM=NFILT
11120 PRINT CHR$(27)+"="+CHR$(43)+CHR$(72);"Max  =";NFILTM;
11130 RETURN
11140 NFILJ=0
11150 FOR JP=1 TO N
11160 IF A(I,JP)<>0 THEN NFILJ=NFILJ+1
11170 NEXT
11180 GOTO 11090
```

DISTRIBUTION:

U.S. Government Printing Office
Receiving Branch (Attn: NRC Stock)
8610 Cherry Lane
Laurel, MD 20707
375 copies for RV

Ansaldo Impianti
Centro Sperimentale del Boschetto
Corso F.M. Perrone, 118
16161 Genova
ITALY
Attn: C. Bozzolo

Ansaldo Impianti
Via Gabriele D'Annunzio, 113
16121 Genova
ITALY
Attn: S. Grifoni

ASEA-ATOM
Department KRD
Box 53
S-721 04
Vasteras
SWEDEN
Attn: A. Kjellberg

ASEA-ATOM
Department TQD
Box 53
S-721 04
Vasteras
SWEDEN
Attn: T. Granberg

ASEA KABEL AB
P.O. Box 42 108
S-126 12
Stockholm
SWEDEN
Attn: B. Dellby

Atomic Energy of Canada, Ltd.
Chalk River Nuclear Laboratories
Chalk River, Ontario KOJ 1J0
CANADA
Attn: G. F. Lynch

Atomic Energy of Canada, Ltd.
1600 Dorchester Boulevard West
Montreal, Quebec H3H 1P9
CANADA
Attn: S. Nish

Atomic Energy Research Establishment
Building 47, Division M.D.D.
Harwell, Oxfordshire
OX11 ORA,
ENGLAND
Attn: S. G. Burnay

Bhabha Atomic Research Centre
Health Physics Division
BARC
Bombay-85
INDIA
Attn: S. K. Mehta

British Nuclear Fuels Ltd.
Springfields Works
Salwick, Preston
Lancs
ENGLAND
Attn: W. G. Cunliff, Bldg 334

Brown Boveri Reaktor GMBH
Postfach 5143
D-6800 Mannheim 1
WEST GERMANY
Attn: R. Schemmel

Bundesanstalt fur Materialprufung
Unter den Eichen 87
D-1000 Berlin 45
WEST GERMANY
Attn: K. Wundrich

CEA/CEN-FAR
Departement de Surete Nucleaire
Service d'Analyse Fonctionnelle
B.P. 6
92260 Fontenay-aux-Roses
FRANCE
Attn: M. Le Meur
      J. Henry

CERN
Laboratorie 1
CH-1211 Geneve 23
SWITZERLAND
Attn: H. Schonbacher

Canada Wire and Cable Limited
Power & Control Products Division
22 Commercial Road
Toronto, Ontario
CANADA M4G 1Z4
Attn: Z. S. Paniri

Centro Elettrotecnico
  Sperimentale Italiano
Research and Development
Via Rubattino 54
20134 Milan,
ITALY
Attn: Carlo Masetti

Commissariat a l'Energie Atomique
ORIS/LABRA
BP N° 21
91190 Gif-Sur-Yvette
FRANCE
Attn: G. Gaussens
       J. Chenion
       F. Carlin

Commissariat a l'Energie Atomique
CEN Cadarche DRE/STRE
BP N° 1
13115 Saint Paul Lez Durance
FRANCE
Attn: J. Campan

Conductores Monterrey, S. A.
P.O. Box 2039
Monterrey, N. L.
MEXICO
Attn: P. G. Murga

Electricite de France
(S.E.P.T.E.N.)
12, 14 Ave. Dubrieroz
69628 Villeurbarnie
Paris, FRANCE
Attn: H. Herouard
       M. Hermant

Electricite de France
Direction des Etudes et Recherches
1, Avenue du General de Gaulle
92141 CLAMART CEDEX
FRANCE
Attn: J. Roubault
       L. Deschamps

Electricite de France
Direction des Etudes et Recherches
Les Renardieres
Boite Postale n° 1
77250 MORET SUR LORING
FRANCE
Attn: Ph. Roussarie
       V. Deglon
       J. Ribot

Energia Nucleare e delle
  Energie Alternative
CKE Casaccia
1-0060 Rome
ITALY
Attn: A. Cabrini

EURATOM
Commission of European Communities
C.E.C. J.R.C.
21020 Ispra (Varese)
ITALY
Attn: G. Mancini

FRAMATOME
Tour Fiat - Cedex 16
92084 Paris La Defense
FRANCE
Attn: G. Chauvin
       E. Raimondo

Furukawa Electric Co., Ltd.
Hiratsuka Wire Works
1-9 Higashi Yawata - 5 Chome
Hiratsuka, Kanagawa Pref
JAPAN 254
Attn: E. Oda

Gesellschaft fur Reaktorsicherheit (GRS) mbH
Glockengasse 2
D-5000 Koln 1
WEST GERMANY
Attn: Library

Health & Safety Executive
Thames House North
Milbank
London SW1P 4QJ
ENGLAND
Attn: W. W. Ascroft-Hutton

ITT Cannon Electric Canada
Four Cannon Court
Whitby, Ontario L1N 5V8
CANADA
Attn: B. D. Vallillee

Imatran Voima Oy
Electrotechn. Department
P.O. Box 138
SF-00101 Helsinki 10
FINLAND
Attn: B. Regnell
      K. Koskinen

Institute of Radiation Protection
Department of Reactor Safety
P.O. Box 268
00101 Helsinki 10
FINLAND
Attn: L. Reiman

Instituto de Desarrollo y Diseno
Ingar - Santa Fe
Avellaneda 3657
C.C. 34B
3000 Santa Fe
REPUBLICA ARGENTINA
Attn: N. Labath

ISMES S.p.A.
Viale G. Cesare, 29
24100 BERGAMO, Italy
Attn: A. Castoldi
      M. Salvetti

Japan Atomic Energy Research Institute
Takasaki Radiation Chemistry
  Research Establishment
Watanuki-machi
Takasaki, Gunma-ken
JAPAN
Attn: N. Tamura
      K. Yoshida
      T. Seguchi

Japan Atomic Energy Research Institute
Tokai-Mura
Naka-Gun
Ibaraki-Ken
319-11, JAPAN
Attn: Y. Koizumi

Japan Atomic Energy Research Institute
Osaka Laboratory for Radiation Chemistry
25-1 Mii-Minami machi,
Neyagawa-shi
Osaka 572
JAPAN
Attn: Y. Nakase

Kalle Niederlassung der Hoechst AG
Postfach 3540
6200 Wiesbaden 1,
WEST GERMANY
Biebrich
Attn: Dr. H. Wilski

Kraftwerk Union AG
Department R361
Hammerbacherstrasse 12 + 14
D-8524 Erlangen
WEST GERMANY
Attn: I. Terry

Kraftwerk Union AG
Section R541
Postfach: 1240
D-8757 Karlstein
WEST GERMANY
Attn: W. Siegler

Kraftwerk Union AG
Hammerbacherstrasse 12 + 14
Postfach: 3220
D-8520 Erlangen
WEST GERMANY
Attn: W. Morell

Motor Columbus
Parkstrasse 27
CH-5401
Baden
SWITZERLAND
Attn: H. Fuchs

National Nuclear Corporation
Cambridge Road, Whetstone
Leicester LE8 3LH
ENGLAND
Attn: A. D. Hayward
       J. V. Tindale

NOK AG Baden
Beznau Nuclear Power Plant
CH-5312 Doettingen
SWITZERLAND
Attn: O. Tatti

Norsk Kabelfabrik
3000 Drammen
NORWAY
Attn: C. T. Jacobsen

Nuclear Power Engineering Test Center
6-2, Toranomon, 3-Chome
Minato-ku, #2 Akiyana Bldg.
Tokyo 105
JAPAN
Attn: K. Takumi

Ontario Hydro
700 University Avenue
Toronto, Ontario M5G 1X6
CANADA
Attn: R. Wong
       B. Kukreti

Oy Stromberg Ab
Helsinki Works
Box 118
FI-00101 Helsinki 10
FINLAND
Attn: P. Paloniemi

Radiation Center of
  Osaka Prefecture
Radiation Application-
  Physics Division
Shinke-Cho, Sakai
Osaka, 593, JAPAN
Attn: S. Okamoto

Rappinl
ENEA-PEC
Via Arcoveggio 56/23
Bologna
ITALY
Attn: Ing. Ruggero

Rheinisch-Westfallscher
Technischer Uberwachunge-Vereln e.V.
Postfach 10 32 61
D-4300 Essen 1
WEST GERMANY
Attn: R. Sartori

Sydkraft
Southern Sweden Power Supply
21701 Malmo
SWEDEN
Attn: O. Grondalen

Technical University Munich
Institut for Radiochemie
D-8046 Garching
WEST GERMANY
Attn: Dr. H. Heusinger

UKAEA
Materials Development Division
Building 47
AERE Harwell
OXON OX11 ORA
ENGLAND
Attn: D. C. Phillips

United Kingdom Atomic Energy Authority
Safety & Reliability Directorate
Wigshaw Lane
Culcheth
Warrington WA3 4NE
ENGLAND
Attn: M. A. H. G. Alderson

Waseda University
Department of Electrical Engineering
3-4-1 Ohkubo, Shinjuku-ku
Tokyo 160
JAPAN
Attn: Y. Ohki

```
1200    J. P.  VanDevender
1800    R. L.  Schwoebel
1810    R. G.  Kepler
1811    R. L.  Clough
1812    J. M.  Zeigler
1812    K. T.  Gillen
1813    J. G.  Curro
2126    J. E.  Gover
2126    O. M.  Stuetzer (10)
6200    V. L.  Dugan
6300    R. W.  Lynch
6400    A. W.  Snyder
6410    J. W.  Hickman
6417    D. D.  Carlson
6420    J. V.  Walker
6433    F. V.  Thome
6440    D. A.  Dahlgren
6442    W. A.  Von Riesemann
6444    L. D.  Buxton
6446    L. L.  Bonzon (10)
6446    W. H.  Buckalew
6446    L. D.  Bustard
6446    J. W.  Grossman
6446    M. J.  Jacobus
6446    J. D.  Keck
6446    F. J.  Wyant
6447    D. L.  Berry
6449    K. D.  Bergeron
6450    J. A.  Reuscher
8024    P. W.  Dean
3141    S. A.  Landenberger (5)
3151    W. L.  Garner
```

2 TITLE AND SUBTITLE	3 LEAVE BLANK
Correlation of Electrical Reactor Cable Failure with Materials Degradation	
	4 DATE REPORT COMPLETED

	MONTH	YEAR
5 AUTHOR(S)	February	1986

Otmar M. Stuetzer

	6 DATE REPORT ISSUED
	MONTH	YEAR
	March	1986

7 PERFORMING ORGANIZATION NAME AND MAILING ADDRESS *(Include Zip Code)*	8 PROJECT TASK WORK UNIT NUMBER
Qualification Methodology Assessment Division 6446 Sandia National Laboratories Albuquerque, New Mexico 87185	**9 FIN OR GRANT NUMBER** A-1051

13 ABSTRACT *(200 words or less)*

Complete circuit failure (shortout) of electrical cables typically used in nuclear power plant containments is investigated. Failure modes are correlated with the mechanical deterioration of the elastomeric cable materials. It is found that for normal reactor operation, electrical cables are reliable and safe over very long periods. During high temperature excursions, however, cables pulled across corners under high stress may short out due to conductor creep. Severe cracking will occur in short times during high temperatures (>150°C) and in times of the order of years at elevated temperatures (100°C-140°C).

A theoretical treatment of stress distribution responsible for creep and for cracking by J. E. Reaugh of Science Applications, Inc. is contained in the Appendix.

14 DOCUMENT ANALYSIS - a KEYWORDS/DESCRIPTORS	15 AVAILABILITY STATEMENT
	Unlimited
	16 SECURITY CLASSIFICATION
	(This page)
b IDENTIFIERS/OPEN-ENDED TERMS	Unclassified
	(This report)
	Unclassified
	17 NUMBER OF PAGES
	120
	18 PRICE